Department of Electrical and Computer Engineering

Characterization of Power Transformer Frequency Response Signature using Finite Element Analysis

Naser Hashemnia

This thesis is presented for the Degree of
Doctor of Philosophy
of
Curtin University

December 2014

DECLARATION

To the best of my knowledge this thesis contains no material previously published by any other person except where due acknowledgment has been made. This thesis contains no material that has been accepted for the award of any other degree or diploma in any university.

Signature: *Naser Hashemnia* Date: 11/05/2015

ABSTRACT

Power transformers are a vital link in power system networks. Monitoring and diagnostic techniques are essential to decrease maintenance and improve the reliability of the equipment. The problem of transformer winding and core deformation is increasing due to the long–term exposure of transformers to systemic faults and the continued growth of the power grid [1, 2]. Winding movements may lead to serious faults and subsequent damage to the transformer and draining the transformer oil to carry out winding inspection is not recommended. Winding deformation results in relative changes to the internal inductance and capacitance of the winding structure. These changes can be detected externally by the frequency response analysis (FRA) technique, which has been successfully used for detecting winding deformations, core and clamping structure. The frequency response analysis (FRA) is an off-line test that is used to measure the input/output relationship as a function of a wide frequency range. This provides a transformer fingerprint for future diagnosis. Because of its dependency on graphical analysis, FRA calls for trained personnel to conduct the test and interpret its results in order to identify and quantify internal mechanical faults. Another drawback of the FRA test is that the transformer has to be de-energized and switched out of service causing complete interruption to the electricity grid.

This research has developed a novel, versatile, reliable and robust technique for high frequency power transformers modelling. The purpose of this modelling is to enable engineers to conduct sensitivity analyses of FRA in the course of evaluating mechanical defects of power transformer windings. The importance of this new development is that it can be applied successfully to industry transformers of real geometries.

The FRA test requires identification of any winding displacement or deformation in the early stages. A comprehensive model is ideal, but it is normally difficult to obtain full design information for a transformer, as it requires exclusive manufacturing design records that most manufacturers would be reluctant to reveal. In order to validate the appropriateness of the model for real transformers, a detailed Finite Element Model (FEM) is necessary. To establish the capabilities of a high-frequency power transformer model, the construction and geometric data from the

manufacturer, together with transformer material characteristics are utilized. All electrical circuit parameters in the distributed lumped model representation are calculated based on FEM analysis.

The main conclusions drawn from the work in this thesis can be summarized as follows:

1. A very simple, analytical method using lumped RLC parameters cannot accurately represent the performance of high-frequency power transformers. The reason is that simple models normally ignore the iron core element of the transformer. Inclusion of the iron core in models simulating performance of power transformers can improve the accuracy of the calculated inductance. To overcome limitations of simple models, a frequency-dependent complex permeability can be used in a FEM to represent both the core and the windings in a realistic manner.

2. This study has produced diagnostic charts, which correlate the percentage change in each electrical parameter (involved in a transformer) with the level of mechanical fault for a variety of faults. This can provide precise simulation of mechanical failures using a combination of the transformer's equivalent circuit and the deterministic analysis of the FRA signature.

3. FRA has the potential to detect Bushing faults and oil degradation in the high frequency range.

Keywords: Power transformer, High-frequency model, Condition monitoring, Finite Element Analysis, Lumped parameters model, Frequency response analysis (FRA), internal stresses, Mechanical faults.

ACKNOWLEDGMENTS

First and foremost, I would like to express my immense gratitude and love to the closest of people in my circle, my wife, Sahar Baraei, who has provided unconditional and unrelenting support during my pursuit of study and learning. I recognize that her hard work and determination was largely for the betterment of my life for which I am eternally grateful. For my wife, it is with great pleasure and deep felt love that I dedicate this work to you.

Special thanks must go to several people in connection with the research documented in this thesis. I am especially grateful for the active and enthusiastic involvement of my primary Supervisor, Dr. Ahmed Abu-Siada, who has selflessly given countless hours of his time in discussing my research in-depth. Associate Supervisor, Professor Mohammad-Ali Masoum, is to be thanked for his contributions in this research project serving as co-author in some of my publications. Likewise, Professor Syed M. Islam has been extremely supportive in my research endeavors.

Department Secretary Margaret Pittuck and Technical Manager Mark Fowler deserve special mention as they have been very helpful in all my administration and study material needs. For providing valuable technical hardware support in the experimental aspects of my work on power transformers, I am grateful to the skillful laboratory technicians, Mr. Zibby Cielma and Mr. Russell Wilkinson. Without their help, I would not have been able to carry out safe and accurate measurements for validation and testing of theoretical and simulation model findings.

Finally, a great many thanks must go to the people who helped in reviewing and proofreading this thesis. The behind-the-scenes and often unsung contributors, the reviewers and examiners of this thesis and related publications, should be acknowledged for their time in helping to ensure the work is of a high standard.

PUBLICATIONS

The main results from this work have either been published in the following journals and conference proceedings:

Journal Papers

1. **Naser Hashemnia**, Ahmed Abu- Siada, Syed Islam, “Improved Power Transformer Winding Fault Detection using FRA Diagnostics Part 1: Axial Displacement”, Dielectric and Insulation, IEEE Transaction on, Vol.22, No.1, Feb. 2015.
2. **Naser Hashemnia**, Ahmed Abu-Siada, Syed Islam, “Improved Power Transformer Winding Fault Detetcion using FRA Diagnostics Part 2: Radial Deformation” Dielectric and Insulation, IEEE Transaction on , Vol.22, No.1, Feb. 2015.
3. **Naser Hashemnia**, Ahmed Abu-Siada, Syed Islam, “Detection of Bushing Faults and oil degredation of Power Transformer using FRA Diagnostics”, Dielectric and Insulation, IEEE Transaction on,2014 (under review).
4. A. Masoum, **N. Hashemnia**, A. Abu Siada, M. Masoum, and S. Islam, "Online Transformer Internal Fault Detection Based on Instantaneous Voltage and Current Measurements Considering Impact of Harmonics," Power Delivery, IEEE Transactions on, vol. PP, pp. 1-1, 2014.
5. A.Masoum, **Naser Hashemnia,** Ahmed Abu-Siada**,** A.S. Masoum and Syed Islam, ‘’Finite-Element Performance Evaluation of On-Line Transformer Internal Fault Detection based on Instantaneous Voltage and Current Measurements” AJEEE: Australian Journal of Electrical & Electronics Engineering, 2013.
6. A. Abu-Siada, **N. Hashemnia**, S. Islam, and M. A. S. Masoum, "Understanding power transformer frequency response analysis signatures," Electrical Insulation Magazine, IEEE, vol. 29, pp. 48-56, 2013.

Conferences

1. **Naser Hashemnia**, M.A.S. Masoum, Ahmed Abu-Aiada, Syed Islam, “Transformer Mechanical Deformation Diagnosis: Moving from Offline to Online Fault Detection”, AUPEC, Australia, 2014.
2. **Naser Hashemnia**, Ahmed Abu-Siada, Syed Islam, “Detection of Power Transformer Disk Space Variation and Core Deformation using Frequency Response Analysis”, South Korea, International Condition Monitoring Conference,2014.
3. A. S. Masoum, **N. Hashemnia**, A. Abu-Siada, M. A. S. Masoum, and S. M. Islam, "Performance evaluation of on-line transformer winding short circuit fault detection based on instantaneous voltage and current measurements," in PES General Meeting | Conference & Exposition, 2014 IEEE, 2014, pp. 1-5.
4. **N. Hashemnia**, A. Abu-Siada, and S. Islam, "Impact of axial displacement on power transformer FRA signature," in Power and Energy Society General Meeting (PES), 2013 IEEE, 2013, pp. 1-4.
5. A. Abu-Siada, **N. Hashemnia**, S. Islam, and M. S. A. Masoum, "Impact of transformer model parameters variation on FRA signature," in Universities Power Engineering Conference (AUPEC), 2012 22nd Australasian, 2012, pp. 1-
6. **N. Hashemnia**, A. Abu-Siada, M. A. S. Masoum, and S. M. Islam, "Characterization of transformer FRA signature under various winding faults," in Condition Monitoring and Diagnosis (CMD), 2012 International Conference on, 2012, pp. 446-449.
7. **Naser Hashemnia**, A. Abu-Siada, Mohammad A.S. Masoum, and Syed M. Islam, “Toward the Establishment of Standard Codes for Power Transformer FRA Signature Interpretation in Condition Monitoring and Diagnosis (CMD), International Conference, 2012.

TABLE OF CONTENTS

LIST OF FIGURES

LIST OF TABLES

1. INTRODUCTION

1.1 BACKGROUND OF RESEARCH

Power transformers are vital links and one of the most critical and expensive assets in electrical power systems. Majority of in-service power transformers have already exceeded their expected life span as they were mostly installed prior to 1980 [1]. This poses a significant risk for existing utilities, since the impacts of in-service transformer failures can be catastrophic. In addition to the risk above, the daily increase in load demand, the global trend towards developing smart grids and the growing number of nonlinear loads (such as smart appliances and electric vehicles) will further increase the likelihood of unusual loads on transformers (non-sinusoidal operations) and eventual failure. These combined effects of aging plus nonlinear and unusual loads on transformers are increasing the rate of faults in existing networks, which renders inspection of transformers and detection of incipient faults inevitable. Unfortunately, current fault-detection methods are unable to detect and identify all sorts of faults during routine condition monitoring of assets. Accordingly, there is an increasing need for advanced methods of condition assessment that can readily detect transformers faults so that the rate of faults can be kept at a manageable level. To this end, it is essential to develop simple, reliable and accurate diagnostic tools that can perform the following functions for transformers:

1. determine the current status of a transformer;
2. detect incipient faults and estimate the remaining life of the existing in-service power transformers in order to prevent failures; and
3. decrease maintenance costs and improve the reliability of power systems .

The technique of Frequency Response Analysis (FRA) is one of those promising methods that can be used to achieve the goals above, because it offers excellent sensitivity and accuracy in detecting mechanical faults in transformer windings. An aging transformer is more prone to mechanical deformations due to the reduction of its capability to ride through short-circuit faults. On the other hand, less severe deformations lead to partial discharges and insulation ruptures, which can normally be detected by oil analysis. Whilst minor deformations show no important variations

in their functional characteristics, the mechanical properties of the copper winding may be altered, seriously, risking a break during the next occurrence. This can cause reduction in impulse strength due to degraded insulation and reduced distances. FRA has proved to be a reliable method in both laboratory investigations and in practice. However, there is little understanding about why and how FRA works and how the FRA signature can be classified and interpreted. All interpretational characteristics relating to FRA should be studied before standardizing this technique for the purpose of condition monitoring of power transformers. To establish this test as a standard method, separate or combined experimental and theoretical investigations (transformer model) should be performed [3-5].

During the last few decades, transformer modelling has attracted much attention, because of its importance in power networks, which are normally characterized by the complexity of their various components. Some disagreements still exist in the literature as to which assumptions should be permitted ideally, accurate models of transformers would use data directly from transformers' manufacturers, but such data is not generally available.

1.2 SCOPE OF WORK

The main objectives of the work presented in this thesis are as follows:

- development of a high-frequency model of power transformer using a software based on the Finite Element Method (FEM);
- investigation of the 3D model based on the actual geometry of a transformer;
- development of charts that correlate the percentage change of all the parameters pertinent to a transformer's equivalent circuit with levels of winding deformations and displacement that result by mechanical faults.

Another goal in this thesis is to use the model developed for investigating the FRA technique to study the following aspects:

- the impact of various winding deformations and displacements;
- the FRA sensitivity to different types and levels of fault;
- other faults that might vary the FRA-signature, such as bushing faults and oil degradation;

- determination of the type of fault and the corresponding frequency band that the FRA signature may be altered or modified by such fault.

The results obtained from the above investigation will be used to improve the understanding of the FRA technique and consequently, achieve a better interpretation of the FRA signature.

1.3 RESEARCH METHODOLOGY

This thesis introduces detailed analyses of the mechanical faults and their impacts on the electrical parameters of the transformer detailed equivalent circuit and hence on its FRA signature. In this regard, a comprehensive review on transformer design as well as Frequency response analysis (FRA) technique are carried out. Then detailed physical single-phase and three phase transformer's geometry are simulated using 3D finite element software to emulate real transformer operation. Finally, a guideline for FRA signature's interpretation is introduced.

1.4 THESIS OUTLINE

This thesis has two main parts: methodology and modelling. The subdivisions of this thesis reflect the progress of the work when it comes to the choice of methods.
The remaining chapters of this thesis are as follows:

- Chapter 2 describes background material regarding condition assessment and transformer modelling;
- Chapter 3 illustrates how FEM software calculates the elementary quantities used in a transformer model, and then presents a model developed using ANSYS, a FEM-based software for high-frequency modelling of power transformers;
- Chapter 4 describes the results obtained from the FEM model. This chapter explains the specific effects of mechanical faults on changing the electrical parameters of the distributed power transformer model. In addition, the chapter investigates the impact of mechanical failures on the signature of FRA;
- Chapter 5 discusses the main conclusions drawn from this work and recommends topics for further investigation.

2. BACKGROUND

Power transformers are the most expensive and vital assets in a power system. It is, therefore, highly expected that suitable care should be practiced in the commissioning and in the preventative and detective maintenance of power transformers. Since maintenance demands a considerable investment of time, with spare units not always obtainable, it is important to regularly monitor the condition of the power transformers of a network. An international survey of monitoring the condition of large power transformers such as the one conducted by the CIGRE [6] shows that the annual transformer failure rate is between 1% to 2%. Even though the survey shows that the failure rate is relatively low, a single incipient fault in a large transformer normally incurs huge losses for the overall utility. Thus, the significance of condition monitoring of power transformers is listed as a key priority in any utility. Frequency response analysis, FRA, is a relatively novel detective method used for evaluating the mechanical condition of transformer windings. This technique compares the FRA signatures obtained with baseline measurements and any variation between the two signatures may be interpreted as potential mechanical failures. Hence, a reliable high-frequency model of power transformer is essential to establish and interpret the sensitivity guidelines for various mechanical failures.

Different methods of transformer modelling have been established, depending on the application of the model [7-9]. Experimental work was the starting point for the first 50 years. Then, the advent of computer technology provided engineers the capacity to solve complex problems such as development of internal voltages within transformer windings at high frequencies by using computational logic [6].An appropriate technique of modeling has been investigated in order to examine the FRA technique and to assess various internal faults [1, 2, 10].

2.1 CONDITION MONITORING – PURPOSE AND PRACTICE

During the last decade, condition monitoring of power transformers has attracted much attention from the utilities. Asset management and asset life expectancy have become significant because financial considerations have altered the technical strategies of power utilities. In order to decrease the costs of maintenance and

increase the life expectancy of the components at the same time, the maintenance policy has been changed from time-based maintenance to condition-based maintenance. Since many of the global power transformers currently in service will reach their designated lifespan in just a few years [11] regular monitoring of the condition of these units is very important for estimating the remaining lifespan and avoiding any incipient failures as well as long power outages. Failure of a power transformer can fall into one of the following categories:

- Defects or deficiencies that will eventually represent incipient faults;
- Problems originating from aging processes;
- Problems induced by operating conditions exceeding the transformer capabilities.

Normally, transformers defects persist for some time before they lead to catastrophic failures. Condition assessment of transformers contributes to prolonging the lifespan by enabling knowledge-based decisions regarding refurbishment, replacement and retirement to be made reliably. In order to establish efficient lifespan management, a comprehensive model that calls for several parameters is required. Therefore, comprehensive investigation is needed to identify these parameters and assess their role in the condition of the various components of a transformer. Some important factors which should be considered during investigation of a transformer's conditions are listed below [12-14].

- Insulation of windings and conductors, cellulose structure, mechanical strength, decomposition and aging products;
- Transformer oil analysis such as dissolved gas analysis (DGA), partial discharges (PD), etc.;
- On-load Tap Changers (OLTC);
- Core, circulating currents, local overheating due to faulty grounding-leads, overrated flux-levels, local short-circuit faults;
- Mechanical condition of windings, withstand strength, displacement and deformation, supportive structure and clamping force;
- Bushings, oil-level, and pollution;
- Tank and components involved and cooling system.

Various diagnostic techniques have been developed by several studies to assess

the condition of the transformer and its components [6-8].These studies were undertaken to establish statistics for power transformer faults and the types of parameters associated with these faults. Some of the most popular power transformer condition monitoring techniques are briefly elaborated below:

2.1.1 Condition Monitoring By Partial Discharge Analysis

When the strength of the electric field exceeds the strength of the dielectric breakdowns of a localized area, an electrical partial discharge bridges the insulation in between conductors as well as ground. This indicates a partial discharge (PD) activity within the transformer [15]. The dielectric properties of insulation might be affected significantly if it is subject to consistent partial discharge activity over a long period of time [16-19]. In addition, if the PD activity persists and is not attended it might ultimately lead to complete electrical failure of the system. Partial discharge activity can be an important symptom of the deterioration of a transformer and the aging of its insulation .Investigations of PD events in liquid dielectrics (such as oil) are not very common and consequently are less well understood than solid dielectrics [20].

Partial discharge activity can be defined and categorized by the type of defect/fault responsible and the area where it occurs. The range of fault classes is as follows [21]:

- Floating component – caused by conducting objects that have become disconnected and acquired a floating potential;
- Bad contact – caused by sparking, e.g. between the threads of loose nuts and bolts;
- Suspended particle – caused by small, moving conducting objects or debris within the insulating oil;
- Rolling particle – caused by particles lying on a conductive surface until they become influenced by the electric field, causing them to roll or bounce around;
- Protrusion – caused by fixed, sharp metallic protrusions on HV conductors;
- Surface discharge – caused by moisture ingress or as a result of interactions between cellulose material and the insulating oil, causing surfaces to become semiconducting;

- Floating electrodes – caused by components such as stress shields that may have become partially detached from the chamber, resulting in ineffective bonding and capacitive sparking [22].

PD is determined and detected by using piezoelectric sensors [23, 24]. Also, optical fiber sensors can be used to successfully capture the PD signal [25]. Ultra-High Frequency (UHF) sensors are relatively newer than conventional PD measurement methods [26, 27].

The type of discharge is determined by a variety of factors, such as [28]:

- The pulse amplitude;
- The time of occurrence (point on wave) on the mains cycle;
- The number of discharges per second;
- The interval between discharges.

Because of the fact that a significant number of insulation problems are induced by partial discharge (PD), it is used extensively to monitor the condition of the transformer insulation[29].

2.1.2 Condition Monitoring By Vibration Analysis

Vibration analysis is effective for detecting mechanical failures, and it can be used to diagnose the transformer's condition online, even when the transformer is electrically connected [30-32]. Critical information can be provided by vibrations recorded on the transformer tank under normal operational conditions [33]. Many different sources can cause a transformer tank to vibrate. Examples of these are the windings and the core (which contributes significantly to vibration) .Other sources of vibration include On-Load Tap Changers (OLTCs), cooling fans and oil pumps, which can readily be distinguished from other important components that may contribute to vibration [34-36]. Both the internal core and windings can create vibrations signals that may be very difficult and complex to model. Historical records show that winding deformations can cause 12%-15% of transformers failures [37, 38]. Therefore, it is essential to develop a vibration model that can reflect the status of the windings with high accuracy [39].

The process involved in using vibration analysis to monitor the condition of a transformer can be described as follows:

Vibrations generated by windings and core spread through the transformer's oil. The

signatures generated by the vibrations [40] reach the transformer walls, which are picked by vibration sensors. After that, accelerometers are to gather the vibration signals by connecting them to the transformer walls. The signal recorded could be interpreted as a series of decaying bursts, with each of the bursts being the consequence of a mixture of a finite number of decaying sinusoidal waveforms [41]. Limiting vibration analysis to diagnose a few important parts may be inadequate, and this entails more investigation to evaluate the condition of all of the transformer parts [35, 37, 39].

2.1.3 Condition Monitoring By Dissolved Gas Analysis

Dissolved gas-in-oil analysis (DGA) is an outstanding method to detect the incipient insulation (or concealed) faults in an oil-immersed power transformer. Some small quantities of gases are liberated when insulating oils face abnormal electrical or thermal stresses [20, 42, 43]. By means of DGA, it is feasible to differentiate a variety of faults, such as PD, thermal faults or arcing in a great variety of oil-filled equipment. To distinguish trends and determine the severity of incipient faults, oil samples must be taken regularly over a period of time. The information obtained from the analysis of gases dissolved in insulating oil is essential. This information can form a part of preventive maintenance programs. Data from DGA can provide [44-46] :

- Information on the rate of fault development;
- Confirmation of the existence of faults;
- Justification for repair schedules;
- Condition monitoring data within overload [47-49].

Thermal decomposition of oil and paper produces gases such as methane, hydrogen, ethylene, ethane, acetylene, CO, CO_2 in addition to organic compounds, alcohols, aldehydes and peroxide acids [49].

The concentration of fault gas in an oil sample can be used to identify and quantify various faults. Many DGA data interpretation such as the Rogers ratio[47, 50], Doernenburg ratio[49], IEC, [48] Logarithmic Nomograph, [51] Key gases[52] and the Duval triangle[47, 52, 53] are currently widely used.

2.2 POWER TRANSFORMERS DESIGN

A power transformer is a static electrical device that uses electromagnetic induction to transfer power from one circuit to another without a change in frequency [54]. Power transformers are essential components of a power system which is typically designed to have a 30 year operating life. Their function is to transform voltages to suitable levels between the generation, transmission and distribution stages of a power system. Power transformers can be classified into three categories based on their power ratings, small (500 to 7500kVA), medium (7500kVA to 100MVA) and high (100MVA+) [54]. A power transformer consists of different parts as following:

2.2.1 Cores and Windings

The active part where the transformation takes place consists of the core and the windings. A transformer utilises the low reluctance path provided by a magnetic core to transfer energy from one winding to another. The materials used to make the core are normally iron and steel to reduce hysteresis loses. The limbs are made of a number of thin core steel sheets to reduce eddy current losses and they are kept by means of glue for the small transformers and by means of steel straps around the limbs or an epoxy-cured stocking for large transformers.

The conductor material is generally made of copper or aluminium and they can arranged in either disk winding, helix winding or layer-type winding [54].

2.2.2 Transformer insulation and cooling

The main insulation system of a power transformer consists of a combination of paper and pressboard cellulose material which is immersed in mineral oil. The oil impregnated cellulose material is of low cost and has excellent insulation properties. It is used to insulate winding turns and is is circulated in ducts for cooling purposes [54].

2.2.3 Transformer Tank

The tank is primarily the container for the oil and is acting as a physical protection for the active parts within the transformer. It is also serves as a support structure for accessories and control equipment [54]. Fig 2.1 shows the main components of a power transformer.

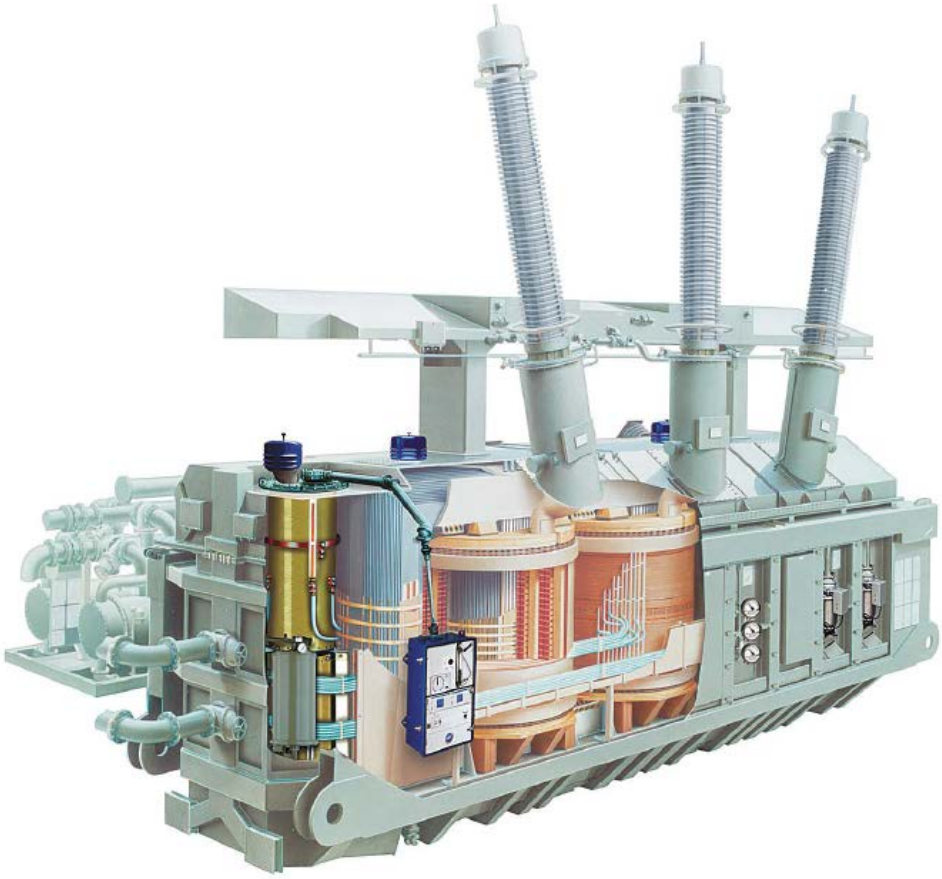

Figure2-1 Power Transformer[54]

2.3 ROOTS OF MECHANICAL FAULTS IN POWER TRANSFORMER

It has been reported that transformer winding and core failures are at the top of the list of failures. It is assumed that some dielectric defects occur due to mechanical displacements inside the winding. Mechanical condition assessment of the winding and the core can prevent occurrence of such faults at an earlier stage [55, 56].

Several mechanisms exist to analyse the root of mechanical failures found in transformer windings:

- Very high short-circuit forces, because of close-up secondary faults;
- Careless during transport;
- Dynamic forces in service (for example, seismic forces or vibrations);
- Aging, which decreases clamping force to supportive structure and insulation, leading to reductions in the withstand strength of dielectric insulation against the above factors.

It is recommended to diagnostically detect deformations at an earlier stage before

they lead to catastrophic failures or any unexpected outages. Short-circuit forces due to secondary faults are the most common reasons for mechanical deformations [51, 57, 58]. The main mechanical fault modes are[53]:

- Axial displacement (e.g. displacement of the complete winding), telescoping, stretching and bending;
- Radial deformation (e.g. free and force buckling).

Secondary faults (associated faults) are usually caused by the disruption of strand and turn insulation, resulting in local short circuits[57]. This normally creates hot-spots and cause partial discharges or strand ruptures, and casual gassing. The latter symptom of gassing is where DGA usually can be used to detect and classify the fault [51, 59] .

Frequency response analysis is known as the most reliable nondestructive technique in identifying mechanical deformation within power transformers [60].The SFRA calls for experts to conduct the test and analyse its results. This thesis is aimed at establishing a comprehensive interpretation guideline for SFRA signatures.

2.4 FREQUENCY RESPONSE ANALYSIS (FRA)

Frequency response analysis (FRA) is a powerful diagnostic technique currently used to identify winding deformations within power transformers [2, 61-64] The FRA technique is based on the fact that deformations and displacements of a transformer winding alter its impedance and consequently its frequency response signature. The change in the transformer's FRA signature is used for both fault identification and quantification.

Transformer components such as windings, core, and insulation can be represented by equivalent circuits, comprising resistors, capacitors, and self or mutual inductances whose values will be altered by a mechanical fault within the transformer. Thus the frequency response of the relevant equivalent circuit will change. Changes in a transformer's geometry or in the dielectric properties of its insulating materials due to aging or increasing water content also affect the shape of the frequency response, especially the resonant frequencies and their damping [8]. Frequency response analysis is an off-line technique, in which a low-voltage AC signal is injected at one terminal of a winding and the response is measured at the other terminal of the same winding with reference to the grounded tank. The FRA

analyzer measures the transfer function, impedance or admittance of the winding, typically over the frequency range 10 Hz to 5 MHz, and one or all of these three properties can be used for fault diagnosis. FRA equipment can be connected to the transformer in different ways [12]–[14].

A typical FRA signature (winding transfer function in dB against frequency) is shown in Figure 2-2 [6]. The figure shows 3 responses from the 3 phases of the same transformer. For a normal (healthy) transformer, they should closely follow each other (overlap). In this case, the one that stands out is indicative of abnormality on that phase. The point is that in cases where historical data is not available, it is still possible to reveal the fault through comparison between phases. This signature can be compared with a previously recorded signature to detect any mechanical deformation that may have developed between the recordings of the two signatures. A FRA diagnosis has also been used recently to identify winding deformations in rotating machines [65, 66]. While the measurement procedure using commercial test equipment is quite simple, skilled and experienced personnel are required to interpret the FRA signatures and correctly identify the type and location of a fault. Although much research has been performed on the topic of FRA signature interpretation, a reliable interpretation code on the method has not yet been published [5]. In [66] the FRA frequency range is subdivided into the following:

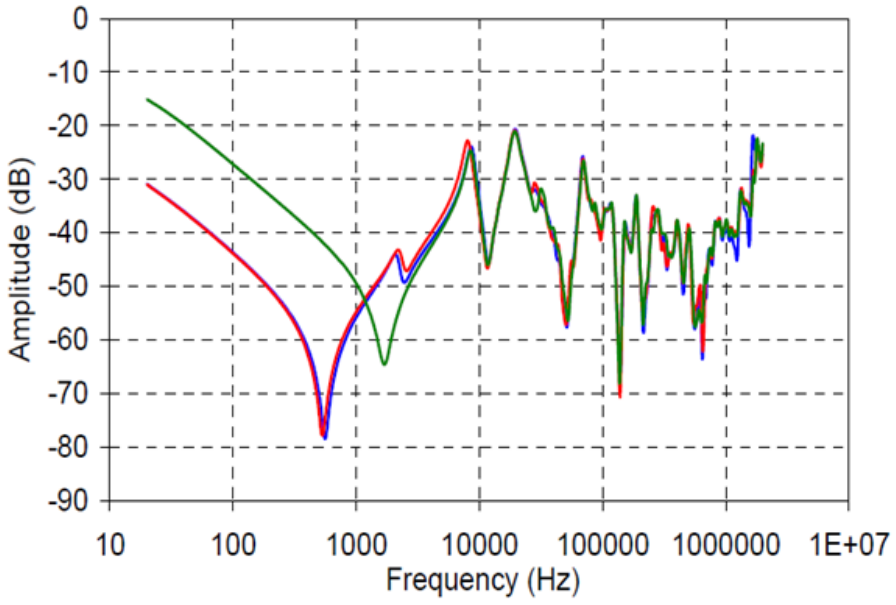

Figure 2-2 Typical FRA signature with shorted turns on phase C [6]

- The low frequency range (<20 kHz), within which inductive components dominate the transformer winding response;
- the medium frequency range (20–400 kHz), within which the combination of inductive and capacitive components results in multiple resonances;
- the high frequency range (>400 kHz), within which capacitive components dominate the FRA signature [15].

These ranges and the associated fault types are summarized in Table 2.1 [16], [17].

Table 2.1. Frequency Response Analysis Bands and their sensitivity to faults

Frequency band	Fault sensitivity
<20 kHz	Core deformation, open circuits, shorted turns and residual magnetism, bulk winding movement, clamping structure loosening
20-400 kHz	Deformation within the main or tap windings
>400 kHz	Movement of the main and tap windings , ground impedance variations

If the original transformer FRA signature in the healthy condition status is not available, the reference signature can be either from similar transformers (construction-based comparison) or other phases (symmetric comparison) [67]. In order to investigate the FRA technique specifically, it is therefore assumed that a comprehensive internal model is the best way to study the sensitivity and impact of various sorts of faults[68].

The methods of shunt reactors and impulse testing were invented 60 years ago, by examining current measurements for faults. The FRA that was first invented by Dick and Erven [69] in 1978 is actually an improved version of impulse testing technique [70].

2.3.1 Measurement Techniques

Currently there are no consistent, reliable guidelines for FRA signature quantification and classification, and different signature setups are used throughout the world. Different interpretation setups would produce different fault detection results[71]. Standardizing interpretation setups is actually inevitable. A comparison of the two measurement techniques of low voltage impulse (LVI) and sweep frequency analysis (SFRA) is explained in the following section [72]:

2.3.1.1 LVI (Low Voltage Impulse)

The LVI method is adapted from the initial impulse test method. The applied voltage from the impulse generator is measured along with secondary voltages on other terminals and several measurements can be made simultaneously. The time-domain measurements are then transferred into the frequency-domain by the Fast Fourier Transform (FFT), and the transfer function is established from the ratio of the two transformed signals[73].

2.3.1.2 LVI Advantages:

- Several channels/transfer functions can be measured simultaneously, reducing outage time during revision;
- The test is rapid, compared with SFRA; one measurement is usually conducted in one minute (several impulses are applied to establish an average time series)[74, 75].

2.3.1.3 LVI Disadvantages

- It has fixed resolution, resulting in a low resolution at low frequencies; this may be a problem for the detection of electrical faults. In addition, signals are usually high-pass filtered in order to reduce problems with the window-functions of the FFT;
- The power spectrum of the injected signal is frequency-dependent; the resulting precision across the frequency range will then be frequency dependent;
- Slowly decaying signals are not recorded; window-function, zero padding or high-pass filtering is necessary;
- Several pieces of equipment are needed such as broad band noise filters high pass-filterers;
- Noise and errors are related to digitizers;
- Its accuracy is dependent on the mathematical evaluation.
-

2.3.2 SFRA (Sweep Frequency Response Analysis)

This technique is performed by sweeping the desired frequency using a very low

sinusoidal voltage and it is much slower than the LVI technique. The main FRA methods categorized by the CIGRE are as follows [76] :

2.3.2.1 High Voltage winding End-To-End Open Circuit Connection Test

The End-to-end open circuit test is performed by injecting a signal into the end of a winding and measuring the response at the other end of the same winding. It is a very common test, because of its simplicity for examining each winding separately. Satish et al [44] categorized the sensitivity of a broad range of FRA method connections. They quantified the sensitivity by counting the number of natural frequencies obtained in each of FRA test separately. They classified the end- to-end open circuit test in the highest sensitivity category level among other tests. This test can be performed on both high voltage (HV) and low voltage (LV) windings as shown in Figure 2-3[77].

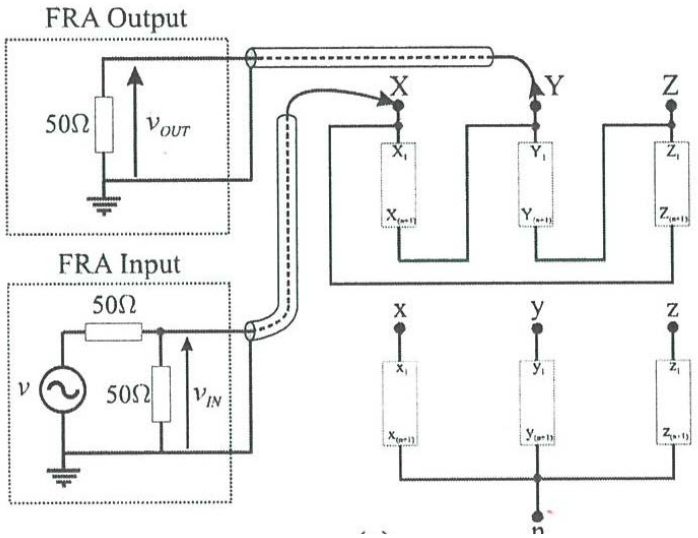

Figure 2-3. HV winding End to End open circuit test [1]

2.3.2.2 Low Voltage Winding End-To-End Open Circuit Connection Test

This test is very similar to the end-to-end open circuit test, but the other winding of the same phase must be short-circuited. Therefore, the influence of magnetizing and leakage inductances which dominate the lower frequency ranges at low frequency is removed. At higher frequency ranges, the result is similar to the end- to-end open circuit test. Figure 2-4 shows the setup of this connection[77]

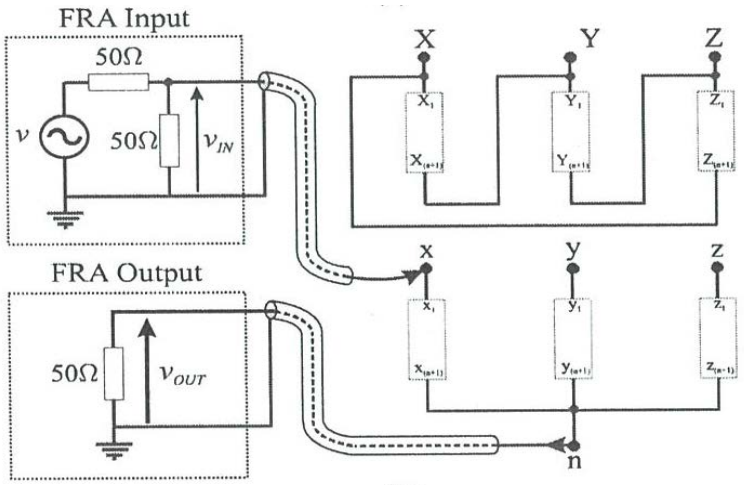

Figure 2-4. LV winding End to End open circuit

2.3.2.3 Capacitive Inter-Winding Connection Test

This test is conducted by injecting a signal into one end of a winding and measuring the response at the other winding of the same phase as shown in Figure.2-5[78]. This test is very sensitive to the inter-winding capacitance existing between windings of the same phase [78, 79]. In research conducted by Jayasinhe [5] in 2006 on the sensitivity of different FRA connections and their capabilities for diagnosing various types of faults, it was revealed that the capacitive inter-winding test is more sensitive to the faults of radial deformation and axial displacement than other tests. In addition, Ryder [80] proposed the capacitive inter-winding test for its sensitivity to axial displacement on 300 MVA transformers in his article in 2003.

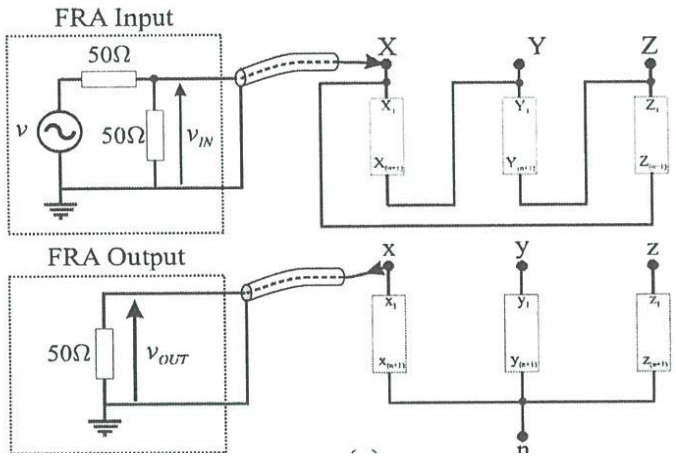

Figure.2-5. Capacitive inter-winding test

2.3.2.4 Inductive Inter-Winding Connection Test

This test is conducted in the same way as the capacitive inter-winding test but the opposite ends of both windings are connected to the ground.

2.3.3 SFRA Advantages [75]

- It gives the ability to sweep an extensive frequency range, from 10Hz -5 MHz;
- By controlling the number of frequency points, the resolution of the signature can be improved;
- With higher resolution, the range of frequency can be divided into different frequency bands in a range from low to high.

The FRA signature can be logarithmic or linear.

2.3.4 SFRA Disadvantages [58]

- Using a standard network analyser, simultaneous determination of several transfer functions is not possible.
- SFRA is an offline test and to conduct this test, the transformer must be shut down and disconnected from the network.
- Each measurement takes time to perform and averaging techniques are very time-consuming.
- Low signal amplitude.

2.5 COMPARISON METHODS

A measurement is compared to a number of different references:

2.4.1 Time-Based Comparison

A signature is obtained during the factory acceptance test. This provides the best sensitivity, because it excludes almost all natural changes. Possible aging and temperature impacts might be observed with this technique[81].

2.4.2 Construction-Based Comparison

In this method the signature obtained is compared to the signature obtained from identical transformers with the same construction. This comparison has a lower

sensitivity, because any small changes to the design and differences in lead layout will influence the measurements [6].

2.4.3 Comparison Based On Symmetry

This is the general method for comparison, because baseline measurements are normally unavailable. On line tap changer (OLTC) is the usual source of inconsistency, together with differences between center and outer phase [82, 83].

2.4.4 Model-Based Comparison

Baseline measurement must be compared with the transformer computer model to ensure accuracy of the latter. This method is adopted in this work for interpreting FRA signatures.

2.6 INTERNATIONAL EXPERIENCE

Numerous FRA projects were carried out at the University of Stuttgart in Germany. They have used the LVI method exclusively:

- Leibfried [82, 83] studied the possibilities of measuring impulse excitation using switching operations. This led to an on-line monitoring system. The frequency spectra of such switching operations are highly variable. The wide tolerance bands established by Leibfried mask the possibility of detecting minor deformations, which favours the use of an off-line measurement technique (Minor deformations are believed to affect the upper part of the frequency range (several MHz)). These large tolerance-bands are mainly a function of the variation in the frequency-content of the excitation signal and the signal to noise level of the measurement system.
- Christian [84] [85]reported time-based, construction-based and type-based comparisons among many transformers, establishing a good statistical foundation. He also presented an experimental setup used at the University of Stuttgart, where sensitivity to radial deformations and axial displacements were investigated. The overall sensitivity to axial displacement is 1%-2% of the total axial height of the winding. Radial deformations have a limit of sensitivity at a buckling-depth of 3% of winding diameter along 10% of its height. These are the only quantified sensitivities found in literature.

Admittance measurements were found to be less sensitive than voltage ratio measurements.

- The sensitivities found by Christian were verified in high-frequency models developed by Rahimpour [86]-[2, 10, 87], using the same constructional details as Christian. These laboratory models were reduced scale models, built to ease the application of radial deformations and axial displacements. The core was replaced by a slit cylinder by assuming the core-flux can be neglected.
- The University of Helsinki in Finland has conducted many tests on different types of transformers utilizing measurements from factory measurements (standard lightning impulse) at full and decreased voltage levels[88]. Testing at full voltage includes the use of dividers and this limits the applicable frequency range rigorously. Additionally, they applied different grounding typologies such as establishing one point of grounding or grounding each terminal at the flange.
- Many experiments were performed by the University of Stuttgart (as described above) on similar transformers with different tapping positions and phases. In addition, the impact of various types of windings was investigated. Capacitances with different values were added to the windings to artificially simulate damage such as deformations. In these experiments, the tank and core were replaced by two metallic cylinders. However, the artificial damage could not show the different degrees of deformations directly. Therefore, the application of these results is limited.
- Wang and Vandermaar[89], [90] reported that large variations in measured admittance over 1 MHz before and after reclamping of various transformers specifically on a 140 MVA and a 630 MVA unit. Another investigation was carried out by Wang et al. [91] identifying significant features of FRA during field measurements. When the admittance is being measured, the shunt impedance applied for current measurements is essential. Different values between 1 and 50 Ω were tested; the result showed that sensitivity increases with decreasing shunt impedance. This result shows that 50 Ω shunt affects the measured response over 500 kHz, while a 10 Ω shunt affects the

measured response above 3 MHz and hence, based on these results, the use of a current transformer instead of a measuring shunt is encouraged.

- Studies by Wang [91] on the influence of connecting cables at the top or bottom of the bushing indicated that some changes below 1 MHz, which becomes more noticeable over 3 MHz. The effect with/without neutral grounding indicates only minor differences over 2 MHz and major difference at lower frequencies. Minor local axial displacements are obviously identified above 4 MHz, while small buckling deformations show only minor changes over 7 MHz. The biggest variation is detected above 1 MHz for connecting different lengths of the measurement leads. They concluded that the lengths of the measurement leads affect the FRA response and should be as short as possible. In addition, their conclusion shows that the size of the transformer is critical, because the size of the bushings restricts the upper usable frequency owing to the increasing length of the leads.
- ERA [92] reported the successful application of FRA by using the LVI technique on winding deformation and distortion as well as axial displacement. Their experience underlines that severe winding damage does not always cause secondary effects such as ruined conductors or low insulation resistance and that substantial distortions can occur without detracting from the normal performance at power frequency. They emphasized the need for FRA.
- Dobble and Omicron are the well-known providers of FRA tools for diagnostic purposes throughout the world. In their user guide for one of the instruments [93] applicable to FRA measurements, they draw on wide-ranging experience. The application examples indicate transformers in both healthy and faulty condition, which connections should be applied and how to distinguish normal variations from faulty deviations due to mechanical or electrical failures.
- Høidalen [94] conducted experiments on radial and axial faults on a 35 MVA single-phase transformer. He recorded low sensitivity to both axial and radial faults during the experiments. The buckling deformation occurred locally within 1%-3% of the winding height, whereas the outer winding was displaced axially at 5% of the total winding height. One of the expectations

for the low sensitivity in this testing is the complexity of the winding; two identical sets of windings were placed on each core leg and cross-connected in a certain order. The authors also studied the influence of the oil, the bushings and the tank.

2.7 ALTERNATIVE TECHNIQUES

As stated earlier, currently there are no methods that can detect mechanical deformations in transformers with adequate sensitivity. Techniques such as stray inductance, turns ratio and impedance measurements have a rate of inaccuracy of 2% or more [95].During the last decade, the Frequency Response Stray Losses (FRSL) [95] technique, which is a newer and simpler technique than FRA, was developed. In this technique, the stray losses in the frequency range of 10 Hz to 1 kHz are measured. It is reported that the FRSL method can readily diagnose and interpret deformations with less dependency on the measurement-setup than FRA, because the method operates within a low frequency range. Other methods such as vibro-acoustic techniques for detecting winding slackness and other clamping defects related to the windings and core are casually used [96], [97]-[96].Finally, there is a special application for detecting buckling deformations of the winding called “ultrasonic measurements” for in-service assessments [96].

2.8 FRA SUMMARY

As revealed from scrutinizing the literature, it is essential to have interpretational guidelines and criteria to interpret FRA results. In order to establish a comprehensive guideline for FRA, a detailed study considering actual transformer geometries is urgently needed through a computer model.

In addition, and as iterated above, standardizing the equipment and methods for FRA testing is recommended.

Fortunately, the literature indicates that most the mechanical failures are diagnosable with the limitation that minor damage is diagnosed at frequencies where the inherent limitation of the measuring devices can affect the results. This is obviously a restriction, reflecting the need to perform more comprehensive investigations into this area. Apparently, small deformations can be detected at frequencies above 1 MHz, which promotes the SFRA method, since the LVI method is limited (both in

frequency and dynamic performance) in terms of noise and digitizing problems. Minimizing the loops of the measurement-leads connected to the bushings is important. It should be noted, that FRA is not yet totally accepted by the industry as a diagnostic method.

2.9 TRANSFORMER MODELLING

For decades, simple analytical methods have been utilized widely in transformer modelling. Such approaches are assumed to have some limitations related to details of transformer geometry. However, these methods are investigated due to their convenience for studying of winding deformation.

Due to the absence of a reliable and reproducible technique, existing methods are used despite of their limitations and disadvantages. However, these methods can be used as a basis for developing a new, reliable fault detecting technique.

2.8.1 Inductance Calculation

The main streams of inductance calculation for the analysis and design of transformers in general, has traditionally been classified [1], [39] into the following categories:

2.8.1.1 Modelling Based On Self and Mutual Inductances

This model is based on a lather network. It was first proposed by Weed [86], neglecting mutual inductances. The method was supported experimentally where empirical data was used to include losses and to modify inductances. Wilcox has recently improved the model by including the core and winding losses [98], [99].This model seems to be accurate for the calculation of self and mutual inductances of the windings, sections, or turns of transformers. This is the model usually used in high-frequency models and was used in earlier sensitivity-analysis of FRA.

2.8.1.2 Modelling Based On Leakage Inductance

This approach was proposed by Blume[100] following which the method was improved by McWirther [101] and Shipley [102]. The method is used to represent the leakage inductance of the transformer at low frequencies; however the low frequency core- properties are not considered properly. This method is usually applied at low frequencies to represent short-circuit data for a transformer, and it can be extended to higher frequencies [103].

2.8.1.3 Transmission Line Modelling

The method was initiated by Wagner [104]. The transformer winding is modelled as a multi-conductor transmission-line.

2.8.1.4 Modelling Based On Terminal Measurements (Black-Box Modelling)

This is not an appropriate method for the investigation of geometrical influences such as mechanical failures in windings, because of its nonphysical nature. This method is still applied for domain models into time domain[105].

2.8.1.5 Analysis Based On Electromagnetic Fields

This is not a separate method but a tool for establishing the parameters of the above methods. This approach is used by designers of large transformers using electromagnetic field methods for calculating the design parameters. Finite element method (FEM) is the most accepted numerical solution for field problems [106]. There is general agreement that three-dimensional (3D) field analyses are essential in the design process (e.g. such as the evaluation of eddy-current stray losses) [107].

The methods listed above concern mainly the inductances in the transformer model, since this has traditionally been the biggest challenge in transformer modelling. Other important elements in a high-frequency transformer model are briefly reviewed below.

2.8.2 Capacitance Calculation

Capacitances can be calculated either by using conventional analytical methods or computer approaches such as the Finite Element Method, where the geometry and material parameters are important and can be included [108]. Shunt capacitances (capacitance between windings and from winding to ground) can be calculated by simplifying the transformer geometry and analytical formulas. The series capacitance is the capacitance between disks of windings and is a determinant for the electrostatic voltage distribution. More details for the calculation of this parameter can be found in [60].

2.8.3 Losses

Accounting for losses in a fault detecting model is crucial, particularly when internal stresses are assessed in the design of a transformer. Without the consideration of the losses, the stresses predicted by the simulation will be higher than in reality, leading

to a design that is both costly and less competitive [60].

There are various loss-mechanisms in a transformer, as follows:

- Series resistance in windings (DC-resistance);
- Frequency dependent losses in the conductors due to eddy currents; eddy currents cause skin effect and Proximity effect ;
- Eddy currents in core laminations (core reaction) due to magnetic field in the core ;
- Insulation dielectric losses for series- and shunt conductance .

2.8.4 Iron Core

Depending on the application, transformer modeling is divided into two different paths. In order to handle the nonlinear influences such as saturation and hysteresis effects of core, the time-domain models have been developed for the frequency range of slow transient from 50Hz to 10 kHz. Since it is assumed that the behavior of transformers in the high-frequency range is linear, high-frequency models are typically applied in the frequency domain .Many studies have shown [109] that although the iron core was neglected in high-frequency transformer models, reasonable results of fault detection were obtained.

2.10 MODELLING ACCURACY

High-frequency transformer models can be developed with a high degree of conformity to terminal measurements, provided that construction information is available. Detailed internal transformer models are always developed on the basis of construction details. If an internal model is properly defined, including all relevant phenomena, it should also comply with expected behaviour, reflected to the terminals of the transformer. If not, there must be other elements of influence than the construction of the winding. This may be investigated by comparing terminal measurements with the terminal model. Some influences from leads, connections, tap changers, etc. are to be expected, at least in the upper frequency range. These effects may be difficult to account for.

The approach of Rahimpour [10] is based on analytical air-core theory, since it is assumed that all flux is displaced from the core above 10 kHz. His approach seems to obtain a high degree of accuracy for his models compared with terminal

measurements. This approach was tried on three different windings which were manufactured for investigating axial deformation, radial deformation and disk-to-disk short-circuits (one for each application, in experimental work carried out by Christian[85]).

Rahimpour employed the models developed for FRA sensitivity analysis, using an analytical approach. The results of Rahimpour's work showed the highest level of agreement between models and measurements seen so far, and thus constitutes the starting-point for this work.

De Leon's approach [110]focuses on a simple implementation based on analytical equations for the magnetic field. The leakage field is adjusted using mirror currents inside the core, but this requires calibration. His method established turn-to-turn parameters, which are reduced to a terminal equivalent. Losses are also calculated on a turn-to-turn basis, but represented by a Foster-equivalent at the terminals. The accuracy of this approach is questioned, since all terminal behaviour is dependent on the internal representation. De Leon's work is concluded by a comparison to measurements on a small, simplified transformer with layer windings. The transfer function incorporates one resonance frequency; unfortunately, the agreement between measurement and model was not satisfactory. This approach seems to be suitable for simplified geometries but will probably fail in a real and complex transformer's geometry.

Other methods are claimed to have good agreement with measurements. Most of these method are time-domain based models [111], [112], where simulated and measured time-domain responses are compared. This provides incomplete overview of the model's ability to reproduce a broad frequency-spectrum of the transformer represented.

Fergestad [113] obtained close agreements when comparing time-domain responses, but empirical corrections are needed for the inductance calculation. In addition, all losses are added on an empirical basis.

Wilcox et al. [114], [99]obtained a high degree of resemblance to measurements of inductances on iron cores, but their method needs measurements on each specific core in order to establish the different parameters needed for the calculation. In addition, the formulas seem to be difficult to implement numerically. Accurate formulas for inductance-calculation are also reported by Mombello [115].

2.11 CONCLUSIONS

The increased focus on condition monitoring has led to novel techniques for detecting very incipient failures such as mechanical faults. Normal operation of power transformers may not be degraded by such failures, but their presence over a long period of time might lead to short circuits and over voltages, which damage the windings severely. A few studies were undertaken to investigate the sensitivities and drawbacks of this technique. To this end, high-frequency transformer modelling based on construction information seems to be an appropriate approach to examine the sensitivities and drawbacks of the FRA method. In addition, this approach can show the effect of the different mechanical failures on the FRA signature[116].

3. FINITE ELEMENT ANALYSIS

Finite element analysis (FEA) is a sophisticated tool widely used by engineers, scientists, and researchers to solve engineering problems arising from various physical fields such as electromagnetics, thermal, structural, fluid flow, acoustic, and others. Currently the finite element method is clearly the dominant numerical analysis method for the simulation of physical field distributions, with success not paralleled by any other numerical technique. In essence, the finite element method finds the solution to any engineering problem that can be described by a finite set of spatial partial derivative equations with appropriate boundary and initial conditions. It is used to solve problems for an extremely wide variety of static, steady state, and transient engineering applications from diverse sectors such as automotive, aerospace, nuclear, biomedical, etc.

The finite element method has a solid theoretical foundation. It is based on mathematical theorems that guarantee an asymptotic increase in the accuracy of the field calculation towards the exact solution as the size of the finite elements used in the solution process decreases. For time-domain solutions, the spatial discretization of the problem must be refined in a manner coordinated with the time steps of the calculation according to estimated time constants of the solution (such as magnetic diffusion time constant).

Maxwell solves the electromagnetic field problems by solving Maxwell's equations in a finite region of space with appropriate boundary conditions and, when necessary, with user-specified initial conditions, in order to obtain a solution with guaranteed uniqueness. In order to obtain the set of algebraic equations to be solved, the geometry of the problem is discretised automatically into tetrahedral elements (for 3D problems)[78]. The model domain (solids) is meshed automatically by a mesher code. Assembly of all tetrahedral is referred to as the finite element mesh of the model or simply, the mesh. Inside each tetrahedron, the unknown characteristics for the field being calculated are represented as polynomials of a second order degree. Thus, in regions with rapid spatial field variations, the mesh density needs to be increased for good solution accuracy (see Figure 3-1 for an example of adaptive mesh refinement).

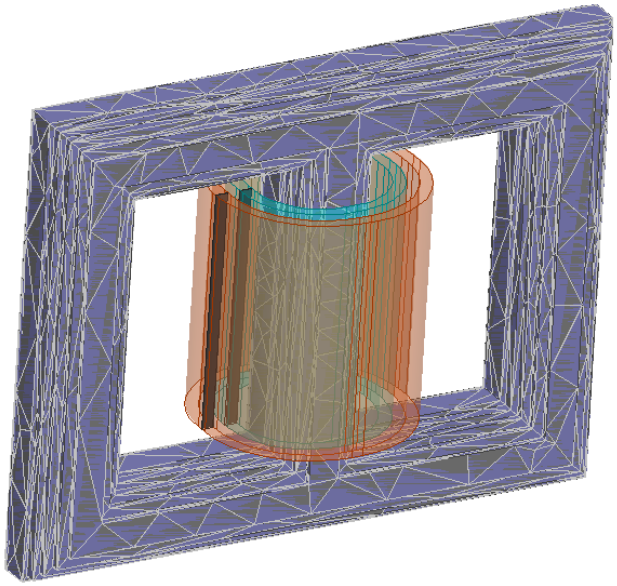

Figure 3-1. Mesh shown on the Transformer core

In the 3D Model, the solver uses the Maxwell formulation. Motion (translational or cylindrical/non-cylindrical rotation) is allowed, excitations, currents and/or voltages-can assume arbitrary shapes as functions of time, and nonlinear BH material dependencies can also be modelled. The support of voltage excitations for the windings means that the winding currents are unknown and thus the formulation has to be modified slightly to allow Maxwell to account for source fields resulting from unknown currents in voltage - driven solid conductors (where eddy effects are evaluated) and in voltage-driven stranded conductors - where the eddy effects (such as skin and proximity effects) are ignored. Also for a simpler formulation of problems where motion is involved, Maxwell adopts a particular convention using the fixed coordinate system for Maxwell's equations in the moving and the stationary part of the model. Thus, the motion term is completely eliminated for the translational type of motion while for the rotational type of motion a simpler formulation is obtained by using a cylindrical coordinate system with the z axis aligned with the actual rotation axis[79] .

The formulation used by Maxwell transient module supports Master-Slave boundary conditions and motion-induced eddy currents throughout the model, for both stationary and moving parts. Mechanical equations associated with the rigid-body moving parts allow complex formulation with the electric circuits being strongly

coupled with the finite element part and also coupled with the mechanical elements whenever transient mechanical effects are included by users in the solution. In this case the electromagnetic force/torque is calculated using the virtual work approach. For problems involving rotational types of motion, a "sliding band" type of approach is followed and thus no re-meshing is performed during the simulation. For translational types of motion, the mesh in the band object (surrounding the part in motion) needs to be re-created at each time step with a degree of refinement that is dependent upon the mesh size in the moving object. In this latter case, the mesh in both stationary and moving objects remains unchanged as initially created by the user. For transient types of electromagnetic field analysis (with or without motion), the user is responsible for creating the mesh that is capable of "catching" the respective physics such as skin and proximity effects (if any) -when they are present in the resulting fields.

The following three Maxwell's equations are being used in the programmer[121] :

$$\nabla \times H = \sigma(E) \tag{1}$$

$$\nabla \times E = -\frac{\partial B}{\partial t} \tag{2}$$

$$\nabla \times D = \rho \tag{3}$$

Where the following two equations directly result from the above equations:

$$\nabla \times \frac{1}{\sigma} \nabla \times H + \frac{\partial B}{\partial t} = 0$$

(4)

$$\nabla \times B = 0 \tag{5}$$

where σ is the electric conductivity, ε the dielectric permittivity, μ the magnetic permeability, B is the magnetic flux density and H is the magnetic flux intensity.

The final result is a formulation where vector fields are represented by first order edge elements and scalar fields are represented by second order nodal unknowns. Field equations are coupled with circuit equations for both solid and stranded conductors, because, in the case of applied voltage supplies, the currents are unknown [117, 118]. For the case of voltage-driven solid conductors, the following equation is used to account for the Ohmic drop across the i-th conductor loop:

$$V_{Ri} = \int_{RC(i)} \iint J_{0I} (E + V \times B) dR \tag{6}$$

where J_{0i} represents the current density.

The induced voltage can be derived from the following equation:

$$e_i = -\iiint H_i * BdR \tag{7}$$

where the integration is performed over the whole conductor region.

Stranded conductors are assumed to be free from induced eddy currents, and, thus, are placed in the non-conducting region. This means that, for the purpose of calculating the Ohmic voltage drop, the same procedure cannot be used as for solid conductors. Instead, a lumped parameter is used to represent the DC resistance of the winding. Induced voltage is obtained as a result of the total flux linkage in way that is similar to solid conductors. In both cases, it is also possible to add an external inductance and capacitance.

For the nonlinearities allowed in 3D transient applications, the classical Newton-Raphson algorithm is used to solve the equilibrium equations.

The transient solver in Maxwell supports the coil terminals and winding definitions. Thus it is possible in the model to specify the number of turns of coils that is necessary for the calculation of critical engineering parameters such as flux linkage and back EMF of coils. After calculation, the 3D transient solver produces a number of quantities automatically and displays them as 2D plots (functions of time; these plots are voltage (current), flux linkage and back emf. Other global quantities can also be calculated by the 3D transient solver and displayed as 2D plots; examples are power loss, core loss, stranded loss, and electromechanical quantities such as force/torque, speed and displacement.

The 3D (frequency domain or harmonic solver) uses Maxwell formulation for analysis. It is based on the assumption that all electromagnetic fields pulsate at the same frequency (specified by the user) and have magnitudes and initial phase angles calculated by Maxwell. There are no moving objects (velocity is zero everywhere). Permanent magnets cannot be part of the model, and all materials are assumed to be linear. Electromagnetic radiation can also be simulated.

In the non-conducting regions, the magnetic field strength is given by the following equation:

$$\vec{H} = \vec{H}_P + \nabla_\varphi \tag{8}$$

In regions with non-zero conductivity where eddy current calculation has been set up, the following equation where the electric vector potential is calculated using edge elements is true:

$$\vec{H} = \vec{H}_P + \nabla_\varphi + \vec{T} \tag{9}$$

At the interface between conductors and non-conductors, the tangential component of the electric vector potential is constrained to zero. The quantity calculated by Maxwell in this case is the magnetic field H(x,y,z,t). Typical sources for eddy current problems include current and current density. In applying the sources for the magnetic field problems, the applied current distribution must be divergence free in the entire space of the solution as it is physical for (quasi) stationary conduction current density distributions. Thus, the conduction path (s) for the applied current distributions must be closed when totally contained within the solution space for the problem or must begin and end at the boundaries. The total current applied to conductors that touch the boundaries does not require existence of the terminals at the ends where the current is applied; in this case, the respective planar surfaces of the conductors in the plane of the region (background) can be used to apply the excitations.

The insulating boundary condition is of particular use for applications where very thin insulating layers are impractical to model due, for example, to high aspect ratio geometries that would be generated in association with meshing difficulties. Thus insulating boundary conditions can be assigned to surfaces of separation between conductors. Another remarkable situation where such a boundary condition proves to be extremely useful is in modelling faults in conductors (cracks for example). Thus, modelling 2D (sheet) objects at the location of the respective cracks and applying the insulation boundary condition proves to be a very effective way of modelling the flaws without having to generate 3D cracks that would be difficult and impractical to mesh.

3.1 PARAMETER CALCULATION

3.1.1 Inductance and Resistance Matrices Calculation

To compute an inductance matrix, the software performs a sequence of magnetostatic field simulations. In each field simulation, one ampere is allowed to flow in a single conductor[60, 81]. For an n-conductor system, *n* field simulations are automatically performed. The energy stored in the magnetic field that couples two conductors is:

$$W_{ij} = \frac{1}{2}\int_{\Omega} B_i \times H_j \, d\Omega \tag{10}$$

where W_{ij} is the energy stored in the magnetic field linking conductor *i* with conductor *j*., I_i is the current in conductor *I,* B_i is the magnetic flux density where one ampere is

allowed to flow through conductor i andH_j is the magnetic field where one ampere is allowed to flow through conductor j.

The inductance coupling conductors i and j is therefore:

$$L_{ij} = \frac{2W_{ij}}{I^2} = \int B_i \times H_j d\Omega \tag{11}$$

For multi-turn conductors, the net value of inductance is the value given by:

$$L_{net} = N^2 L_{matrix} \tag{12}$$

where N is the number of turns in the coil.

By solving the 3D model, winding resistance and inductance can be estimated using the energy balance method as shown below:

$$L_{ii} = 2lm(jW_{ii})/I_i^2 \tag{13}$$

$$R_{ii} = 2w\,\mathrm{Re}(jW_{ii})/I_i^2 \tag{14}$$

where L_{ii} and R_{ii} are the self-inductance and resistance of the i^{th} section, respectively, and $W_{ii}$is the magnetic energy when current I is applied to the i^{th} section of the winding.

Mutual inductance and resistance between i^{th} and j^{th} winding sections can be calculated using the parameters obtained in equations (15) and (16) along with additional solution for energy stored when current is applied to both winding sections [60, 119].

$$M_{ij} = \frac{n_i.n_j.\mathrm{Re}\{W_{mag,ij}\} - \frac{1}{2}L_{ii}.I_i^2 - \frac{1}{2}L_{jj}.I_j^2}{I_j.I_i} \tag{15}$$

$$R_{ij} = \frac{n_i.n_j.\omega.\mathrm{Im}\{W_{mag,ij}\} - \frac{1}{2}R_{ii}.I_i^2 - \frac{1}{2}R_{jj}.I_j^2}{I_j.I_i} \tag{16}$$

where W_{ij} is the entire magnetic energy when currents I_i and I_j are applied to winding sections i and j, respectively.

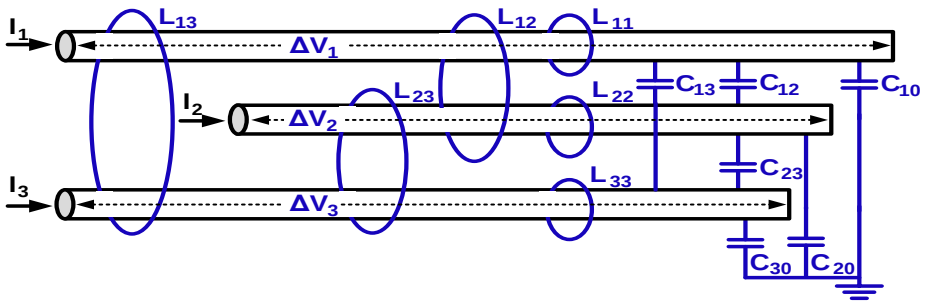

Figure 3-2. Inductance/capacitance matrix configurations for a three disks winding

Given the three current loops shown in Figure 3-2, the relationship between induced flux and currents can be expressed in the following matrix form:

$$\begin{bmatrix}\lambda_1\\ \lambda_2\\ \lambda_3\end{bmatrix}=\begin{bmatrix}L_{11} & L_{12} & L_{13}\\ L_{21} & L_{22} & L_{23}\\ L_{31} & L_{32} & L_{33}\end{bmatrix}\begin{bmatrix}i_1\\ i_2\\ i_3\end{bmatrix} \tag{17}$$

3.1.2. Capacitance Matrix Calculation

Similar to inductance-calculation, capacitance can be calculated using the electrostatic energy W_{el}.

$$W_{el}=\frac{1}{2}CV^2 \tag{18}$$

The capacitances between disks/windings are calculated as below:

$$C_{ij}=\frac{\mathrm{Re}\{W_{el,ij}\}-\frac{1}{2}V_i^2.C_{ii}-\frac{1}{2}V_j^2C_{jj}}{V_j.V_i} \tag{19}$$

$$C_{ii}=2\frac{\mathrm{Re}\{W_{el,ii}\}}{V_i^2} \tag{20}$$

A capacitance matrix represents the charge coupling within a group of conductors. Given a ground reference for the three conductors shown Figure 3-2, the net charge on each object is [120]:

$$\begin{bmatrix}\mathrm{Q}_1\\ \mathrm{Q}_2\\ \mathrm{Q}_3\end{bmatrix}=$$

$$\begin{bmatrix}\mathrm{C}_{10}+\mathrm{C}_{12}+\mathrm{C}_{13} & -\mathrm{C}_{12} & -\mathrm{C}_{13}\\ -\mathrm{C}_{21} & \mathrm{C}_{20}+\mathrm{C}_{21}+\mathrm{C}_{23} & -\mathrm{C}_{23}\\ -\mathrm{C}_{31} & -\mathrm{C}_{32} & \mathrm{C}_{30}+\mathrm{C}_{31}+\mathrm{C}_{32}\end{bmatrix}\begin{bmatrix}\mathrm{V}_1\\ \mathrm{V}_2\\ \mathrm{V}_3\end{bmatrix} \tag{21}$$

Any change in the winding geometry due to faults will lead to alteration of the capacitive and inductive elements of the transformer's equivalent.

3.2 COUPLING MAXWELL DESIGNS WITH ANSYS STRUCTURAL

Stress feedback coupling between Maxwell and ANSYS Structural is supported via the Workbench [120]. Stress feedback is supported for Maxwell magnetostatic, eddy current and transient types. The design and geometry must be set up appropriately. The process for stress feedback coupling between Maxwell and ANSYS Structural

helps to accurately estimate the resultant mechanical forces considering structural characteristics of the system in the form of stress distribution and displacement of the windings as well as heat losses.

3.3 TRANSFORMER CONSTRUCTION USED IN FEA

3.3.1 Core Characteristics

The configuration of a transformer's core depends on many factors, such as voltage, current, and frequency. In addition, the size of lamination and the construction costs are also factors that should be taken into account. Some materials are commonly used in fabrication of cores, such as soft iron and steel. Each of these materials is appropriate for specific applications and inappropriate for others. Usually, air-core transformers are used when the voltage source has a high frequency (above 20 kHz). On the other hand, iron-core transformers are usually used when the source frequency is low (below 20 kHz)[121]. A soft iron-core transformer is very beneficial where the transformer must be physically small. The iron-core transformer can transfer power more efficiently than the air-core transformer. A transformer core with laminated sheets of steel dissipates heat easily[122].

These steel laminations (see Figure 3-3) are insulated with a non-conducting material, such as varnish, and then formed into a core. The laminations help to decrease eddy current losses. It should be noted that the most efficient transformer core is one that creates a better path for most lines of magnetic flux with the least loss in electrical and magnetic energy.

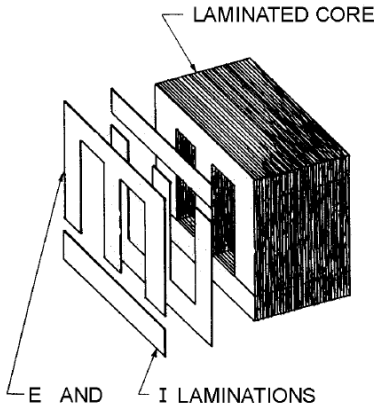

Figure 3-3. Transformer core with laminated sheet[54]

3.3.2 Shell and Core Type Transformer

Shell type transformers are the most popular and efficient transformer core as shown in Figure 3-4. The core consists of layers with E- and I- shaped sections of metal. These sections are stuck together to form the laminations. To form the core these laminations are insulated from each other and then pressed together. In core type each phase is provided with a core of single magnetic circuit together with winding applied around it. On the other hand, more than two shells of magnetic circuit surround the windings in shell type[123].

Figure 3-4. Shell type transformers[54]

3.3.3 Windings Conductor

The windings of power transformers are usually wound in rectangular-shaped conductors for efficient use of the available space as shown in 3-5. Even in small distribution transformers, rectangular-shaped conductors are used to increase the space factor in the core window[124]. To reduce eddy current losses in the windings, the conductor area should be increased and divided into two or more parallel elements. A rectangular-shaped conductor is called a strand and each conductor is insulated with paper and enamel lacquer.

3-5. Rectangular shape conductor[54]

3.3.4 Winding Types

Windings can be categorized into four groups as follows[78]:

3.3.4.1 Layer Winding

Layer windings are more common with shell-type constructions. They permit easy control over the short circuit impedance of the transformer. By placing HV and LV coils together on the same magnetic axis, the leakage is reduced and the mutual flux is increased. By increasing the number of sandwiched coils, the reactance can be substantially reduced[122]. Circular core and coil winding construction with layer windings can improve winding cooling, but usually do not provide complete circulation of the oil to every conductor and every layer of the windings. Even circular layer windings still have significant quantities of winding insulation and although the space factor in the core and coils are an improvement compared to the rectangular core and solid design, it is not as good as a disk and helical circular core and coil construction. An example of a circular core and coil winding assembly utilizing layer windings is shown in Figure 3-6.

Figure 3-6. Layer winding type[54]

3.3.4.2 Helical Windings

One very common cylindrical coil arrangement is the helical winding (Figure 3-7). This is made of a large cross-section rectangular conductor wound on its side. The coil progresses as a helix that is commonly used for LV windings. The insulation requirement also is not too high. Between layers no insulation (other than conductor insulation) is needed, as the voltage between layers is low. The complexity of this type of winding rapidly increases as the current to be handled increases. The conductor cross-section becomes too large and difficult to handle and the eddy current losses in the conductor rapidly increase[123]. Hence two or more conductors have to be wound and connected in parallel. The parallel circuits introduce problems of current sharing between the circuits. Transpositions of the parallel paths have to be adopted to reduce unequal current distribution. The modern practice is to use continuously transposed and bunched conductors. The helical winding is the preferred concept when the number of turns and the total amount of current permit. The quality of conducting material that can fitted inside a given volume is high compared to other types of winding. It is said that helical windings have a high space factor, which is beneficial for an overall total mass-total loss relation. Moreover, it is

mechanically robust and easy to manufacture, particularly when continuously transposed cable is used[54].

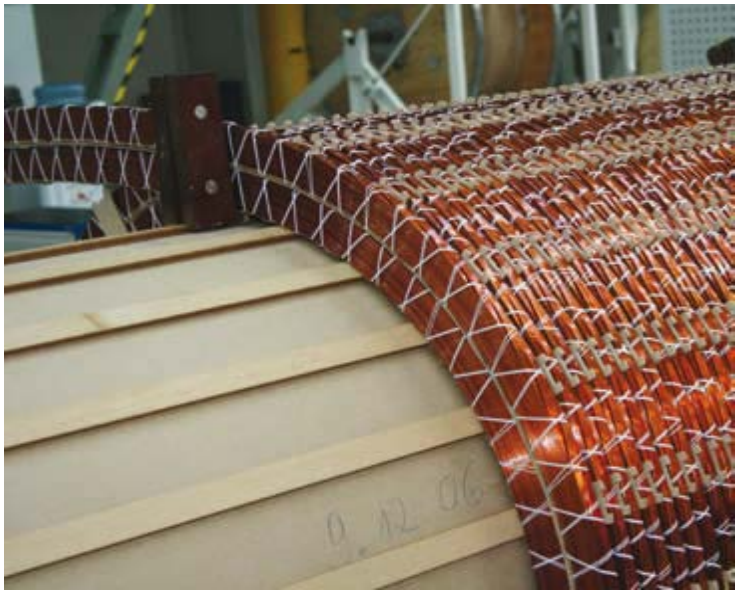

Figure 3-7. Helical winding type[54]

3.3.4.3 Disk Windings

Disk coils consist of conductors wound in a spiral from the centre outwards (Figure 3-8). Alternating disks spiral from the outside towards the centre. Sectional disks or continuous disks may be used. These have excellent thermal properties and the behaviour of the winding is highly predictable. Winding of a continuous disk requires specialized skills.

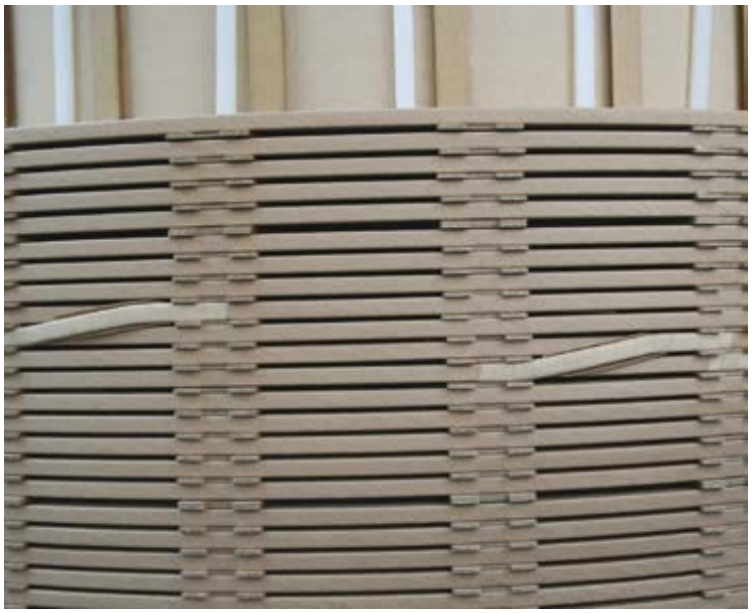

Figure 3-8 Disk winding type[54]

4. INTERPRETATION OF FREQUENCY RESPONSE ANALYSIS (FRA)

In this chapter, the basic features of the FRA concept are investigated. Furthermore, the chapter discusses how different types of winding movement and deformation can be diagnosed by FRA. Also, the chapter discusses the outlook of FRA interpretation and presents some recommendations for further developments.

4.1 BASIC FEATURES OF END-TO-END FRA RESPONSES

The behaviour of a single winding at low frequency is like that of an inductive element, whereby the end-to-end FRA response magnitude tends to fall until the frequency increases with a linear decreasing gradient of about 20dB per decade. The FRA magnitude reduces when the core inductance is larger. The magnetization inductance (Lm) can be calculated as $L_m=N^2/R$, where N is the number of turns of the winding, and R is the reluctance of the magnetic path. Thus, the FRA responses of a transformer with high voltage and large power ratings typically have low magnitude to initiate with at low frequencies, and within the same transformer, and due to the turn ratio, the high-voltage (HV) winding FRA response has a lower magnitude than the low-voltage (LV) winding FRA response. In addition, the FRA response of the middle-phase winding for a three-phase transformer at low frequencies is quite different from the response associated with other phases[125, 126]. This is because of the difference of the magnetic path between the middle phase and other phases. The behaviour of a single winding at high frequency range is similar as a capacitive element. The mutual inductive couplings between windings affect the FRA signature resonances within mid- to high-frequency ranges. The mid-frequency range is affected by the combination of winding leakage inductance and series capacitance (LC paralleled). This combination creates anti-resonances at some certain frequencies on the end-to-end FRA response. These anti-resonances manifest themselves as a local minimum or so-called “valley” with a large negative decibel value. On the other hand, LC in series produces a series resonance that amplify the signal at specific frequencies on the end-to-end FRA signature response of a cascaded LC network.

These resonances manifest themselves as a local maximum or so-called “peak” with a slight negative decibel value[85]. The conductive and dielectric losses affect the FRA response signature by decreasing the sharpness of the resonances and the anti-resonances. Figure 4-1 shows the basic trends and features of FRA signature responses.

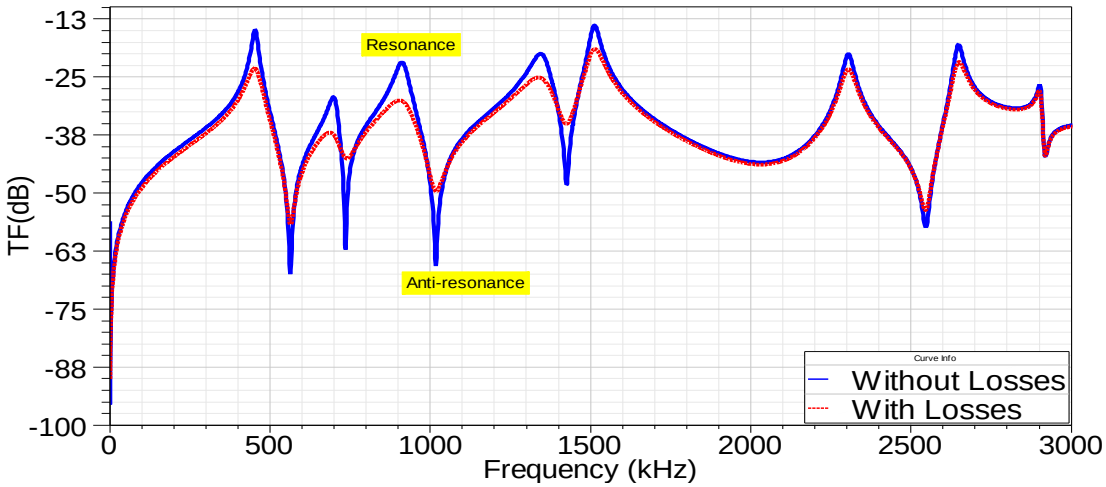

Figure 4-1 Fundamental trends and features of FRA responses.

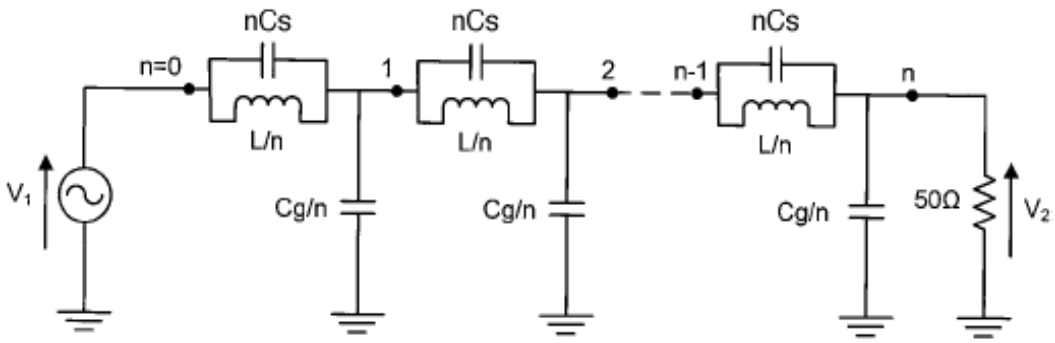

Figure 4-2 N-Stage Transformer Winding Lumped Ladder Network[126]

A regular designed winding can be indicated by a n-stage ladder network as shown in Figure 4-2.The winding consists of leakage inductance, series and shunt capacitances which evenly distributed among the n stages. Equations 21 and 22 calculate the voltage and current at any point on the network [74, 125, 126].

$$u(x, j\omega) = A\cosh(rx) + B\sinh(rx) \tag{21}$$

$$i(x, j\omega) = \frac{1}{Z}[A\sinh(rx) + B\cosh(rx)] \tag{22}$$

Where, $r^2 = \frac{-\frac{LC_g}{n^2}\omega^2}{1-LC_s\omega^2}$ and $Z = \sqrt{\frac{L}{C_g(1-LC_s\omega^2}}$.

, where X is the number of stages along the winding, A and B are constants, Z is the impedance and r is the propagation constant of the winding. At both ends of the winding, the boundary conditions for FRA measurements are:

$$u(0, j\omega) = A, (x = 0) \tag{23}$$

$$u(x, j\omega) = A\cosh(rn) + B\sinh(rn) = 0 \ (x = n) \tag{24}$$

It is assumed that the impedance of 50Ω connected at the end of the winding is much smaller than the total equivalent winding impedance. The end-to-end FRA response can be derived as:

$$\frac{i(n, j\omega)}{u(0, j\omega)} = \frac{1}{Z}\frac{\sinh^2(rn) - \cosh^2(rn)}{\sinh(rn)} = \frac{-1}{Z\sinh(rn)} \tag{25}$$

The end-to-end FRA response is divided into three different frequency regions.

$$\frac{i(n, j\omega)}{u(0, j\omega)} = \left\{ \begin{array}{l} \frac{j}{Z\sin(|r|n)}, \\ \frac{1}{\infty} = 0, \\ \frac{1}{j|Z|\sinh(rn)}, \end{array} \right\} \quad \begin{array}{l} f < \frac{1}{2\pi\sqrt{LC_S}} \\ f = \frac{1}{2\pi\sqrt{LC_s}} \\ f > \frac{1}{2\pi\sqrt{LC_s}} \end{array} \tag{26}$$

In the frequency region where $< 1/2\pi\sqrt{LC_s}$, the FRA response is dominated by inductive components and sin(|r| n)is oscillating between [-1,1]. When sin (|r| n)=0 , some local resonances are created at the frqeuncies as :

$$fk = \frac{k\pi}{2\pi\sqrt{LC_g + (k\pi)^2 LC_2}} \text{ and } rn = k\pi \ k = 1,2,..., n-1 \tag{27}$$

It is seen from (27) that leakage inductances L , series capacitances C_S and shunt capacitances C_g affect the resonances of FRA response of an electric equivalent network made from distributed parameters .In the frequency range where $= 1/2\pi\sqrt{LC_s}$, anti-resonant frequencies are produced and the magnitude drops sharply to the greatest negative decibel value .However, when $f > 1/2\pi\sqrt{LC_s}$, the FRA response behaves capacitively and the magnitude trend increasing.

4.2 TRANSFORMER MODEL (DISTRIBUTED PARAMETER MODEL)

Maxwell software of ANSYS [120]is used to simulate the transformer model geometry shown in Figure 4-3(a) and (b). The model consists of a metal shield core and pressboard spacers between LV and HV windings. In order to maintain the exact position of the low voltage winding, pressboard spacers are placed on core insulation. The 3D transformer model is solved in magnetostatic and electrostatic solvers using Maxwell's equations to extract the inductance and capacitance matrices. Since the vector potential formulation can be easily correlated to both flux and magnetic energy, it is used to solve magnetic problems in FEM and is chosen based on Maxwell's fourth equation [61]. Windings resistance is calculated using eddy current solver because of its dependency on the frequency. The complexity of the model is reduced by lumping several turns into one electrical element. Utilizing a single disk as the smallest discretisation is typically sufficient up to 1MHz or even more, depending on the transformer size. In a real transformer, the parameters are distributed so that each turn has its own electrical and magnetic characteristics, namely losses, capacitance and inductance. When several turns are combined into one electrical lumped element, these parameters are merged. All mutual parameters are considered for the disk as one element. This principle is the same for other winding configurations. The equivalent transformer lumped-parameters electrical model is shown in Figure 4-4. In the model, HV and LV windings are represented by series resistance (R_s) and inductance (L_s) shunted by capacitor (C_s) and conductance (G_s). The capacitance between HV winding and LV winding (C_{HL}) shunted by dielectric conductance (G_{HL}) simulates the insulations between the two windings. Also, the mutual inductances (M) between relevant coils are represented. The dielectric insulation between the LV winding and the earthed core and that is between the HV winding and the earthed tank are simulated by a capacitance (C_g) and dielectric conductance ($G_{\mathbf{g}}$).

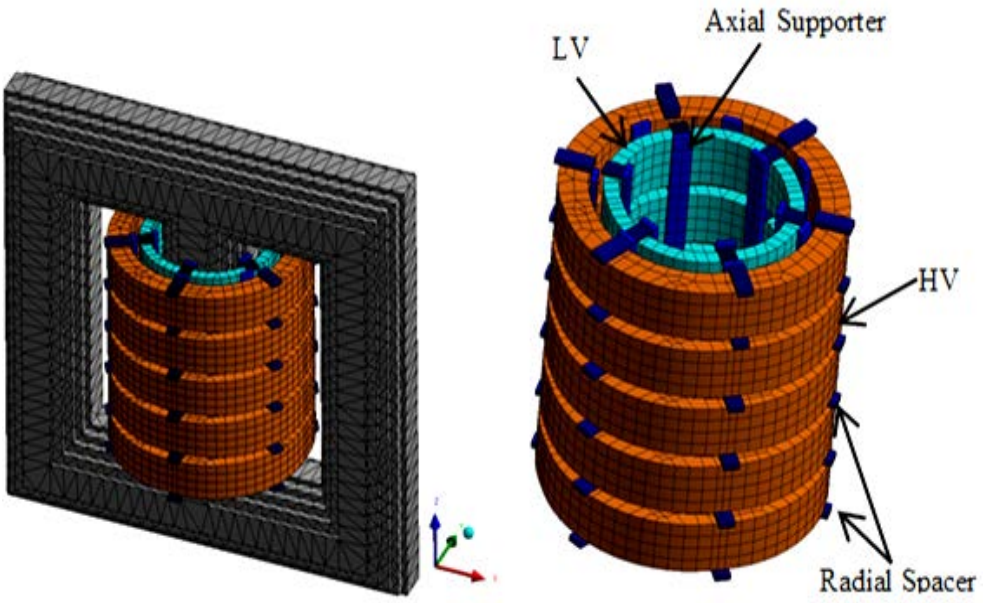

(a)

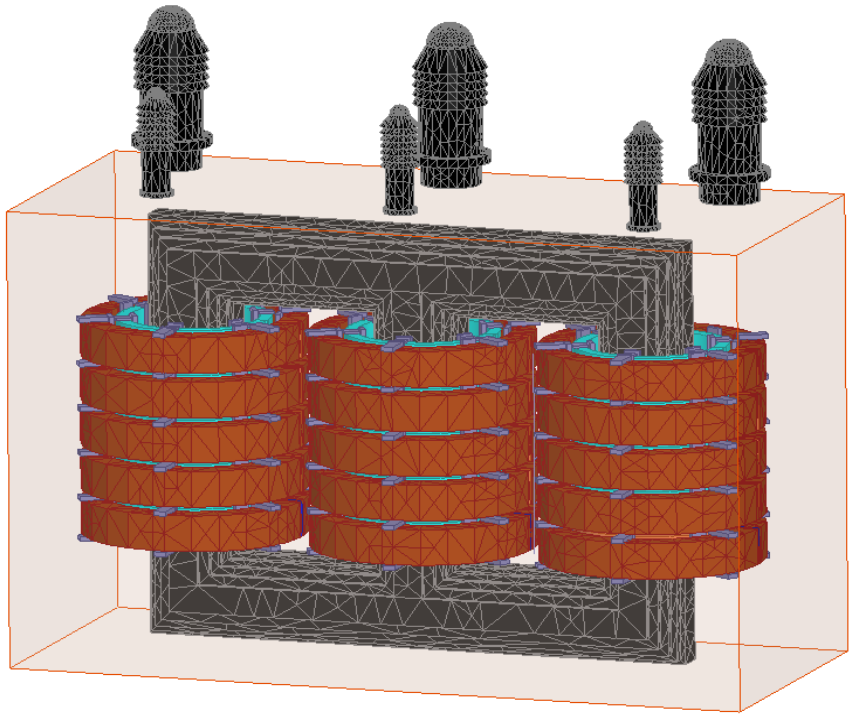

(b)

Figure 4-3 - 3D model of (a) single phase transformer , (b) 3 phase transformer

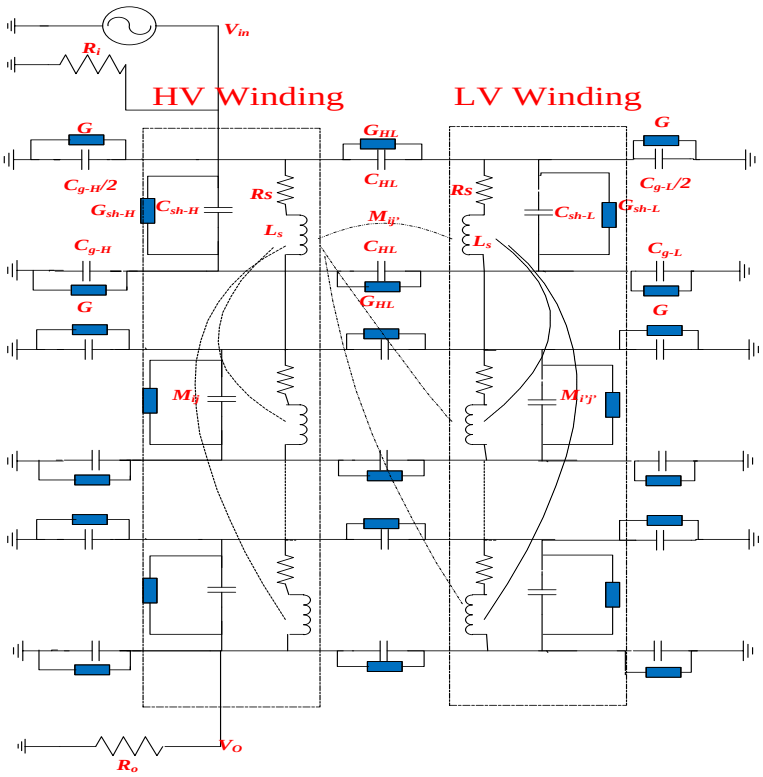

Figure 4-4. Transformer Lumped parameters model

Since mechanical faults cause deformations on the windings and the core of the power transformer, which is simulated as a distributed lumped parameters model, the sensitivity analysis of each parameter on FRA response is very crucial for understanding the variations of FRA response. It is important to understand the effect of each parameter on FRA response. Table 4.1 lists the transformer model parameters, and the mechanical faults that influence them. Various mechanical faults can be simulated by changing the relevant parameters in the transformer model. This can aid in establishing a standard code for FRA signature interpretation.

Table 4.1. Model parameters and the mechanical faults that influence them

Model Parameter	**Type of Fault**
Inductance	Disk deformation, local breakdown and winding short circuits.
Shunt Capacitance	Disk movements, buckling due to large mechanical forces, moisture ingress and loss of clamping pressure.
Series Capacitance	Aging of insulation and disk space variation.
Resistance	Shorted or broken disk and partial discharge.

4.3 AXIAL DISPLACEMENT FAILURE MODE AND TRANSFORMER EQUIVALENT CIRCUIT PARAMETERS CALCULATION

Axial displacement occurs by the imbalanced magnetic forces generated by a short circuit fault in the upper and lower parts of a particular winding. Considering a typical single-phase transformer, the short-circuit current generated is approximately calculated as [61, 127-129]:

$$i(t) = i_0^{e^{-\frac{t}{\tau}}} + \sqrt{2I_{sc}}\left(\cos(\omega t + \psi - \varphi) - e^{-\frac{t}{\tau}}[\cos(\psi - \varphi)]\right) \quad (28)$$

Where

$$\tau = \frac{L_{eq}}{R_{eq}} \quad , \quad I_{Sc} = \frac{V}{\sqrt{{R_{eq}}^2 + \omega^2 {L_{eq}}^2}} \quad , \quad \varphi = \tan^{-1}\frac{\omega L_{eq}}{R_{eq}}$$

where ψ is the voltage angle when the fault occurred, I_{SC} is the steady state value of the short circuit current, I_0 is is the initial current at fault application, R_{eq} and L_{eq} represent the total series impedance of the winding and V is the effective supply voltage.

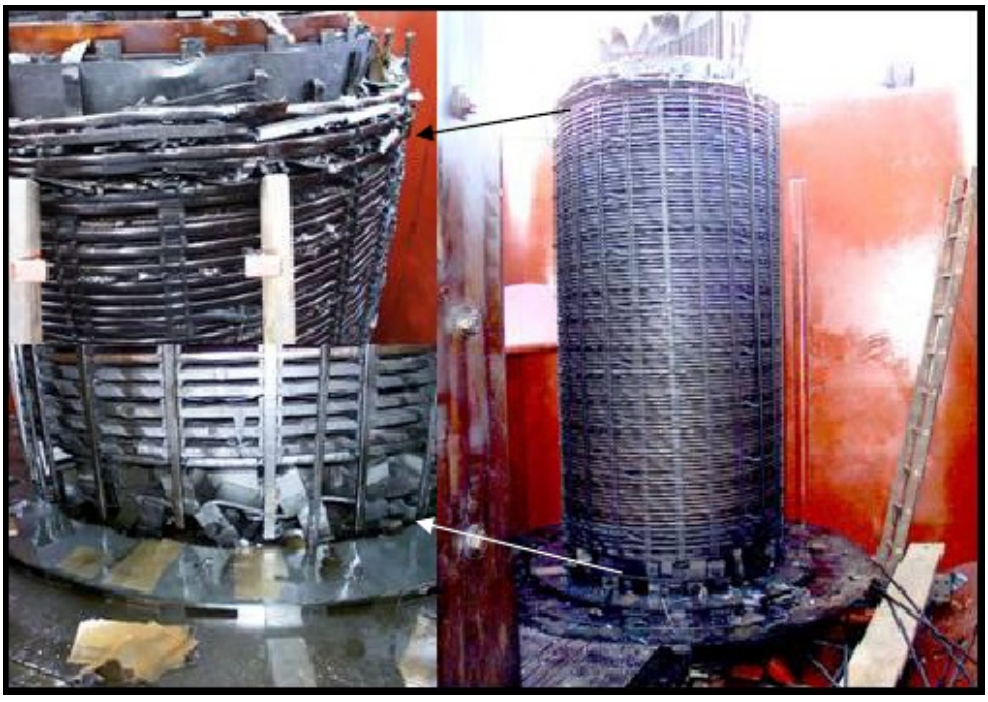

Figure 4-5 Axial displacement[1]

During short circuit faults, the electromagnetic forces acting on the coils may suddenly rise from a few newtons to Mega Newtons. These forces oscillate at double

the circuit frequency of the supply [75, 130-132]. The crushing forces within the coil might be extremely high whilst the forces exerted on the coil clamps may be zero [133], leading to compression of some parts of the winding, whereas other parts of the same winding may be in tension. At the winding terminals, the leakage field tries to spread out and form a radial component that produces an axial force along the winding as shown in Figure 4-5. The net force is equal to zero as long as the magneto motive forces (MMF) produced are completely balanced. Once the MMF are out of axial balance, the net force tends to raise this imbalance, leading to separation of the windings and breakage of the clamping structure [128]. Electromagnetic force on the transformer winding is a result of the interaction of the leakage flux and short circuit current in the winding [134, 135]; its effect on a small volume *dV* of a winding having a current density *J* placed in a point where the radial component of the flux density is *B(r)* can be calculated as [61, 134, 136]:

$$df=JB(r)dV \tag{29}$$

The electromagnetic force on the winding is analysed by means of ANSYS mechanical software as expressed below (see Figure 4-6).

$$F = \int_{vol}(J \times B)dV \tag{30}$$

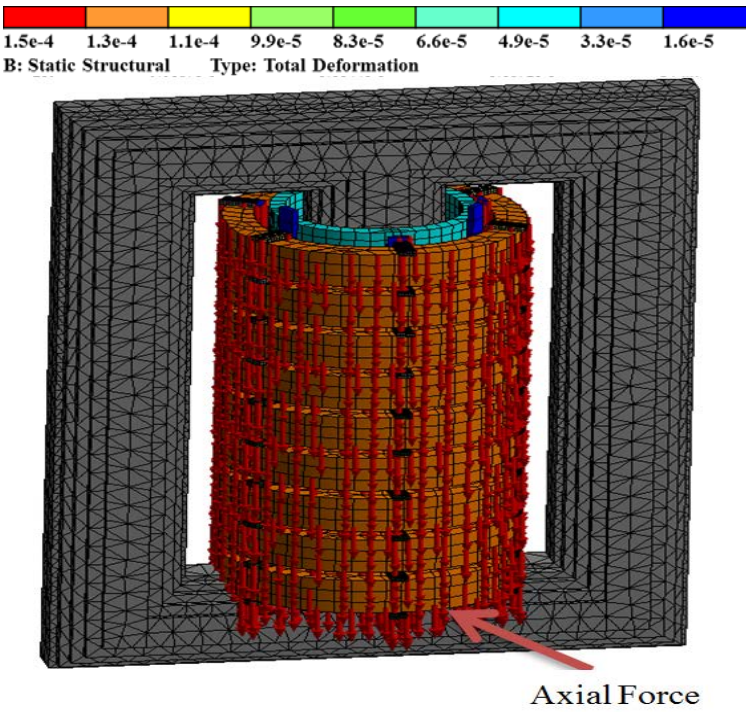

Figure 4-6 Axial displacement after short circuit fault

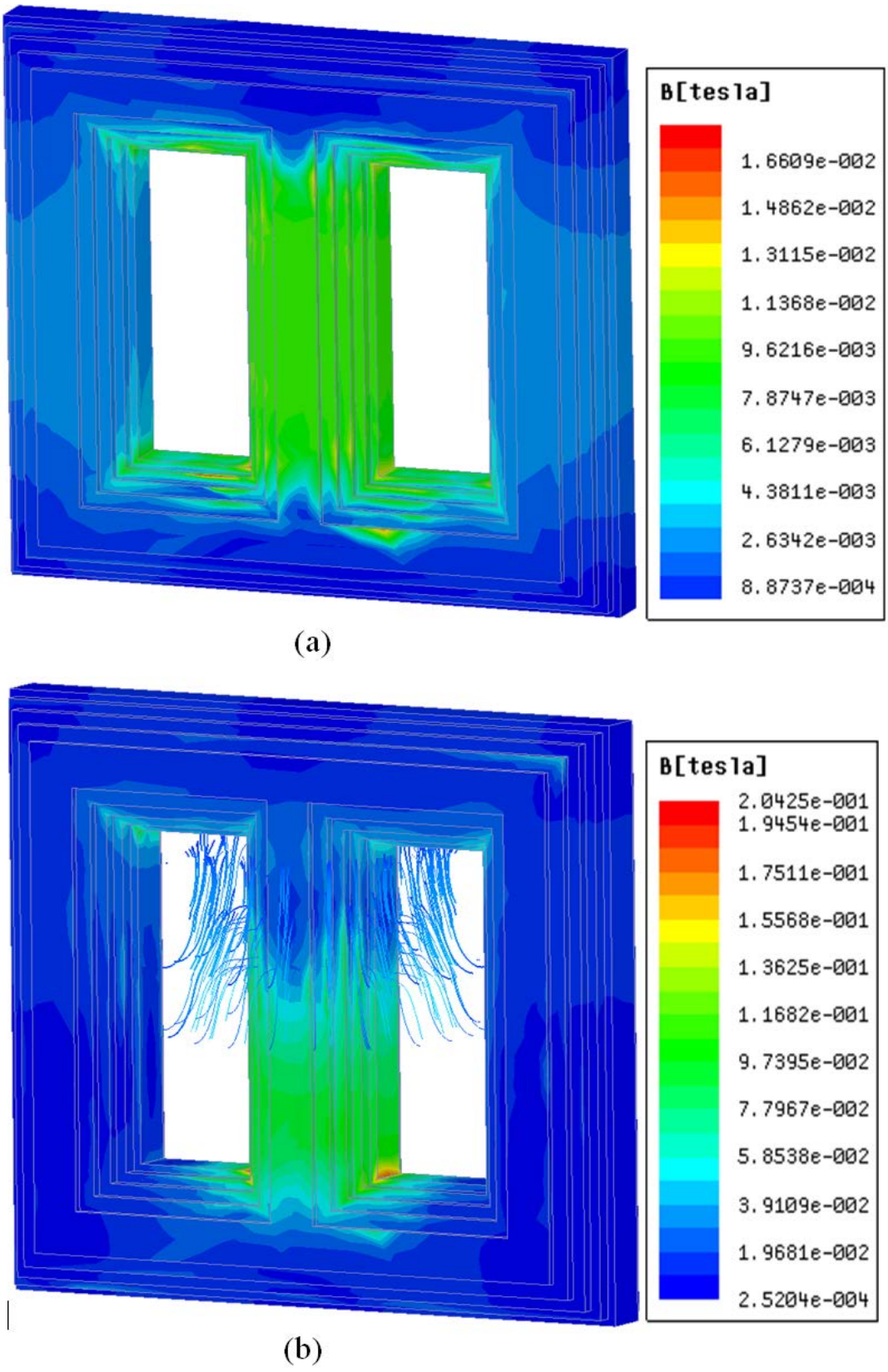

Figure 4-7 Magnetic flux density (a) Healthy Condition (b) Faulty Condition

Figure 4-7a shows a colour shaded plot of the magnetic flux density distribution within the studied transformer under normal operating condition whereas Figure 4-7b shows the magnetic flux distribution within the same transformer under axial displacement of the HV winding. Figure 4-7a clearly shows that the central limb, where the transformer windings are wound on, has higher magnetic flux density than the other two limbs and the flux density distribution is symmetrical around the central limb. On the other hand, the asymmetrical distribution of the electromagnetic flux can be noticed in case of HV axial displacement as shown in Figure 4-7b. Modification of the electromagnetic field in the vicinity of the faulty region can be justified by the increase in leakage flux at the upper part of the central limb due to axial displacement of the HV winding. As leakage flux is directly proportional to the winding current, the resultant electromagnetic force, as given in equation (30), is proportional to the square of the short circuit current. The leakage flux consists of radial and axial components and any change in the flux density before and after the fault causes variation to the transformer equivalent circuit inductance due to the change in the magnetic energy stored W as below[120]:

$$W_{ij} = \frac{1}{2}\int B_i H_j \tag{31}$$

Where, W_{ij} is the energy stored in the magnetic field linking conductor i with conductor j, B_i is the magnetic flux density within coil i and H_j is the magnetic field intensity of coil j. The parameters of the model shown in Figure 4-4 are calculated from the physical geometry (given in the appendix) of the transformer using 3D finite element analysis for normal winding condition. Various fault levels of axial displacement are simulated on the 3D finite element model and the model parameters are recalculated to investigate the impact of axial displacement on all model parameters as elaborated below.

4.3.1 Impact of Axial Displacement on Equivalent Electric Circuit Parameters

When axial displacement occurs in a winding, the equivalent electrical parameters of the winding model are expected to alter due to the change in the physical configuration of the windings [124, 137]. In order to precisely simulate an axial displacement using a transformer electrical circuit model, it is crucial to identify the percentage change in the electrical circuit parameters that is equivalent to a particular fault level [116, 138]. According to [10, 11, 139], axial displacement will alter the

mutual inductance between HV and LV disks windings; however, the change in capacitive components is small and can be neglected. To accurately identify the impact of the axial strain level (which is calculated as the ratio of winding displacement to the winding height, Δh/h as shown in Figure 4-8), on the electrical parameters of the transformer equivalent circuit, the physical dimensions of the two single-phase transformers are simulated using 3D finite element analysis, where various axial displacement levels are simulated in both low voltage and high voltage windings.

The impact of each axial displacement fault level on the electrical parameters of the equivalent circuit is investigated. Two case studies are presented using single-phase transformers (1 and 5 MVA) of different physical geometry to investigate the impact of transformer size on the transformer equivalent electrical parameters change due to axial displacement. The electrical parameters pertinent to normal and faulty conditions are extracted using FEM based on the following 3 steps:

(a) The electromagnetic forces calculated during a short-circuit fault by the Maxwell program is used as the input source of sequential FEM (ANSYS static structural) to accurately estimate the resulting mechanical forces, considering the structural characteristics such as stress distribution and displacement of the windings. The mechanical stress and displacement of HV and LV windings are predicted by the static structural analysis.

(b) The resultant mechanical displacement due to forces achieved from the static structural is solved using the electromagnetic Maxwell software in electrostatic and magnetostatic domains to obtain the inductance and capacitance matrices.

(c) The electrical parameters matrices are extracted for normal and faulty conditions and the percentage change in each parameter due to axial displacement is calculated as:

$$\text{Percentage change } x=\frac{x_n-x_f}{x_n}\times 100\% \quad (32)$$

where x_n and x_f are the values of inductance and capacitance parameters during normal and faulty conditions, respectively.

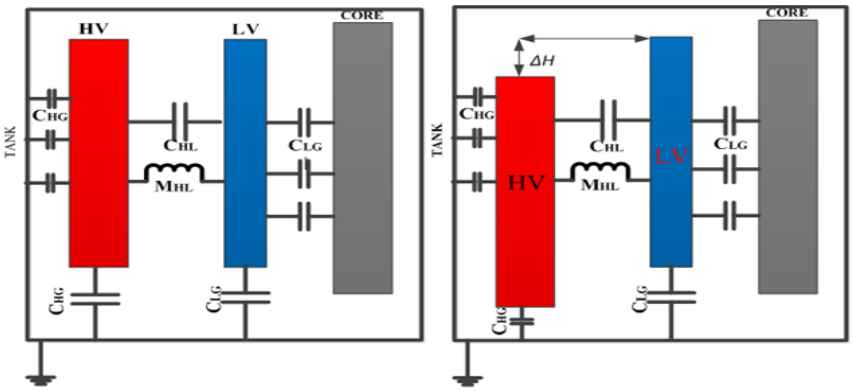

Figure 4-8 configuration of axial fault

4.3.1.1 Case Study 1: 1MVA Single-Phase Transformer

Figure 4-9 shows the percentage change of the mutual inductance between HV and LV windings with respect to the base value of healthy condition for different axial displacement fault levels when it takes place within the HV and LV windings. As shown in Figure 4-9 the percentage change in mutual inductance decreases with the increase of fault level. For small fault levels (up to 4.5%), the percentage change in the mutual inductance due to axial displacement on the HV or LV windings is the same. However, beyond this fault level, a slight difference is observed. This may be attributed to the asymmetry of the produced magnetic field generated by high axial displacement levels in both cases. Since the LV winding is closer to the core, LV winding axial displacement will lead to less change in the mutual inductance between the HV and LV windings than the change caused by axial displacement of the HV winding [114]. In general, the change in mutual inductance between the two windings is quite small due to the fact that FRA is performed on one winding while the other winding is kept open circuited.

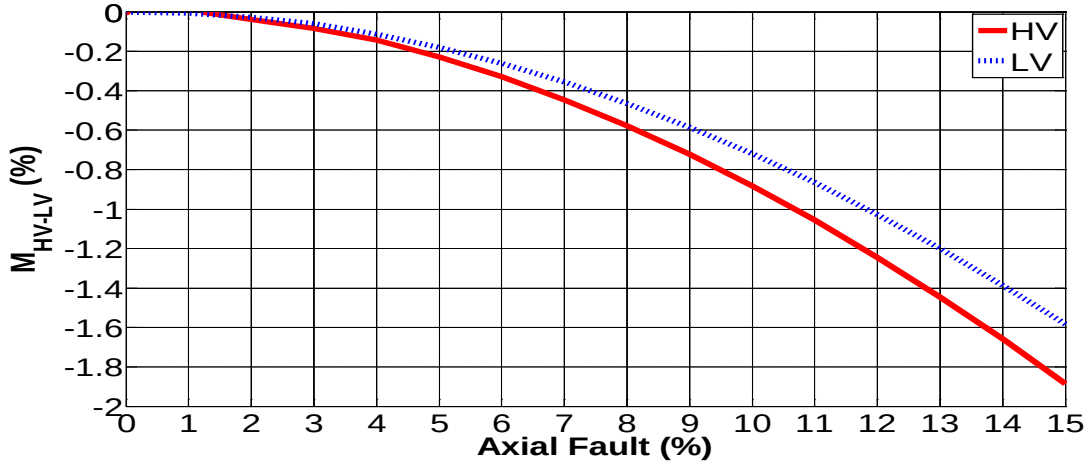

Figure 4-9- Variation of Mutual Inductance for various fault levels

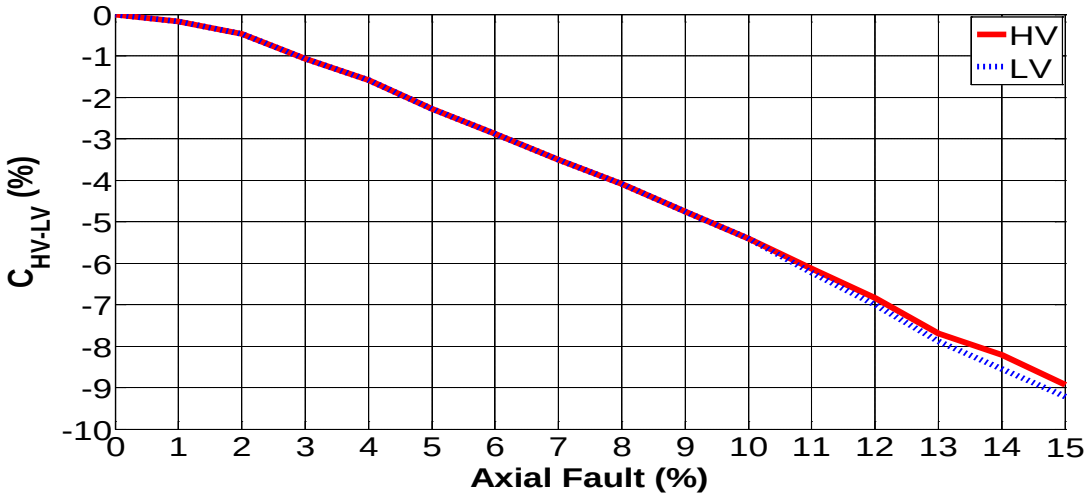

Figure 4-10 Variation of HV-LV Capacitance

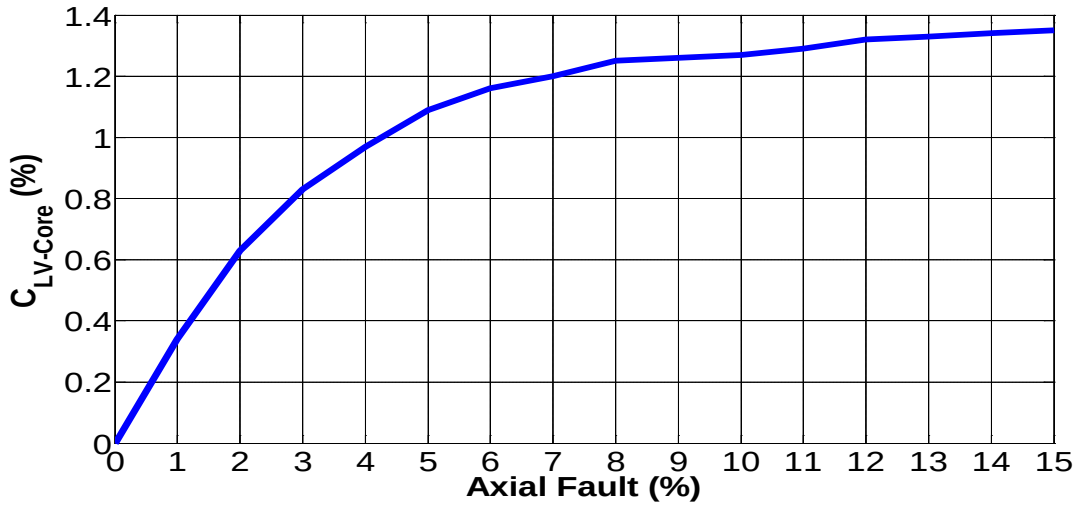

Figure 4-11. Variation of Capacitance between LV-Core (LV Axial fault).

Figure 4-10 shows the percentage change in the capacitance (with respect to the normal condition value) between the HV and LV winding when various axial displacement levels takes place on HV and LV windings. As revealed in Figure 4-10, the percentage change in capacitance between HV and LV windings is decreasing with the increase of fault level. The change in the capacitance is the same for the same axial fault level when it takes place on the HV or LV windings.

Figure 4-11 shows how the capacitance between the LV winding and core changes for various axial fault levels within the LV winding. It can be seen that the percentage change in capacitance increases with the increase of fault level. Figure 4-12 shows the same trend for the change in the capacitance between the HV winding and the tank for axial displacement within the HV winding. However, the percentage change in the capacitance between HV winding and the tank for a

particular HV axial displacement level is higher than the percentage change in the capacitance between the LV winding and the core for the same level of axial displacement on the LV winding. It is worth mentioning that the equivalent electrical parameters of a 3-phase transformer will have a similar trend to the single phase transformer equivalent electrical parameters as the effect of phase coupling will be insignificant and can be neglected.

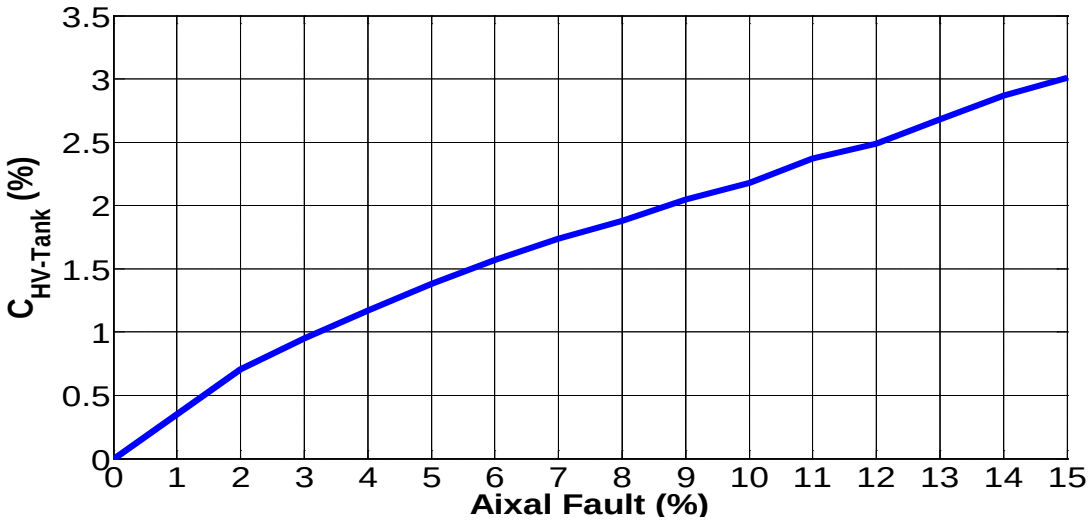

Figure 4-12. Variation of Capacitance between HV-Tank (HV Axial fault).

4.3.1.2 Case Study 2: 5 MVA Single-Phase Transformer

To investigate the impact of transformer sizing on the changes in electrical parameters due to axial displacement, the geometry of 5 MVA transformers is simulated using FEM. The percentage change in the equivalent electrical parameters with respect to the normal condition parameters for various axial fault levels on the HV windings was observed and compared with the previous case study as shown in Figure 4-13. Figure 4-13a shows the change in the mutual inductance between the HV and LV windings due to HV winding axial displacement for the two case studies. Up to 10% fault level, the change in the mutual inductance is the same for the two cases studied. However, beyond this fault level, the percentage change in the mutual inductance for the high rating transformer is slightly higher. Figure 4-13b and Figure 4-13c show that the variation in the capacitance matrices due to various axial fault levels is almost the same for the two cases studied. The results of this analysis reveal that the transformer size has a slight impact on the change in the electrical parameters due to different axial fault levels and the transformer size effect could be

ignored, as the electrical parameter change is calculated with respect to the base value for healthy transformer conditions.

It is worth mentioning that corrective action should be taken as soon as any minor axial deformation is detected, since leaving this fault unattended can lead to winding collapse or failure of the end supporting structure due to the progressive nature of axial deformations [9, 140].

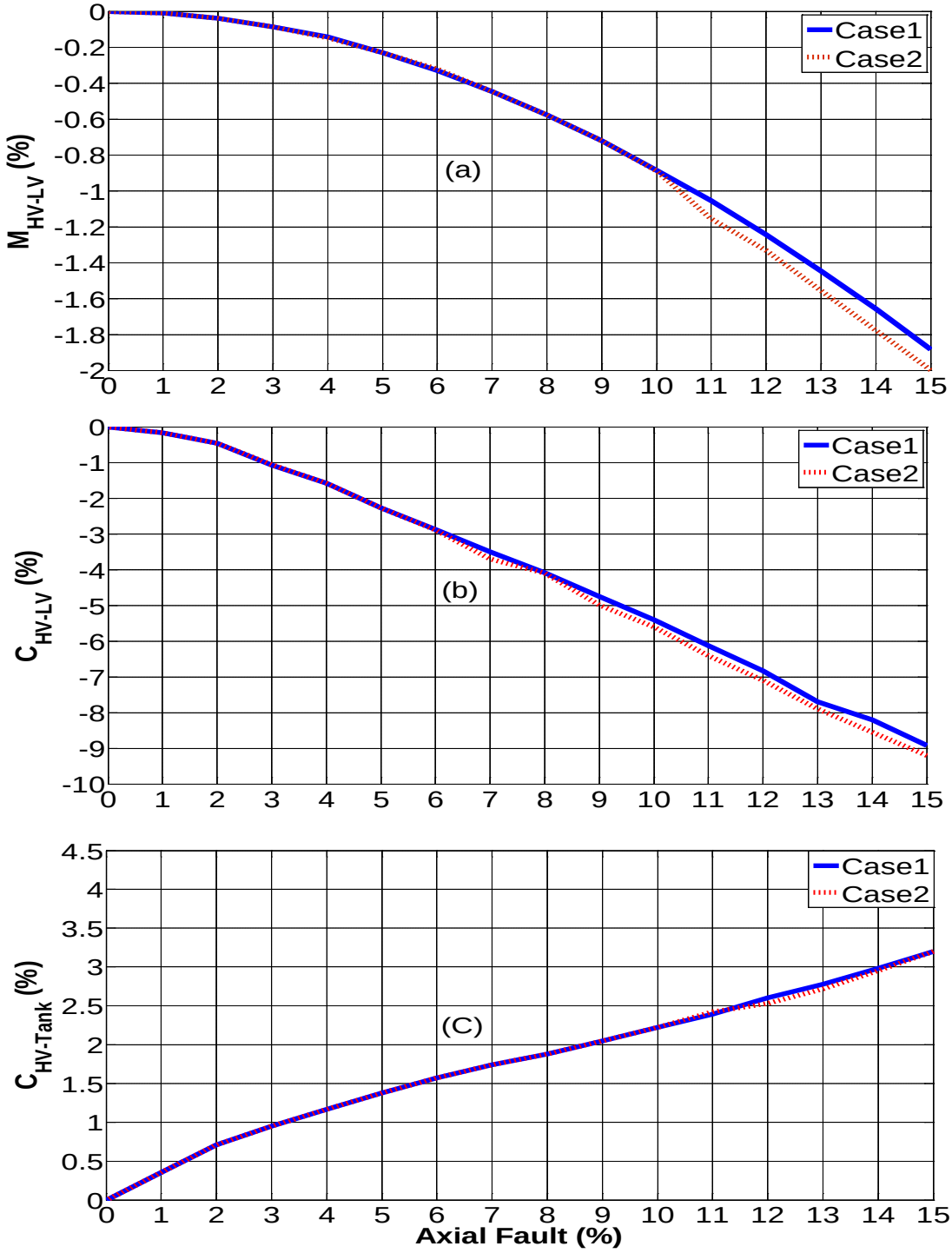

Figure 4-13. Variation of Inductance and Capacitance Matrices (1 and 5 MVA).

4.3.2 Impact of Proposed Parameter Changes on FRA Signature

In order to investigate the impact of the parameters discussed above on the FRA signature, the FRA signature of the lumped transformer model (1 MVA) shown in Figure 4-4 is plotted for both healthy and faulty conditions. As shown in Figure 4-14, the FRA signature for the HV winding is obtained by connecting a low voltage ac sweep frequency source (V_{in}) to one terminal of the winding while the response (V_o) is measured at the other terminal of the same winding with respect to the earth. The input and output resistors (R_i and R_o) shown in Figure 4-4 emulates the resistances of coaxial cables used in practical measurements. The FRA signature is plotted as the magnitude of the transfer function (TF) in dB; 20 $\log_{10}$ (V_o/V_i) against frequency. The FRA signature for the axial fault conditions is first obtained by changing only the mutual inductance between the HV and LV windings, as proposed in the literature [6], and subsequently changing the inductive and capacitive parameters, as discussed above. Figure 4-14a and Figure 4-14b show the influence of various levels of HV and LV winding axial displacement (1%, 3% and 5%) that is simulated by changing only the mutual inductance between HV and LV windings on the FRA signature. The value of the mutual inductance that corresponds to each fault level is calculated based on Figure 4-9. As shown in Figure 4-14(a) and Figure 4-14(b), the fault impact on the FRA signature is hardly observable in the frequency range above 200 kHz, where there is a minor shift of the resonance and anti-resonance frequencies to the right; the shift increases by increasing the fault level.

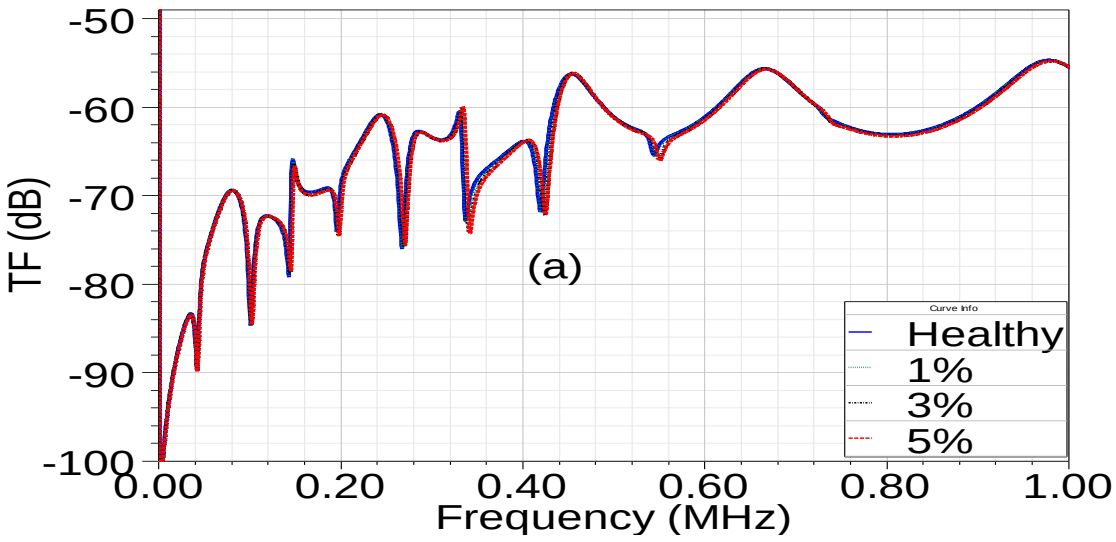

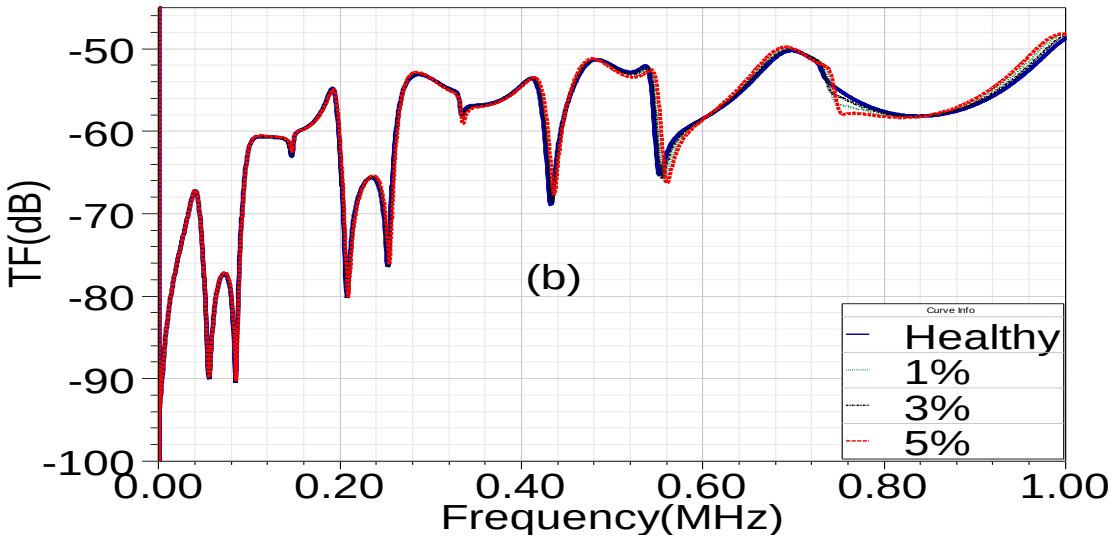

Figure 4-14 Effect of Axial Displacement on FRA signature (simulated by changing MHV-LV only) (a) HV winding (b) LV winding .

Figure 4-15(a) and Figure 4-15(b) show the effect of various axial displacements on the FRA signature of the HV and LV windings, respectively, by considering the changes in both capacitance and inductance matrices. The value of the electrical parameters corresponding to each fault level is calculated based on Figure 4-9 through Figure 4-12. Figure 4-15shows a clear influence of the axial displacement fault on the FRA signature for both windings. Figure 4-15 (c) shows the LV winding FRA signature from 10 Hz to 2 MHz. According to [124] the FRA signature due to axial winding displacement is not predicted for frequencies above 1 MHz.

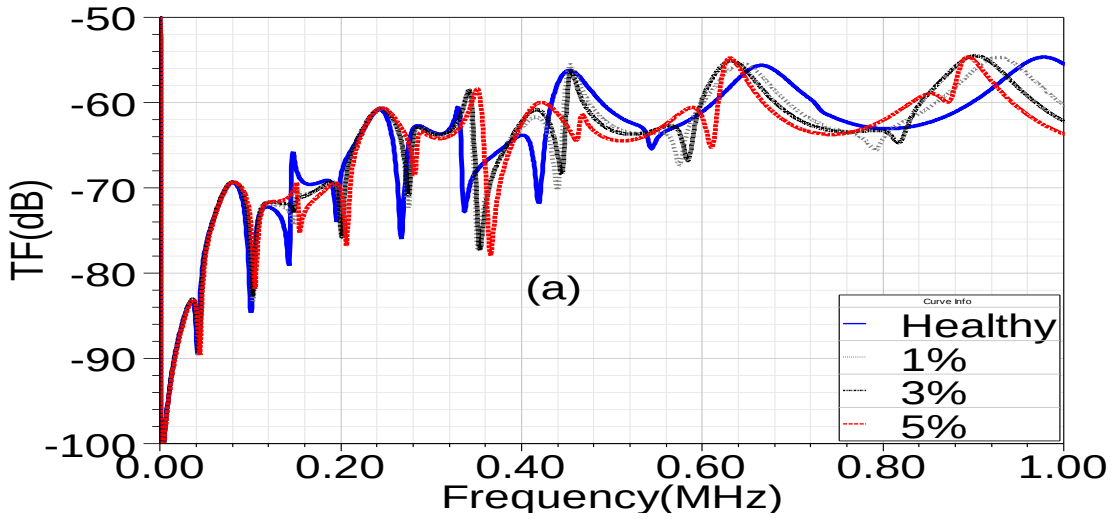

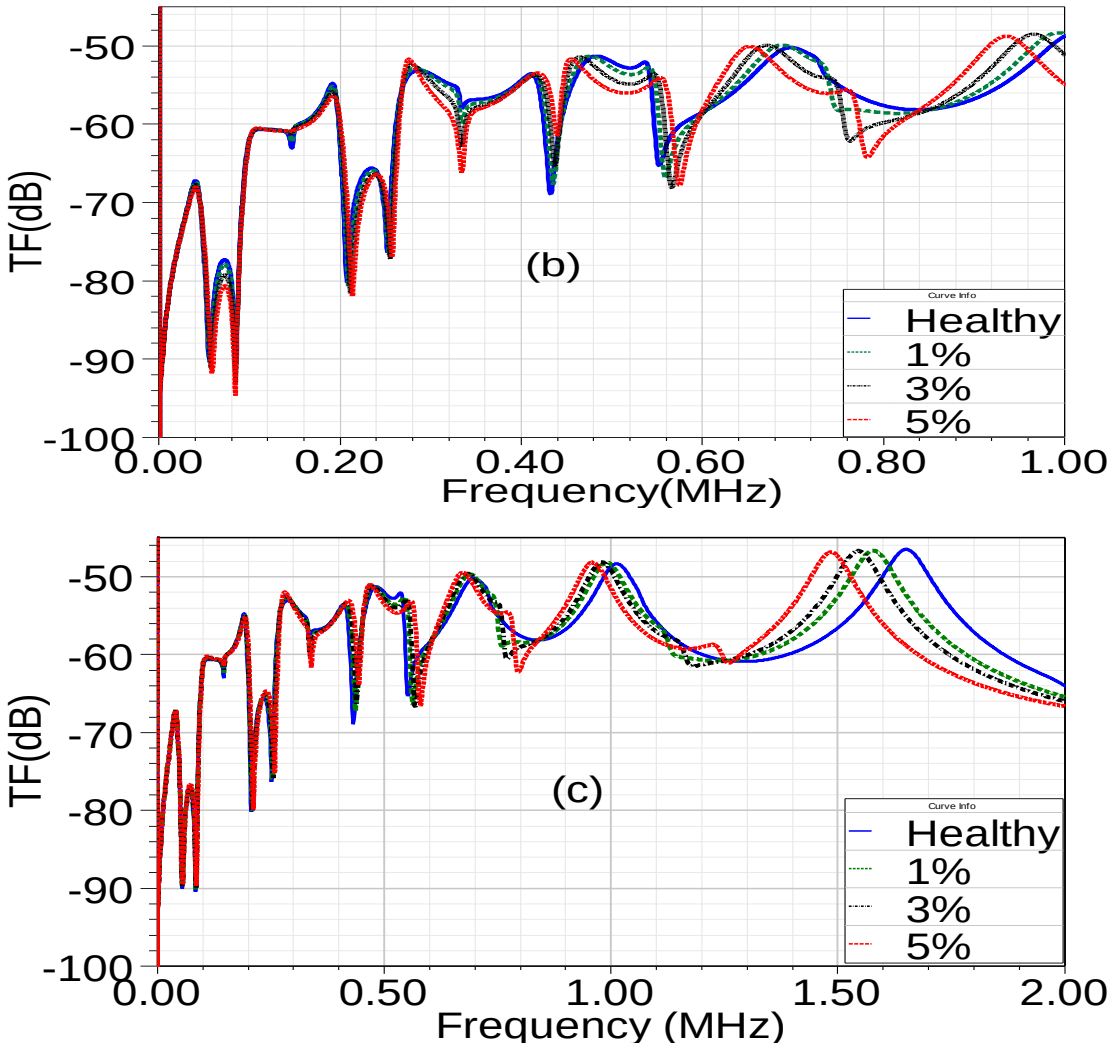

Figure 4-15. Effect of Axial Displacement (simulated by changing Capacitance and Inductance Matrices) on FRA signature (a) HV winding (b) LV winding, (c) LV winding FRA signature till 2 MHz .

The impact is observable for fault as small as 1% in the frequency range above 150 kHz in which resonance and anti-resonance frequencies shift to the right up to about 400 kHz; above this frequency they start to shift to the left due to the fact that within this range, capacitance elements considered in simulating the fault will dominate the FRA signature. Minor deviations in capacitance, ΔC, have more influence at a high-frequency range, since $f_2/f_1 = 1/2\,\pi\sqrt{1+\Delta C/C}$ where f_1 and f_2 are the resonant frequencies of the displaced and intact windings, respectively [139].Table 4.2 and Table 4.3summarise the variation of the resonance frequencies Δf due to 1% axial fault with respect to the healthy condition for both HV and LV windings of 1 MVA and 5 MVA single phase transformers. As shown in the tables, the frequency deviation of the faulty signature compared with the healthy one is much higher when

both inductance and capacitance matrices are considered in simulating the fault. While the shift in resonance frequencies is to the right through the entire frequency range above 100 kHz when inductance variation is considered to only simulate axial displacement, the shift of these frequencies tends to the left in the high frequency range (above 600 kHz) when both capacitance and inductance elements are considered in simulating the fault as proposed herein. This result agrees well with the practical axial displacement impact on the transformer FRA signature provided in [2, 6, 124, 141].

Table 4.2- Average effect of 1% axial winding displacement (1 MVA)

Resonance Frequencies (Normal Condition; kHz)		**Δf of axial fault signature; kHz**			
		considering inductance only		considering inductance and capacitance	
HV	LV	HV	LV	HV	LV
147.321	191.651	0	0	1.01	1.91
242.721	233.491	0	0	2.5	3.2
284.161	271.91	0	0.12	2.8	11.6
329.821	410.791	0.6	0.75	12.11	5.04
402.181	537.091	0.57	0.65	15.61	11
665.071	699.411	1.5	1.8	-33.2	-29.6
977.941	998.411	1.2	1.52	-76.3	-35.08

Table 4.3- Average effect of 1% axial winding displacement (5 MVA)

Resonance Frequencies (Normal Condition; kHz)		**Δf of axial fault signature; kHz**			
		considering inductance only		considering inductance and capacitance	
HV	LV	HV	LV	HV	LV
137.43	180.52	0	0	1.5	2.5
236.73	220.43	0	0	3.52	2.24
286.61	262.49	0.15	0.17	4.28	10.6
350.53	401.61	1.36	1.1	14.11	6.04
420.27	580.39	1.57	0.85	13.61	13
680.75	650.76	2.75	2.5	-40.2	-35.2
970.62	980.36	+3..2	2.532	-73.3	-40.08

4.4 IMPACT OF RADIAL DEFORMATION ON EQUIVALENT ELECTRIC CIRCUIT PARAMETERS

During a short circuit fault, the electromagnetic forces acting on the coils may suddenly rise from a few newtons to Megatons and oscillate at double of the circuit frequency [57, 129]. The radial components of the electromagnetic forces in a transformer with concentric disk windings have never been considered significant due to the fact that the radial strength of the winding is adequate to cope with these forces [61]. Winding radial buckling can be avoided by a perfectly round winding cross-section and by placing adequate radial spacer supports as shown in Figure 4-16 [142-144]. On the other hand, spacer supports influence the buckling strength of windings, which are subjected to radial electromagnetic forces [57, 145]. Radial forces on disk windings of a two-winding transformer produce a hoop stress that tends to extend the radius of the outer winding while, at the same time, produces a compressive stress on the inner winding, resulting in buckling, as shown in Figure 4-16 .The mean hoop stress (σ_{mean}) in the conductor of the outer winding at the peak of the first half-cycle of short-circuit current, assuming an asymmetry factor of 1.8 is [2, 10, 33, 146].

$$\sigma_{mean} = \frac{0.03 W_{cu}}{h e_z^2} \ \text{kN/mm}^2 \ \text{(peak)} \tag{33}$$

where $W_{cu} = I^2 R_{dc}$ is the losses in the winding in kW, h is axial height of the winding in mm and e_z is the voltage applied in per unit.

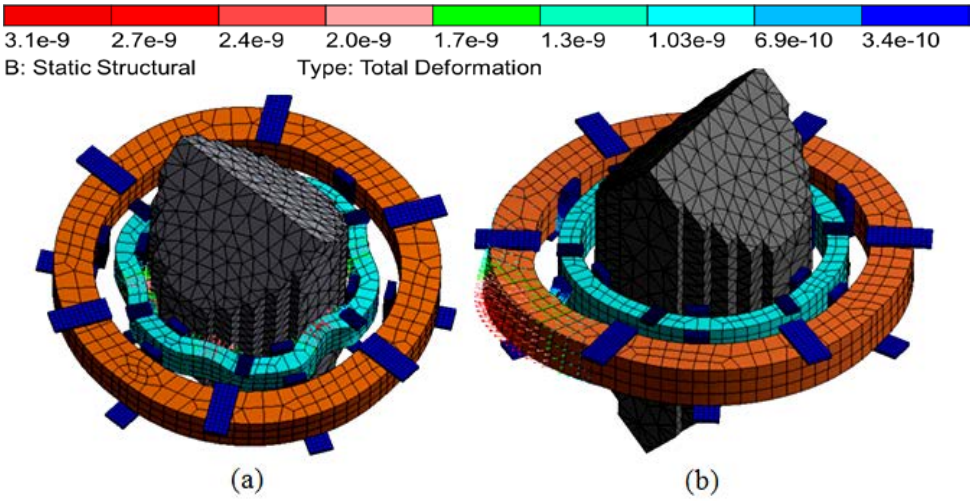

Figure 4-16. (a) Forced buckling (LV), (b) Free buckling (HV).

The inner winding is subjected to radial forces acting inwards (forced buckling), while the outer winding is subjected to outward acting force (free buckling), as shown in **Error! Reference source not found.**. The failure modes include winding collapse or bending between supports. If the winding is of a disk type, each disk is subjected to a radial force that can be calculated as [145, 147]

$$P_r = \frac{2\pi \sigma_{mean} n_c A_c}{D_w} \tag{34}$$

where σ_{mean} is the mean stress calculated in equation (6), P_r is the radial force in kN per mm of length, A_c is the cross-sectional area of the disk in mm^2, n_c is the number of conductors in each disk and D_w is the mean diameter of the winding in mm.

Figure 4-17 Buckling deformation

4.4.1 Impact of Buckling Deformations on Equivalent Electric Circuit Parameters

In order to exactly simulate radial deformation using a transformer equivalent electrical circuit model, it is essential to detect the percentage change in the electrical circuit parameters that corresponds to a particular fault level. According to [11, 78, 139], the radial deformation can be simulated by randomly changing the capacitance value of the HV and of LV windings while the change in inductance is neglected. The study did not emphasize the amount of change in the capacitance that corresponds to the fault levels studied. The main contribution of this section is the investigation of the correlation between various radial fault levels and the corresponding percentage change in electrical circuit parameters to help with accurate simulation of radial faults using transformer high-frequency electrical equivalent circuits and to ease the deterministic analysis of FRA signatures. In this regard, the physical geometrical dimensions of a single-phase transformer is simulated using 3D finite elements and by means of coupling ANSYS magnetic parts with ANSYS static structural mechanical parts; various radial deformation levels, calculated as the percentage ratio of the change in the perimeter of the faulty disk with respect to the disk perimeter prior to deformation, are implemented by controlling the level of the short-circuit current through the windings. In the case of a single-phase transformer, the current during transient conditions can be approximately calculated by equation (28) [61, 128].

Similar to axial displacement study above, the calculated electromagnetic forces are used as input sources of sequential FEM to predict the resultant mechanical forces, considering the structural characteristics such as stress distribution and winding deformation. The radial force due to a short-circuit current and axial leakage flux within the gap between the HV and LV windings is calculated in the finite element analysis as [4, 5, 61]:

$$F_{radial} = \pi D_{ave}\left(\frac{\sqrt{2}\mu_0 NI}{2H_w}\right)\left(\sqrt{2}NI\right) \tag{35}$$

where H_w, D_{ave}, N, I and μ_0 are the winding height, the average winding diameter, the number of turns, the RMS winding current and the permeability of air, respectively.

To investigate the impact of fault location on the percentage change in various electrical parameters of the transformer equivalent circuit, radial deformation was

simulated in three different locations of the HV and LV windings. The impact of transformer size is also investigated as will be explained in the following sections.

4.4.1.1 Case Study 1: 1 MVA Single-Phase Transformer

Figure 4-18 shows variation of the magnetic energy after deformation of the top disk of the HV winding due to a short-circuit current. Inductances associated with the deformed disks are calculated using Maxwell's equations. To calculate the capacitance matrix for the deformed winding, a sequence of electrostatic field simulations was performed to measure the energy stored in the electric field associated with the capacitance between the HV and LV windings, the LV winding and the core and the HV winding and the tank. The electrical parameters matrices are extracted for normal and faulty conditions and the percentage change in each parameter due to buckling deformation is calculated as in equation (32).

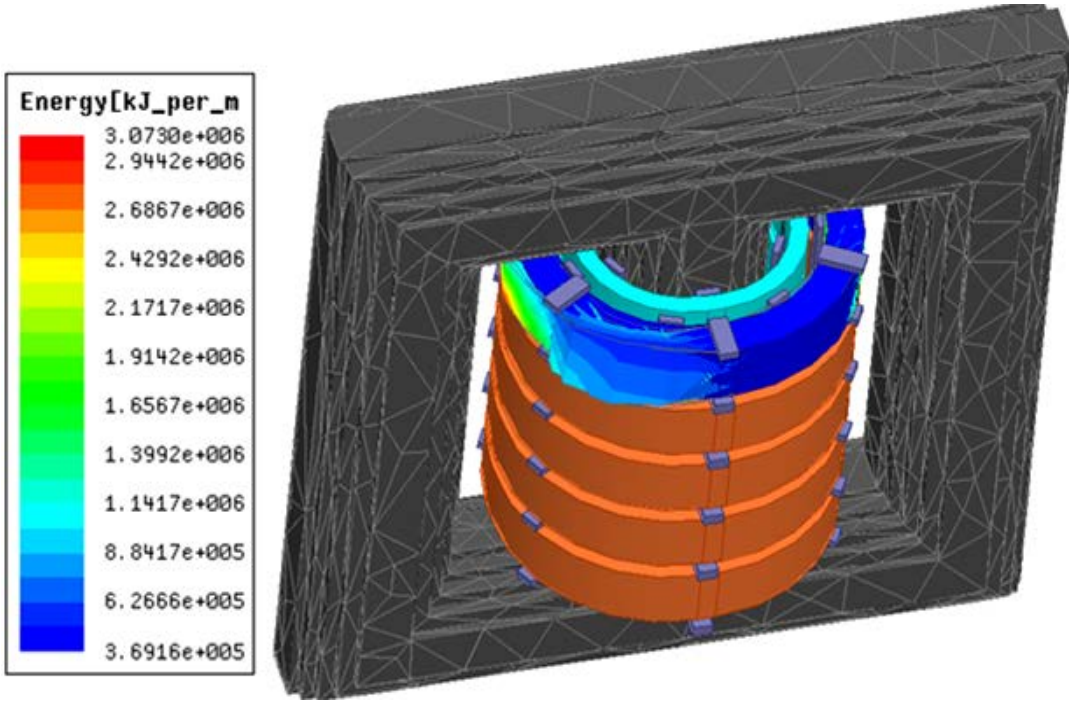

Figure 4-18. Variations of magnetic energy after deformation on top disk of HV.

This procedure is performed for three different fault locations: top, middle and bottom of both HV and LV windings as shown in Figure 4-19. The percentage changes in inductive and capacitive elements as a function of the specific fault level are shown in Figure 4-20 and Figure 4-21 . Figure 4-20 reveals that the percentage change in the self-inductance of the deformed disk winding decreases after buckling

of the LV winding with increasing fault level. The percentage change in the capacitance between LV and HV windings at the fault location decreases with the increase of the fault level whereas the percentage change in the capacitance between the LV winding and the core increases, since the distance between the deformed disk and core decreases. Figure 4-21 shows that, due to the free buckling the HV winding exhibits, the percentage change in capacitance between the HV winding and the tank and the percentage change in the self-inductance of HV winding increase with the increase in the fault level. The percentage change in the capacitance between the HV and LV winding shown in Figure 4-21c has the same trend as the one shown in Figure 4-20c.

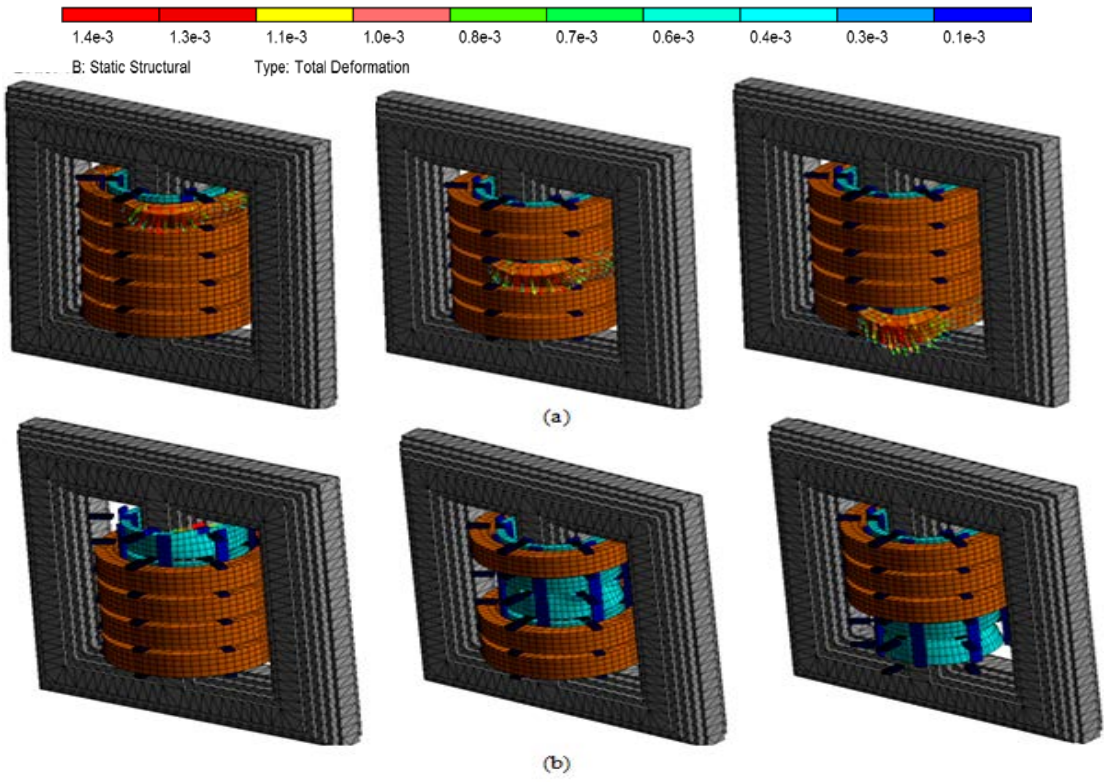

Figure 4-19. (a) Free buckling HV winding (top, middle and bottom). (b) Force buckling LV winding (top, middle and bottom).

Simulation results show that the deformation location has a slight impact on the electrostatic and magneto-static fields. As a result, the percentage change in the electrical circuit parameters is not significantly impacted by the fault location, as shown in Figure 4-20 and Figure 4-21.

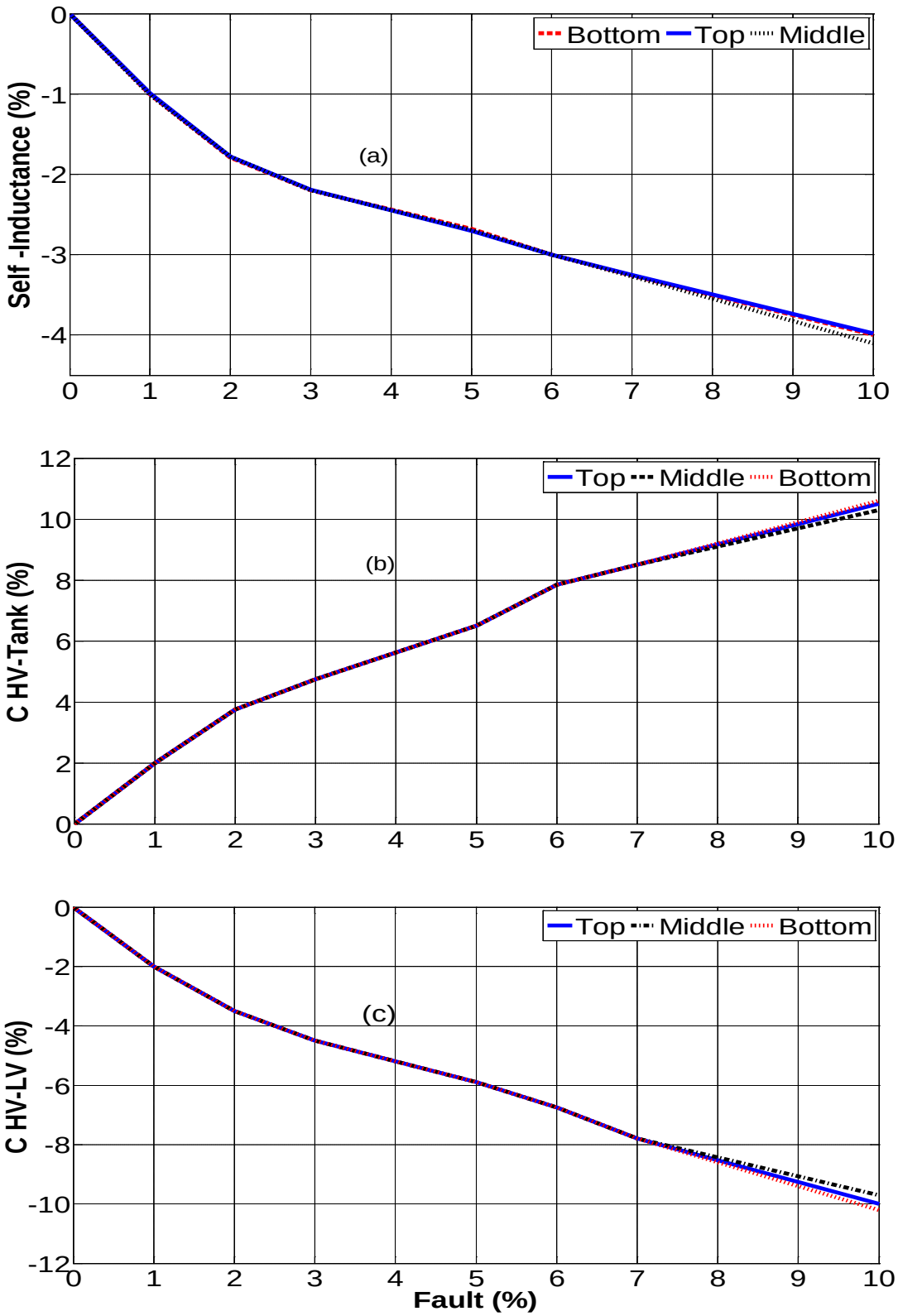

Figure 4-20. Variations of inductance and capacitance matrices (force buckling on LV winding) – 1MVA transformer.

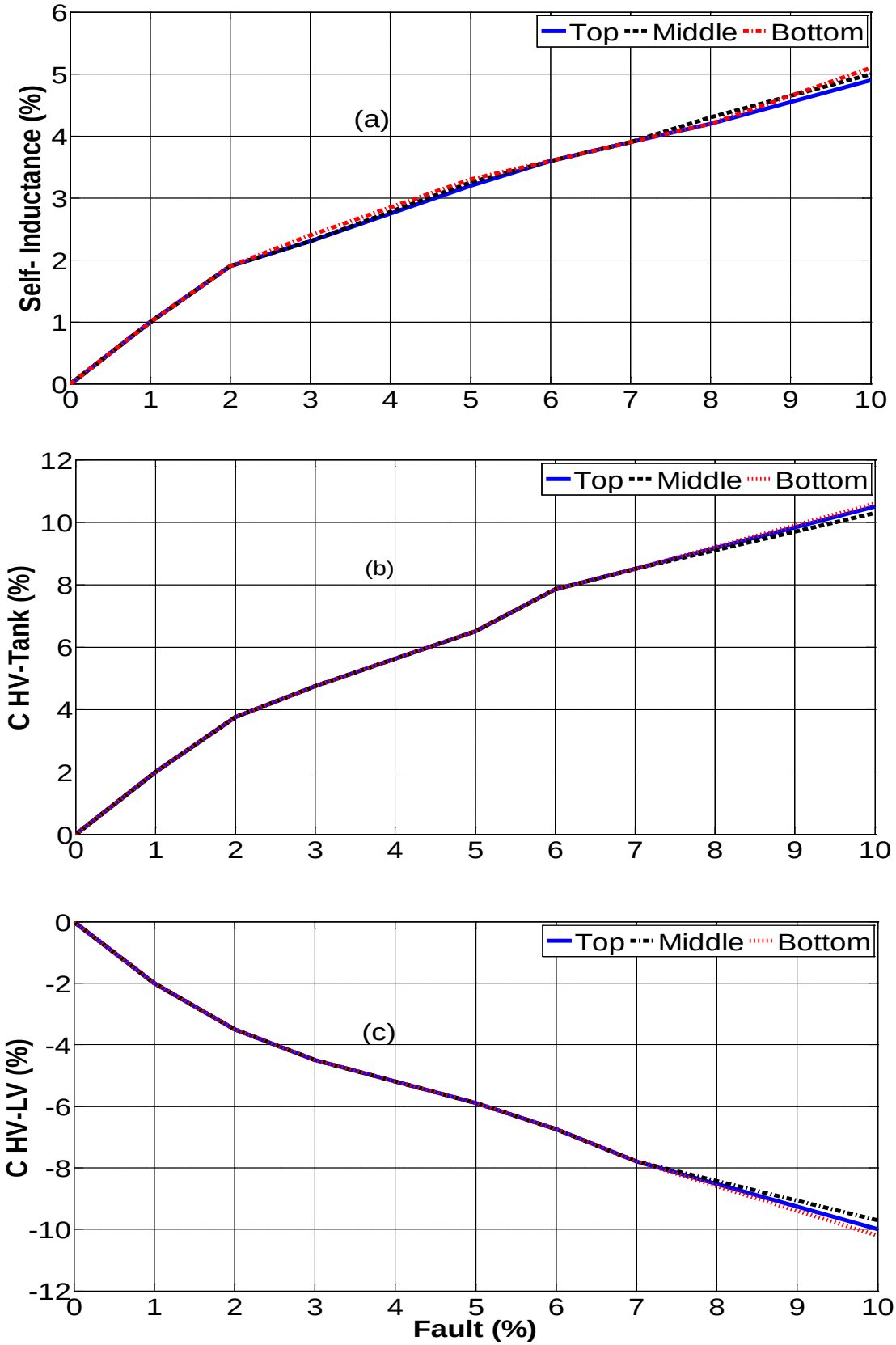

Figure 4-21 Variation of inductance and capacitance matrices (free buckling on HV winding)-1MVA transformer.

4.4.1.2 Case study 2: 5MVA single-phase Transformer

To investigate the impact of transformer sizing on the electrical parameters variations due to radial deformation, the geometry of 5 MVA transformer was simulated and the same approach explained above was used to calculate the percentage change in the equivalent electrical parameters corresponding to various fault levels of free buckling deformation on the HV winding in three different locations. Free buckling on the top of the HV winding is shown in Figure 4-22 and the resulting changes in electrical parameters are presented in Figure 4-23.

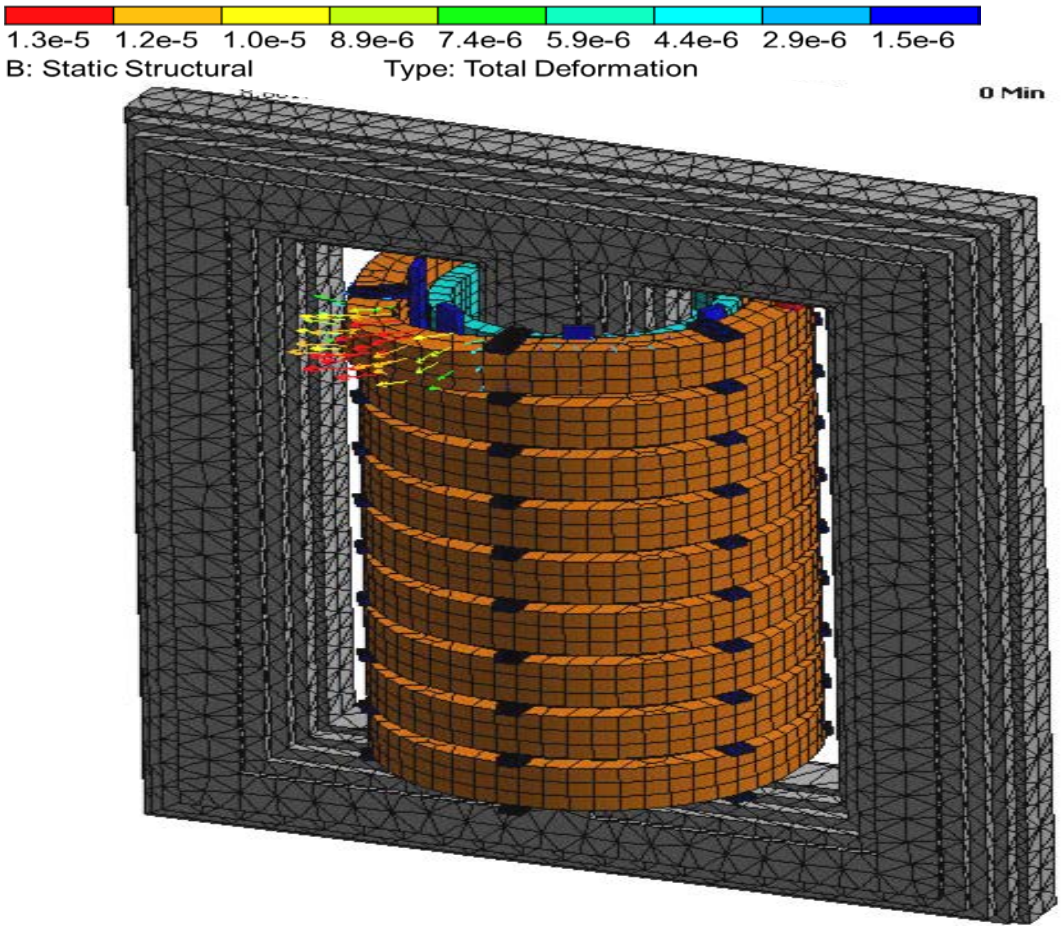

Figure 4-22. Free buckling at the top of the HV winding (5 MVA).

Figure 4-23 reveals that the change in the electrical parameters due to free buckling deformations of the HV winding of a 5 MVA transformer is quite similar to that obtained from buckling of the HV winding of a 1 MVA transformer. However the changes in the parameter associated with the high-rating transformer are slightly higher.

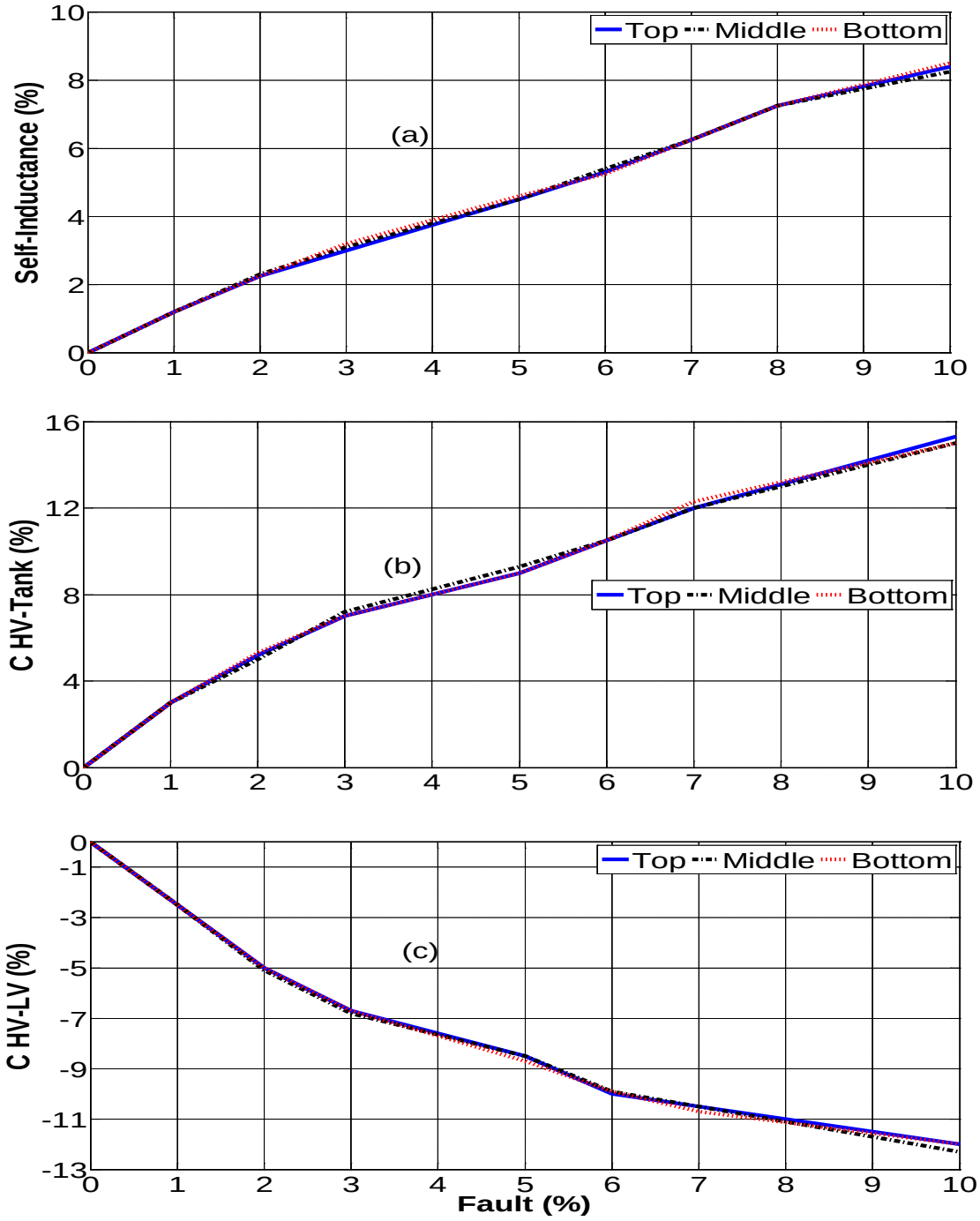

Figure 4-23. Variations of inductance and capacitance matrices (free buckling on the HV winding) - 5 MVA transformer.

4.4.2 Impact of proposed parameter changes on the FRA signature

To investigate the effect of the parameter changes proposed in the previous section on the transformer FRA signature, the transformer model (1 MVA) shown in Figure 4-4 was energized by a sweep frequency AC source (V_{in}) of 10 V and variable frequency (up to 1 MHz); the resulting FRA signature (Transfer function; TF = 20

log10(V_o/V_i)) is plotted against the frequency for healthy and faulty conditions. The value of the electrical parameters corresponding to each fault level is calculated based on Figure 4-20 and Figure 4-21. Figure 4-24shows the influence (on the FRA signature) of two fault levels (1% and 5%) of simulated HV and LV winding buckling deformations by changing only the capacitance matrix as proposed in the literature [11, 139]. As shown in Figure 4-24, the buckling deformation fault impact on the FRA signature is hardly observable in frequency range less than 500 kHz; at higher frequency, the resonance frequencies and magnitude are slightly changed. Figure 4-25 shows the effect of 1% and 5% buckling deformations on the FRA signature of the HV and LV windings by considering both capacitance and inductance variations.

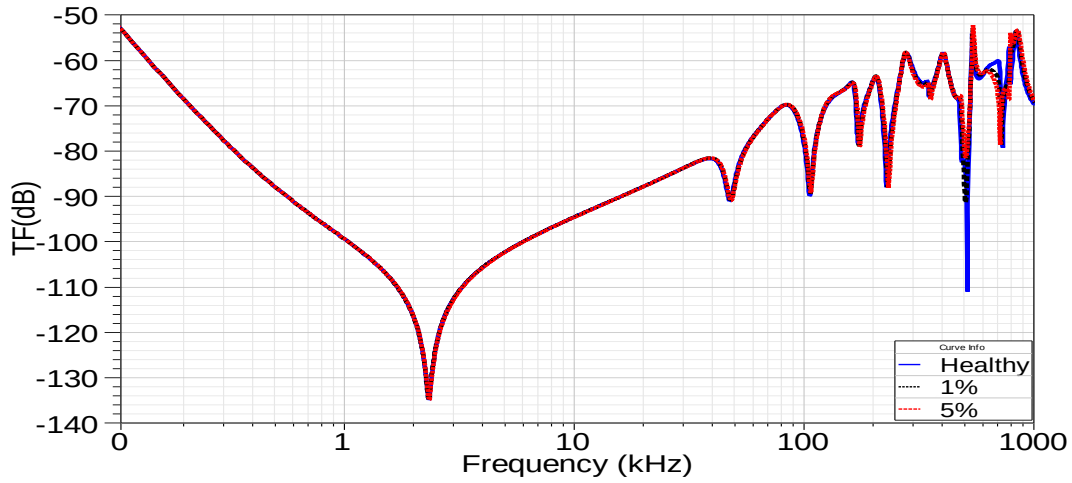

(a)

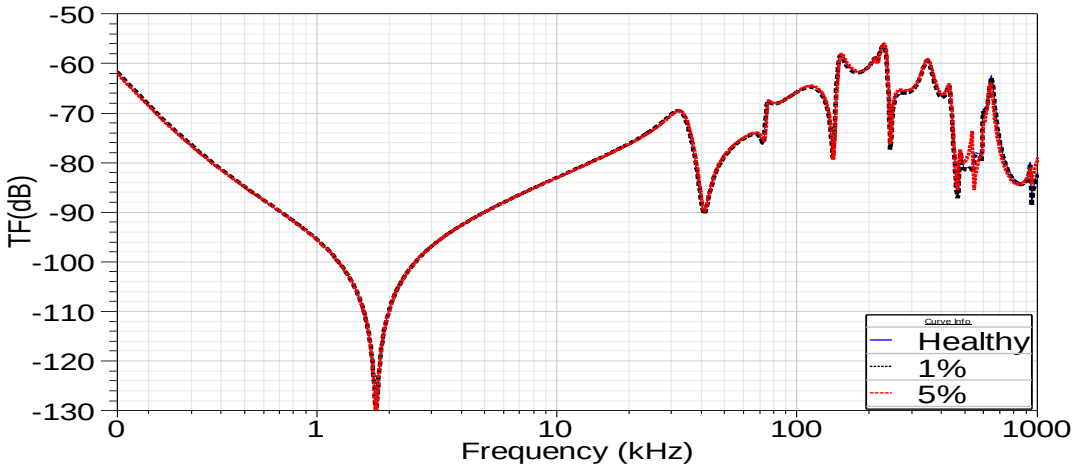

(b)

Figure 4-24. Effect of buckling deformations on the FRA signature (simulated by changing the capacitance matrix only) (a) Free buckling on HV winding (b) Force buckling on LV winding

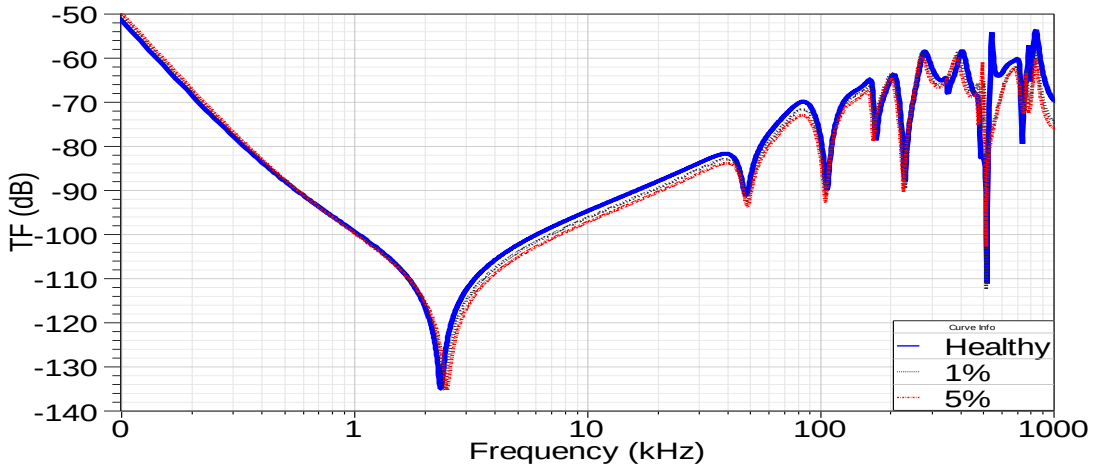

(a)

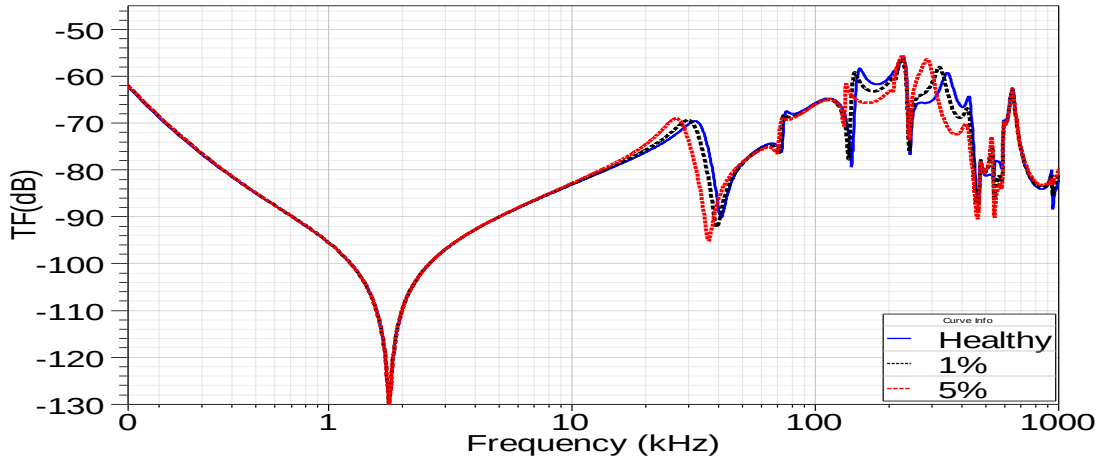

(b)

Figure 4-25. Effect of buckling deformations on the FRA signature (simulated by changing the capacitance and inductance matrices) (a) Free buckling on HV winding (b) Force buckling on LV winding.

In contrast with the FRA signatures shown in Figure 4-24, by considering both capacitance and inductance variations in simulating buckling deformations, the influence of the fault on the FRA signature is observable even at a low fault level of a 1% (see Figure 4-25) . This aligns well with the practical results presented in [85, 124, 148, 149], which indicated that buckling deformation influences the whole frequency range of the FRA signature. The change in the FRA signature in the case of HV buckling faults in the low-frequency range is attributed to the change in the magnetic flux distribution due to the fault.**Error! Reference source not found.**Table 4.4 and Table 4.5 summarize the variations of the resonance frequencies Δf due to 5% radial deformation with respect to the healthy FRA

signature for both HV and LV windings of two single-phase transformers of different ratings, 1 MVA and 5 MVA.. Five resonance peaks in four frequency ranges (10-100 kHz, 100-400 kHz, 400-600 kHz and 600-1000 kHz) are tabulated to quantify the change in peak resonances with and without considering inductance matrix variations. It is noted that the variation in the FRA signature due to buckling faults starts in the frequency range above 400 kHz only if capacitance element variations are considered. Variations in the FRA signature start from the low-frequency range when inductive elements are also considered, which agrees with the practical measurements presented in [6, 124, 148]. Table 4.4 and Table 4.5 show that, with the increase in the transformer rating, the shift in resonance frequencies will increase for the same fault level.

Table 4.4. Average effect of 5% buckling deformation (1 MVA)

Resonance Frequencies (Normal Condition; kHz)		***Δf of Radial deformation* fault signature; kHz**			
		considering capacitance only		considering inductance and capacitance	
HV	LV	HV	LV	HV	LV
74.80	75.36	0	0	-5.01	+8.91
134.9	151.59	0	0	-2.5	+3.2
466.85	425.93	+3.2	+4.1	+ 9.2	+10.02
760.65	641.47	+5.23	+6.75	+ 17.21	+15.2
950.46	930.59	+10.5	+9.65	+ 19.36	+17.5

Table 4.5. Average effect of 5% buckling deformation (5 MVA)

Resonance Frequencies (Normal Condition; kHz)		***Δf of Radial deformation* fault signature; kHz**			
		considering capacitance only		considering inductance and capacitance	
HV	LV	HV	LV	HV	LV
73.75	80.52	0	0	-6.25	+9.62
146.8	153.63	0	0	-3.51	+3.32
500.62	485.83	+4.2	+5.2	+ 10.25	+11.15
790.55	661.52	+6.16	+7.73	+ 18.31	+17.19
970.43	950.45	+11.52	+10.16	+ 20.14	+18.63

4.5 DISK SPACE VARIATIONS

The axial displacement measured between the magnetic centres of the windings results in unbalanced magnetic force components in each half of the winding, which leads to a variation in its relative location [2, 10, 57]. Axial forces cause the conductors to tilt or bend and are recognized to be more destructive when the windings are not spaced equally [150]. Tilting and bending of conductors that cause disk space variations between spacers as shown in Figure 4-26 are the most commonly reported deformations resulting from excessive axial forces [139]. The electrical parameters for normal and faulty windings are extracted using FEM based on the following steps:

(a) large short circuit current is injected into the HV winding;

(b) the structure of HV and LV windings are predicted using static structural analysis;

(c) the resulting mechanical displacement due to forces produced from the static structural analysis is solved using the electromagnetic Maxwell software in electrostatic and magnetostatic domains to obtain the inductance and capacitance matrices.

Results of the finite element analysis show that disk space variations affect several parameters of the transformer model, such as shunt capacitance at the location of the fault and the mutual inductance associated with the location of the fault. Table 4.6 summarizes the changes of these elements at different winding locations. Figure 4-26 (b) shows the variation of the magnetics flux after disk space variation fault.

Table 4.6. Variation of Capacitance and Inductance HV and LV

Fault location	C_S (pF)		Mutual Inductance (μH)	
	HV	LV	HV	LV
Healthy	3	45	142.25	153.45
2 disks Top	3.5	45.6	142.26	153.26
2 disks Middle	3.6	45.8	142.27	153.465
2disks Bottom	3.65	45.7	142.26	153.37

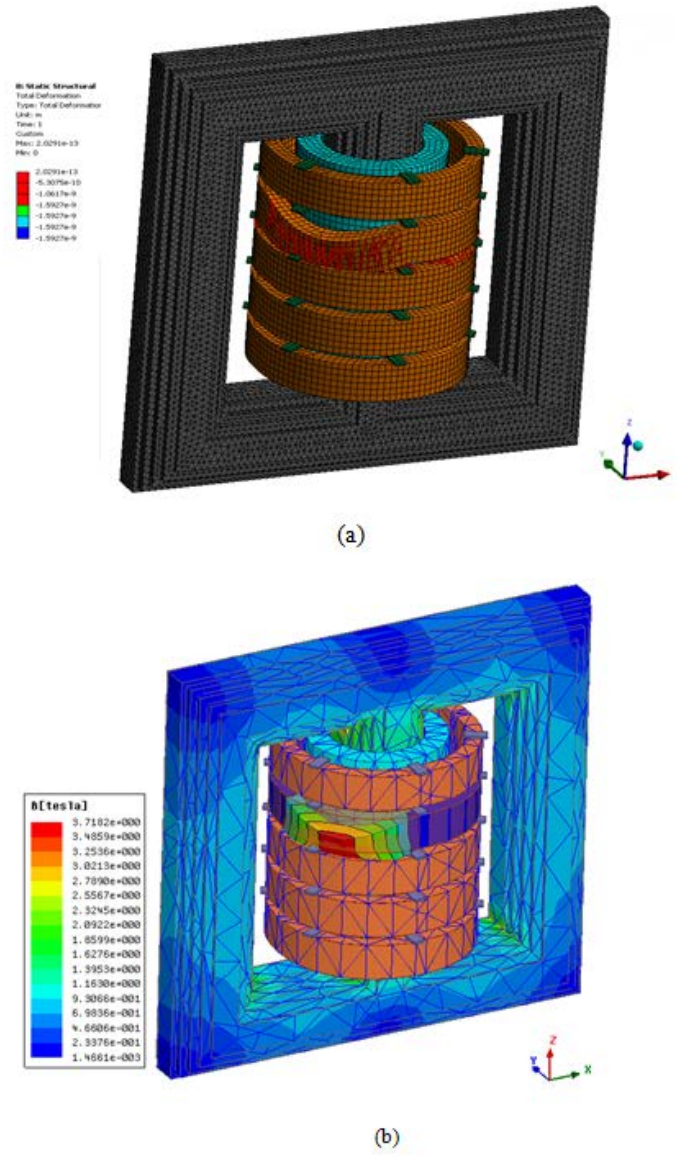

Figure 4-26. Disk space variations after short-circuit fault

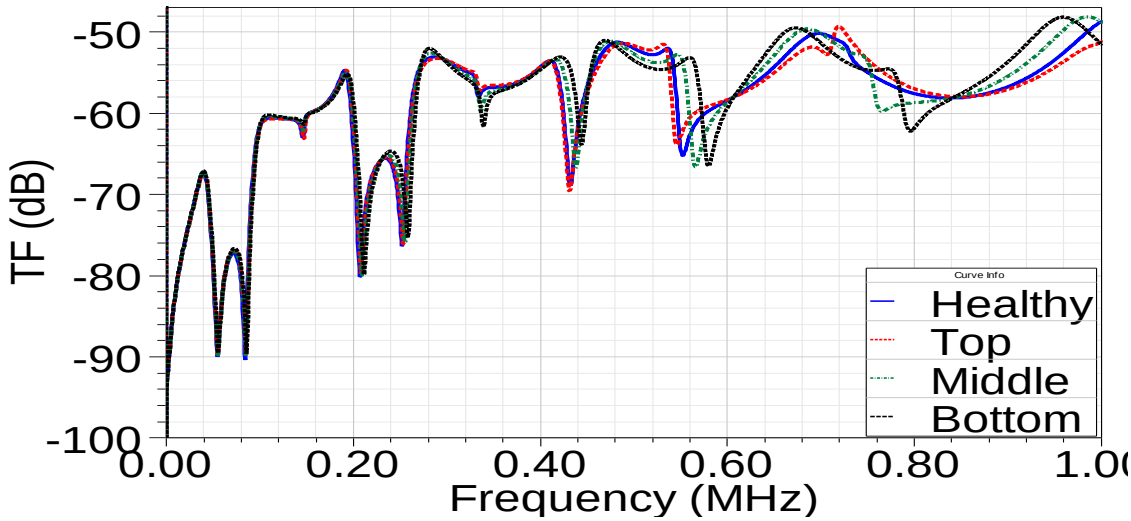

Figure 4-27. FRA signature for Disk Space Variation

Figure 4-27 shows the FRA signature for disk space variations of HV winding at three different locations compared with the FRA signature for healthy winding conditions. Figure 4-27 shows that the impact of disk space variations on the FRA signature is clearly visible at a frequency range above 400 kHz. This is attributed to the fact that capacitive elements dominate the FRA response at this range. Fault location has an impact on the FRA signature, as shown in Figure 4-27 , where the fault in the bottom disk has more impact on the FRA signature, followed by the effect of the fault when it takes place in the middle disk and finally when it takes place in the top disk. This may be attributed to the FRA connection arrangement. . Figure 4-27 shows that the change in C_S due to disk space variation faults is significant when compared with the changes in the mutual inductance that can be neglected in simulating such fault.

4.6 CORE DEFORMATION

Core defects (as shown in Figure 4-28) include shorted/burnt core laminations, multiple/unintentional core grounds, joint dislocations and lost core ground [150, 151]. In addition, there are core defects ensuing from poor insulation of the tightening screws of the core or due to blocked cooling oil ducts that cause the core to exhibit excessive heat [152] that can cause damaging vibrations [152-154]. Figure 4-29 (a) shows the magnetic flux before core deformation.

The winding inductance can be calculated using core material properties and physical dimensions as below [152]:

$$L = \frac{\mu_0 \mu_r N^2 A}{l} \tag{36}$$

where N is the number of turns of the winding, A is the cross-sectional area of the core section, μ_0 is the permeability of the vacuum, μ_r is the relative permeability of the core material and l is the length of the core section.

According to (36) it is expected that the core deformation will change winding inductance. Figure 4-29 (b) shows that the flux density changes when the core is deformed.

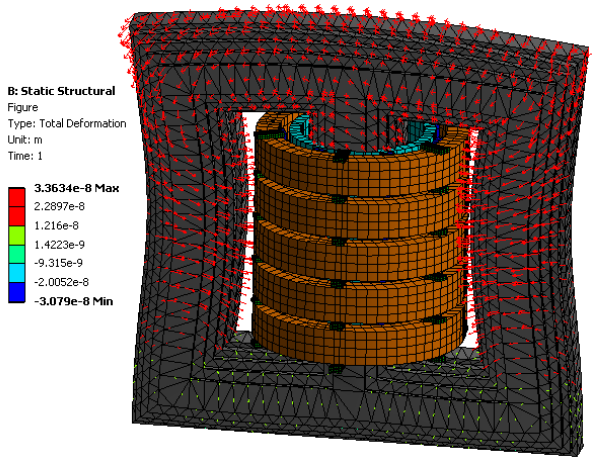

Figure 4-28. Core deformation

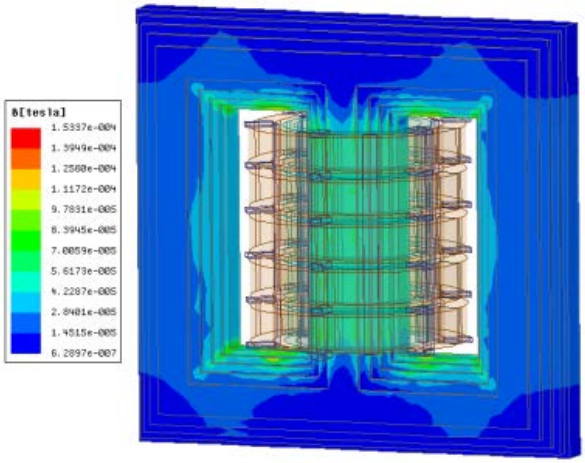

(a)

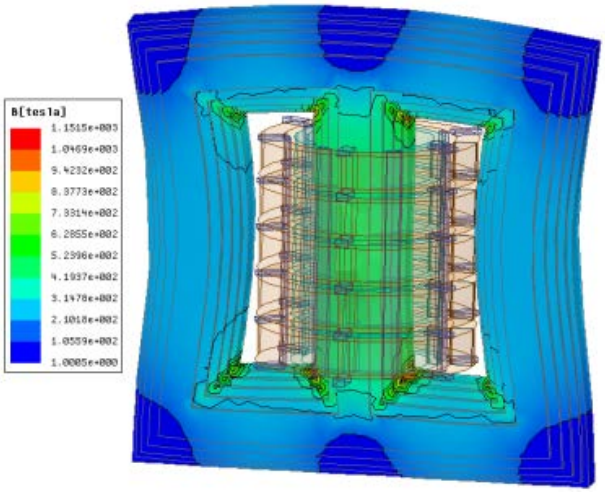

(b)

Figure 4-29. Healthy condition (a)Variations of magnetic flux after deformation on core(b).

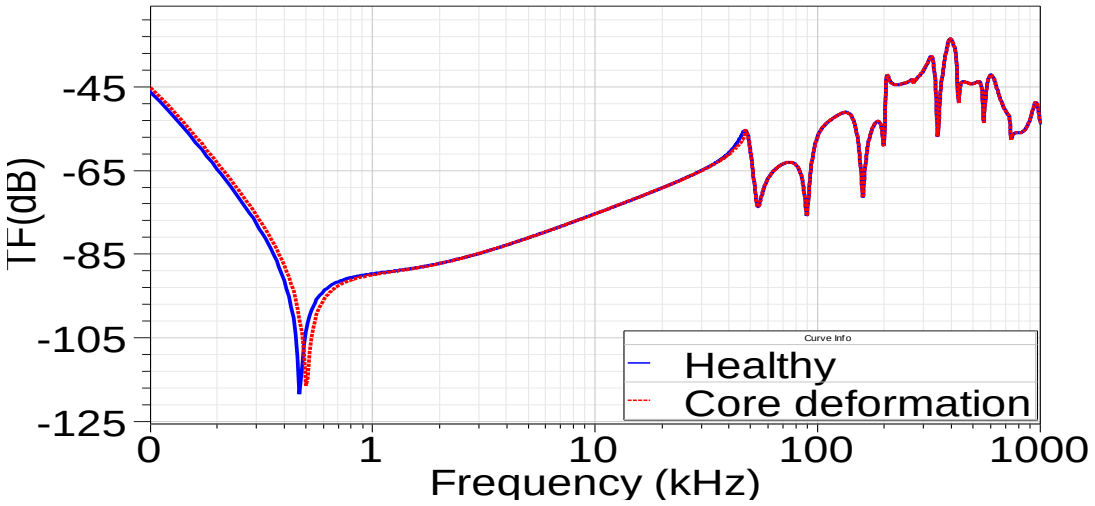

Figure 4-30. HV FRA signature for core deformation

Figure 4-30 shows the core deformation effect on the FRA signature. The impact is clearly visible at the low frequency range (below 10 kHz). This is attributed to the fact that flux penetration into the core is significant at the low-frequencies and its impact dominates the response at this frequency range.

4.7 BUSHING FAULTS AND OIL DEGRADATION

Bushings are one of the major components causing forced outages of power transformers [6]. A CIGRE international survey [6] indicated that the most frequent sources of transformer failures are attributed to tap changers, bushings, and paper-oil insulation systems, which deteriorate mainly due to heat, oxidation, acidity, and moisture [124, 155-159]. There are many issues relating to transformer bushing faults:

- Oxidation, Heat, acidity, and moisture are the major issues related to insulation deterioration.
- Insufficient or inappropriate routine maintenance and operation for transformer bushings.
- Poor dielectric withstand strength of the oil part of the HV bushing due to contamination of transformer oil with conductive particles and penetration of carbon on the lower porcelain surface.
- Temperature stresses due to short circuits and heavy loading conditions.

- Environmental pollution leading to degradation of bushings and finally to failure.

4.7.1 Bushing Fault Detection Techniques

Various diagnostic techniques have been adopted for transformer bushings as follows[160]:

4.7.1.1 Power/dissipation Factor and Capacitance Test

This test should be performed when the bushing is first installed. After that, the test should be conducted at regular intervals (typically 3 years to 5 years). It should be noted that the transformer windings can affect the test after bushing installation, since the temperature affects the dissipation factor test. This test should usually be performed at 20 °C or converted to ambient temperature by using temperature-correction.

4.7.1.2 Gas-in-oil Test

This test is not suggested as a prediction test, because the bushing must be opened and exposed to the outside atmosphere as in this case, the moisture can penetrate the bushing dielectric insulation. While this test is performed by many companies, the degree of expertise required to conduct and interpret the test results makes it impractical for most operators. Unfortunately, there are no IEEE guidelines for DGA tests on bushings[58]. The gas-in-oil test should be used only for the purposes of detecting faults on bushings due to dissipation factor measurements or high power or other situations. The results of gas-in-oil tests should be compared with test results from other bushings. The test oil analysis results from transformers cannot be compared with bushing tests due to the differences in oil volumes and paper/oil ratios.

4.7.1.3 Frequency Response Analysis

While many researchers have investigated the impact of various mechanical winding deformations such as axial displacement[57, 161], buckling deformation[11, 80, 162], disk space variation [142, 143] and short circuit turns[58, 61, 87, 133, 163-165] on the transformer FRA signature, no attention has been given to the impact of transformer oil insulation and various bushing faults on the FRA signature. In the following sections, the impact of insulation system properties as well as the impact

of bushing faults on the transformer FRA signature are elaborated.

4.7.2 Insulation System Properties

Presence of moisture in transformers is due to insulation aging, atmospheric leaks, cellulose decomposition and after the dry-out process where moisture migration between oil and paper insulation takes place [156, 166]. The dissipation factor test is a method that can be used for identifying the moisture content inside the dielectric insulation [124, 160]. The complex permittivity of transformer oil at a given frequency *w* and temperature *T* can be calculated as[1, 124]:

$$\varepsilon_{oil}^{*} = \frac{\sigma_{Oil}(T)}{j.\varepsilon_0.\omega} + 2.2 = \varepsilon^{'}(\omega) - j\varepsilon^{''}(\omega) \tag{37}$$

where σ_{Oil} is oil conductivity, ε_0 is the permittivity of free space.

Dielectric behaviour usually refers to the variations of $\varepsilon^{'}$ and $\varepsilon^{''}$ with frequency, composition, temperature, and voltage [1, 124]. The real and imaginary parts of the dielectric permittivity as a function of the frequency are given by [1]:

$$\varepsilon^{'} = \varepsilon_{\infty} + \frac{\varepsilon_0 - \varepsilon_{\infty}}{1 + \omega^2\tau^2} \tag{38}$$

$$\varepsilon^{''} = \frac{(\varepsilon_0 - \varepsilon_{\infty})\omega\tau}{1 + \omega^2\tau^2} \tag{39}$$

Where ε_{∞} is the infinite-frequency dielectric constant and τ is the dielectric time constant. For an equal thickness of oil-paper composite transformer insulation, τ is given by [167]:

$$\tau = \frac{\varepsilon_{paper} - \varepsilon_{oil}}{\sigma_{paper} + \sigma_{oil}} \tag{40}$$

where, ε_{paper} and ε_{oil} are the absolute value of permittivity of paper and oil insulation, respectively, and σ_{paper} and σ_{oil} are the conductivity of paper and oil insulation, respectively.

The computation of oil conductivity requires details of the transformer physical geometry as shown in Figure 4-31 as well as dielectric permittivity of the test object [1].

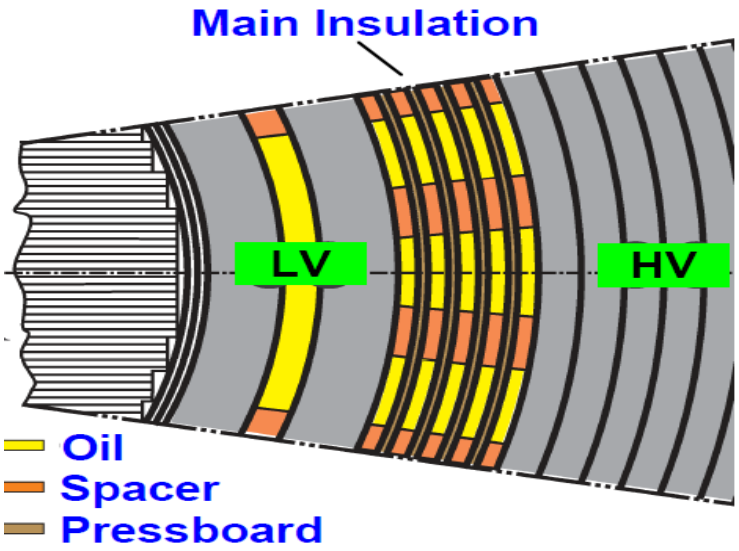

Figure 4-31 Insulation System within a power transformer

4.7.3 Transformer Bushing Construction and Equivalent Circuit

There are two common types of transformer bushings, namely solid porcelain bushings (which are used for low rating transformers) and oil-filled condenser bushing (also known as oil impregnated paper OIP bushing, which is used for high rating transformers [159]. An OIP transformer bushing is composed of insulation paper wound around a central core as shown in Figure 4-32. The portions of the bushing in the air and inside the transformer are also considered in the simulation. At defined intervals, conductive sheets are placed between the paper layers to control the electric field distribution [157]. Layers of paper and foil are usually filled with an insulating fluid such as oil. The main insulation system is represented by capacitance C1 in the equivalent bushing T-model shown in Figure 4-33, while layers near ground are represented by capacitance C2. In the bushing model shown in Figure 4-33. Rs and Ls represent the central conductor within the bushing that connects the line with the transformer energized windings.

Bushings are designed to have a constant dielectric capacitance over the asset life [155]. Therefore, variations in bushing capacitance can be used as an indicator of a potential problem. An increase in capacitance of more than 3% to 5% is typically interpreted as an indication of a problem within a bushing [168]. To accurately identify the effect of bushing faults on the electrical parameters of a bushing equivalent T-model, the physical geometrical dimension of a 10 kVA bushing of a

three-phase transformer Figure 4-33. Transformer Bushing layers and its equivalent T-model was simulated using 3D finite element software (ANSYS) for healthy and faulty conditions. Faulty bushings are emulated through altering their insulation complex permittivity, which is influenced by many factors such as ambient temperature and the structure of the insulation system [155]. Moreover, insulation aging and moisture content have significant effects on bushing dielectric properties.

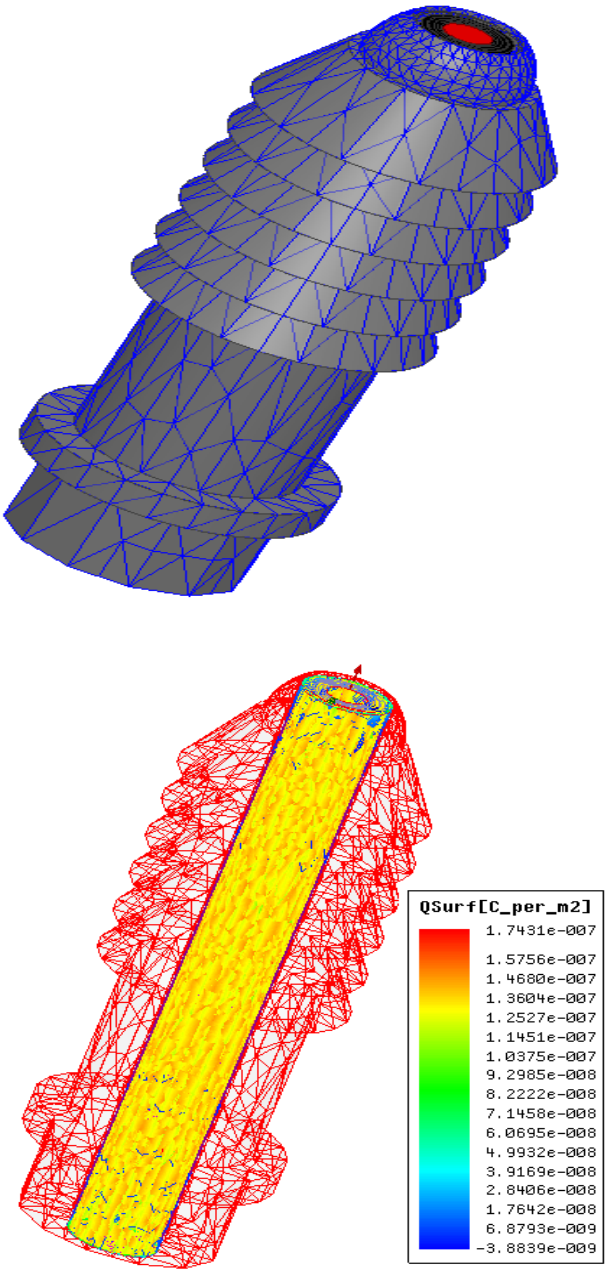

Figure 4-32. 3D model of Bushing solved in electrostatic FEM solver

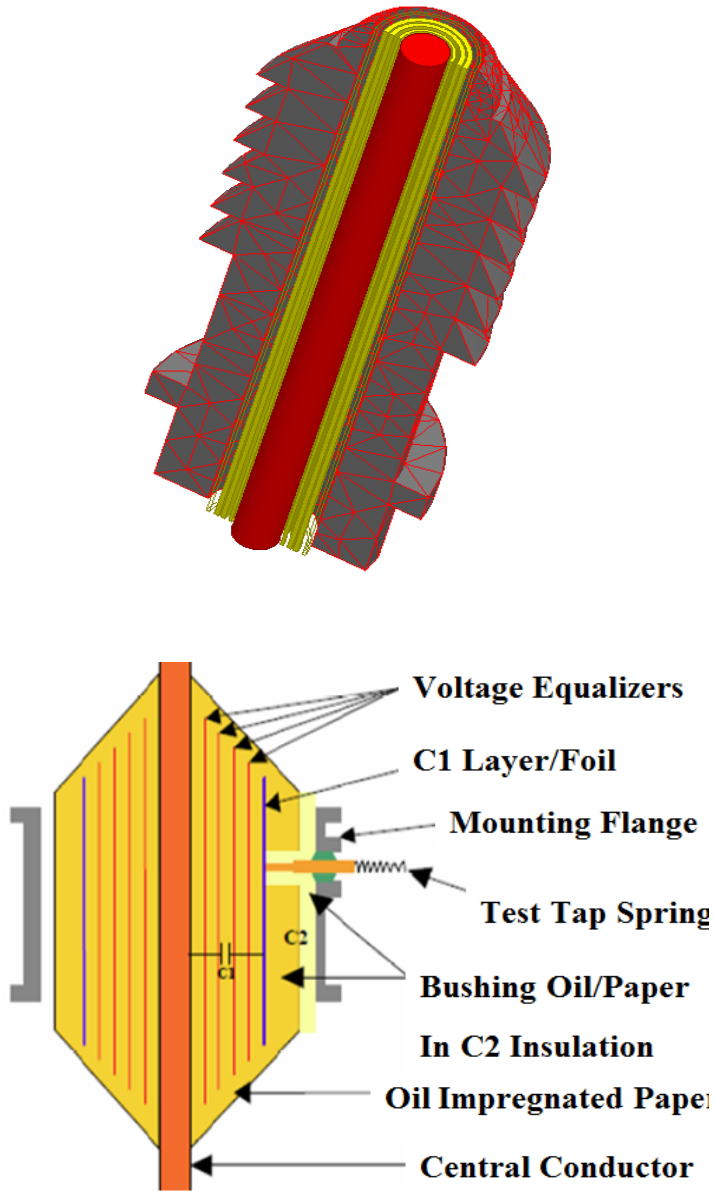

Figure 4-33. Transformer Bushing layers and its equivalent T-model

The electrical parameters for normal and faulty conditions are extracted using FEM based on the following steps:

Step 1: The 3D model of the transformer bushing shown in Figure 4-32 is analysed using electrostatic, magnetostatic and DC conduction solvers to obtain the capacitance, conductance and inductance matrices for the case of healthy condition. To extract the bushing T-model parameters, the effect of capacitive grading on the electric field distribution is also analysed.

Step 2: Faulty conditions are simulated by changing the permittivity of the transformer oil-paper insulation of the bushing, and the corresponding variations in the capacitances and inductance matrices for different faulty condition levels are calculated using the electrostatic, magnetostatic and DC conduction solvers.

Step 3: The FRA signature is plotted as the transfer function $TF_{dB} = 20 \log_{10} |V_0 / V_{in}|$ for healthy and faulty conditions.

Moisture content inside the bushing leads to variations in the capacitive values C1 and C2. In the FEA, moisture content inside the bushing can be simulated through changing the permittivity and/or conductivity of the dielectric insulation. In the transformer model under study, moisture content within the bushing oil was varied by changing the oil permittivity from 1% to 5%. Figure 4-34 shows the corresponding percentage change in the bushing capacitances C1 and C2. These results reveal that the change in C1 is more than in C2 for the same percentage increase in moisture content; for example, a 2% increase in moisture content leads to a 7.5% increment in C1 while C2 increased by only 3%.

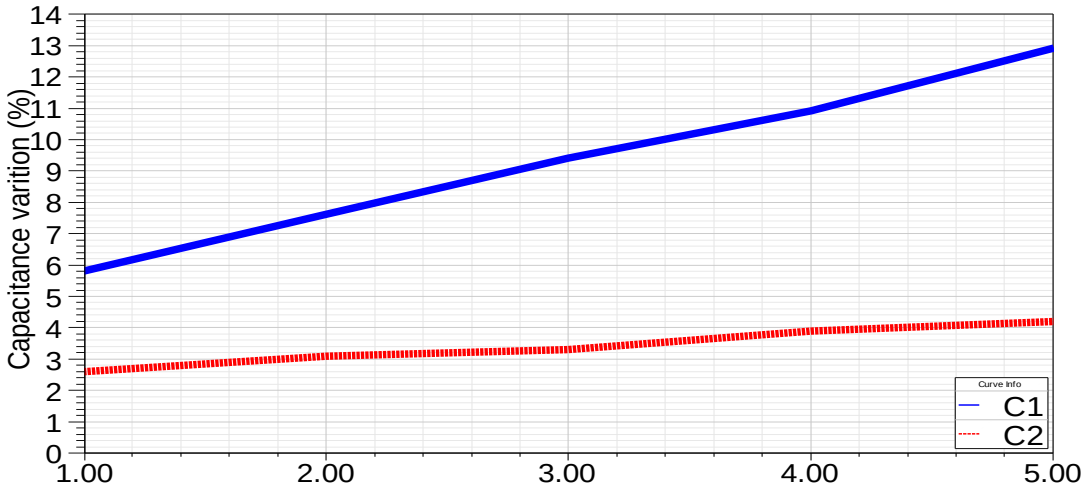

Figure 4-34. Capacitance change of the bushing T-model due to moisture content

Figure 4-35 shows the impact of increasing moisture content on the change of the

total oil capacitance as predicted by the FEA. The figure shows that oil effective capacitance increases with the increase in moisture content in the two types of oil used in the simulation (vegetable and mineral). The increment in vegetable oil capacitance is, however, slightly more than that of mineral oil at the same moisture content. It is worth mentioning that these calculations are conducted based on the assumption that the operating temperature as well as the network frequency are constants.

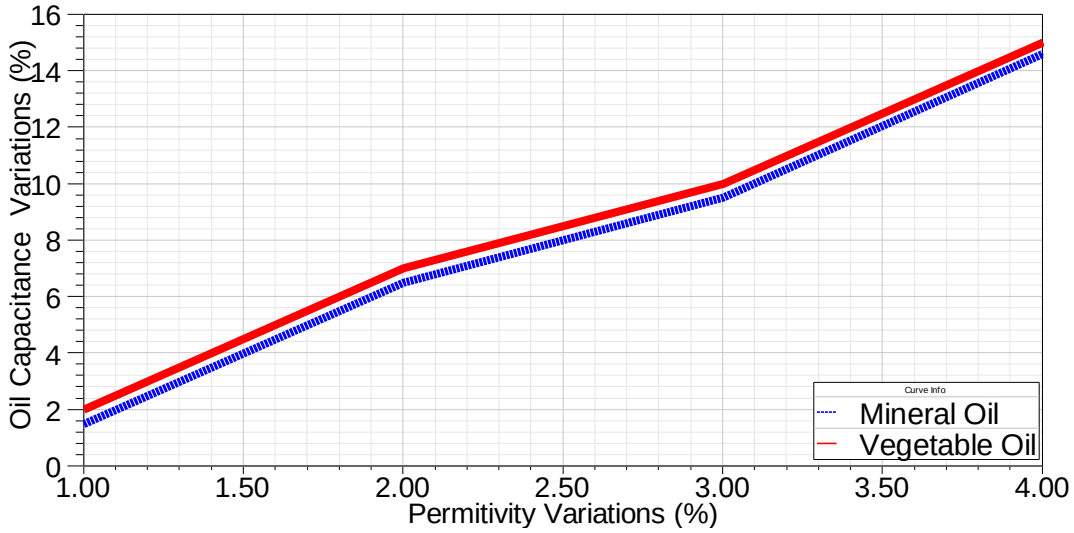

Figure 4-35.Variations in the oil effective capacitance value due to moisture content

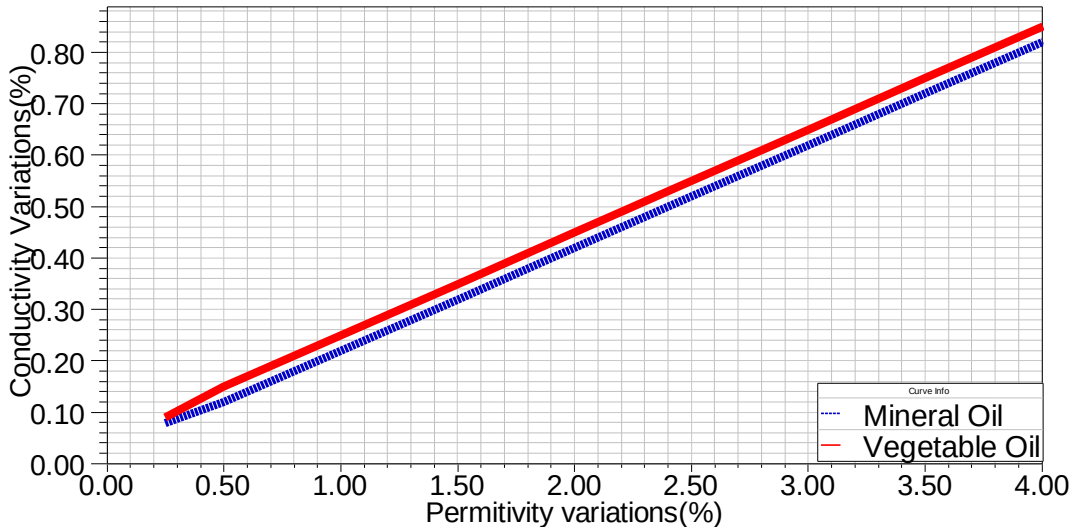

Figure 4-36. Variations in the oil conductivity due to moisture content

Variations in the oil conductivity can be calculated using the DC conduction solver provided by ANSYS as below[120]:

$$J(x,y) = \sigma E(x,y) = -\sigma \nabla \phi(x,y) \tag{41}$$

where J is the current density, E is the electric field intensity, σ is the conductivity of the material (S/m) and ϕ is the electric potential.

Figure 4-36 presents the percentage changes in vegetable and mineral oil conductivity due to the increase in moisture content. Figure 4-36 reveals that the increase in moisture within transformer oil increases its conductivity. Simulation results also show that vegetable oil dielectric strength is slightly more sensitive to moisture content than mineral oil, as can be seen in Figure 4-35and Figure 4-36.

4.7.4 Impact of the Bushing Fault and Oil Degradation on the FRA Signature

To show the impact of a bushing model on the HV winding FRA signature, Figure 4-37 was plotted for the transformer model shown in Figure 4-3(b) with and without the inclusion of the bushing T-model. With the inclusion of the bushing T-model, the transfer function of the transformer produced new resonant peaks after 700 kHz with a slight change in the TF magnitude. On the other hand, the magnitude and the resonant peaks do not change from the low- to mid-frequency range. This is confirmed by the practical test that will be presented in the next section.

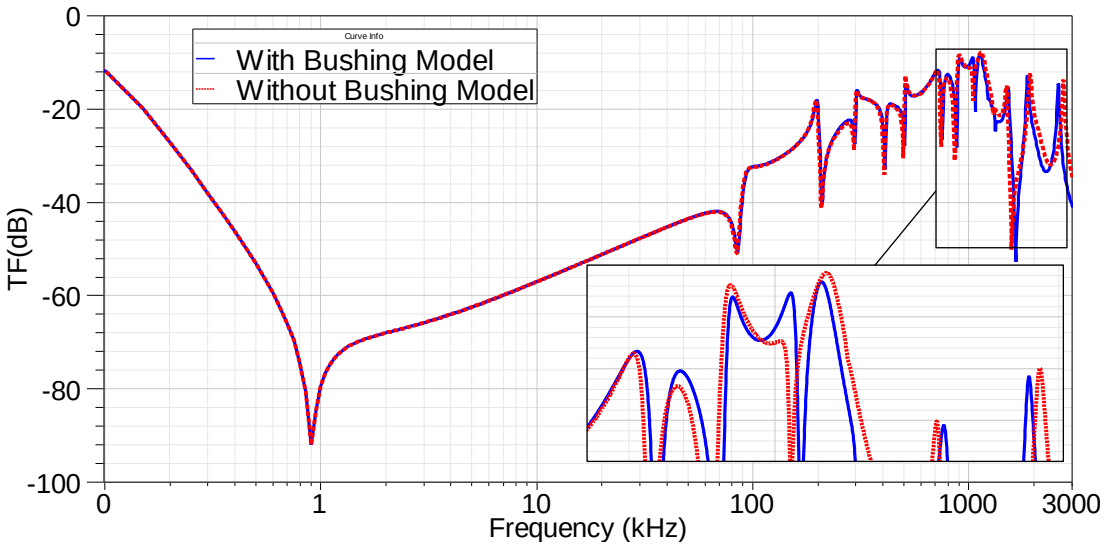

Figure 4-37. FRA signature with and without inclusion of the bushing T-model

The above findings reveal that, for an accurate simulation of transformer FRA signatures, a bushing model should be included in the transformer high-frequency model. The following case studies are conducted using FEA along with the transformer distributed parameters-based equivalent model shown in Figure 4-3 (b) with the inclusion of the bushing T-model as shown in Figure 4-33.

4.7.4.1 Case study 1 (bushing insulation degradation)

Figure 4-38 shows variations in the HV FRA signature for 2% and 4% moisture content (simulated by changing oil/paper permittivity) within the oil and paper of the transformer bushing. The figure shows the impact of the moisture on the FRA signature appears in the frequency range above 700 kHz where the resonance and anti-resonance frequencies along with the peaks alter with respect to the healthy signature. The impact is more pronounced at the high-frequency range and with more moisture content.

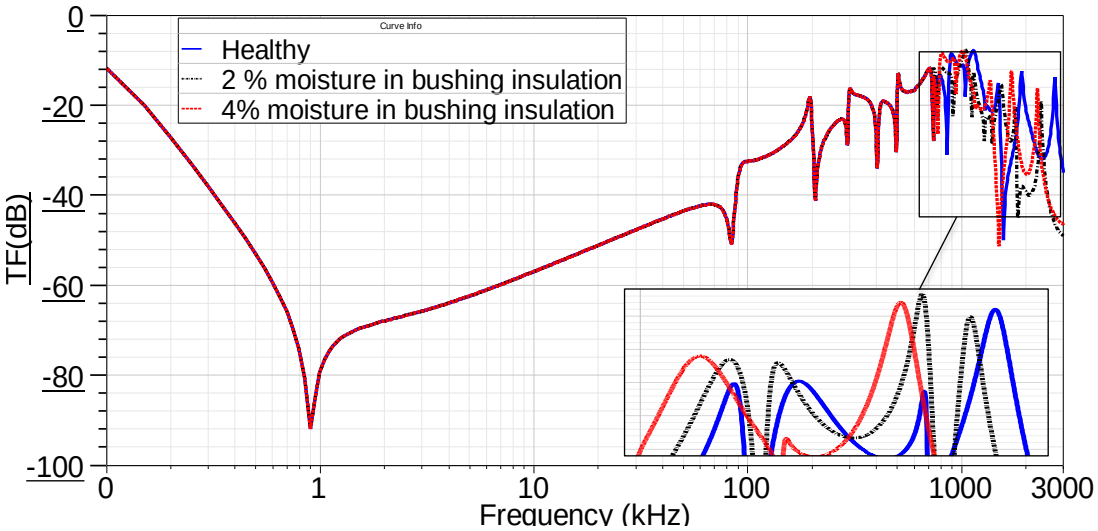

Figure 4-38. Moisture content in bushing insulation effect on FRA test

4.7.4.2 Case study 2 (Transformer oil degradation)

In order to exactly simulate the transformer oil degradation using a transformer distributed parameter model, it is essential to detect the percentage change in the electrical circuit parameters that corresponds to a particular oil degradation level. Figure 4-39 shows the effect of new insulation oil on the transformer FRA signature when compared with the dry transformer FRA signature. As can be seen in Figure 4-39, new insulation oil will shift the resonance peaks to the left on the entire frequency range. This is attributed to the fact that adding insulation oil will increase the overall capacitance and hence reduce the resonance frequencies. The permittivity of the new oil is increased by 4% to simulate moisture content in the oil. As shown in Figure 4-40, oil degradation has a slight impact on the FRA signature from the low to high frequency range.

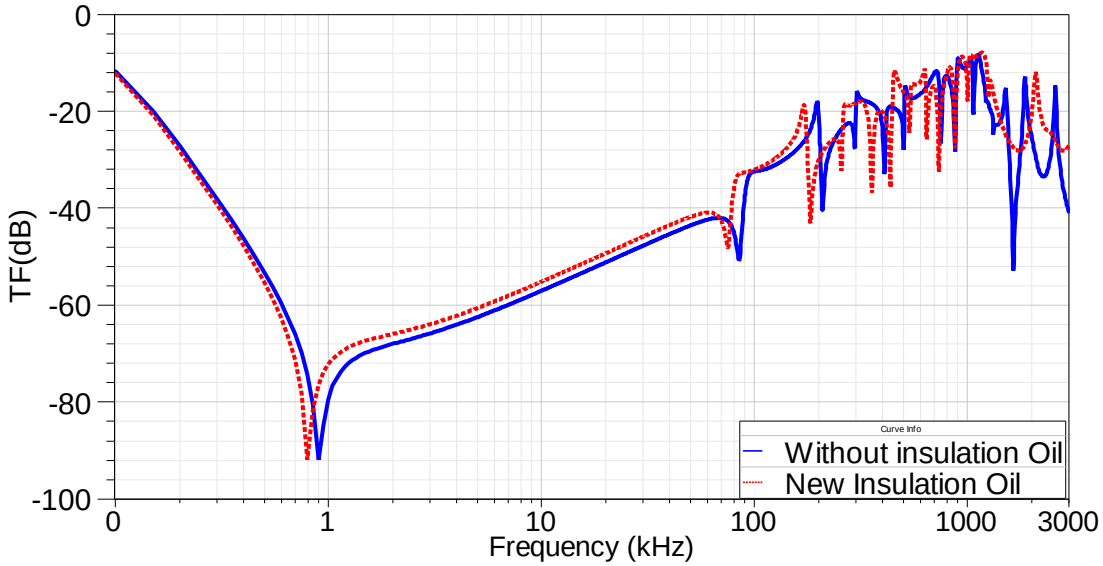

Figure 4-39. FRA signature with and without insulating oil

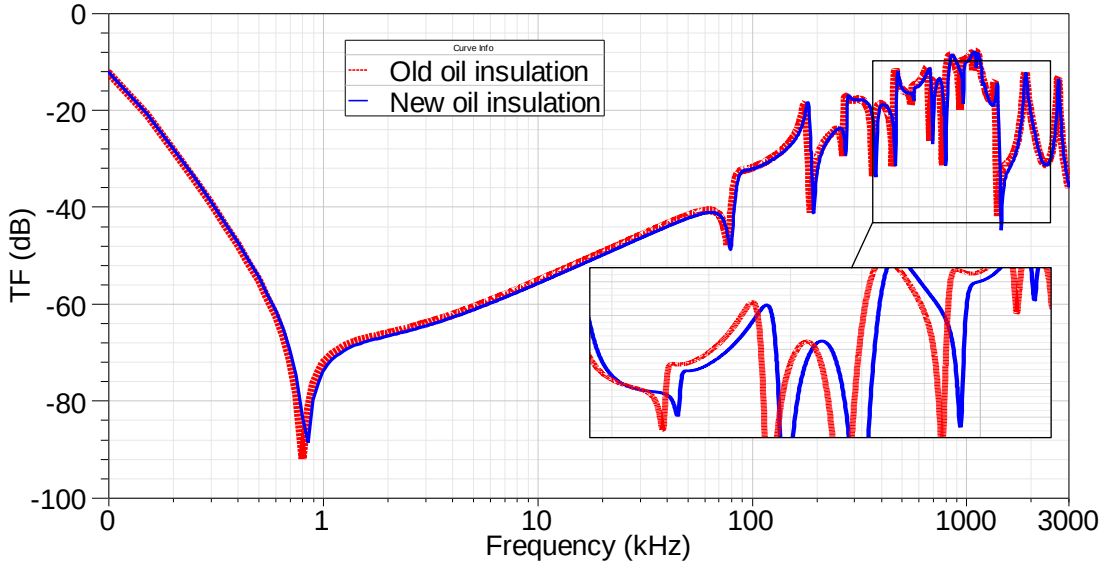

Figure 4-40. Impact of oil degradation on transformer FRA signature

4.7.4.3 Case study 3 (Disk space variation) with bushing model and 3 phase transformer

To show the impact of the consideration of the bushing model in the transformer equivalent circuit, a disk space variation fault is simulated in phase C as shown in Figure 4-41. Finite element calculations reveal that due to disk space variations, the shunt capacitance at the location of the fault and some elements associated with the inductance matrix will change significantly. Table 4.7 and Figure 4-42 show the variations in the resonant peaks with and without the bushing model connected to the distributed parameter transformer model shown in Figure 4-3 (b). Figure 4-42 and

Table 4.7 show that the variations in the resonant peaks start after 300 kHz. Since the T-model adds high capacitance value to the transformer model, the difference between resonant peaks with and without the bushing model increases, particularly in the high-frequency range.

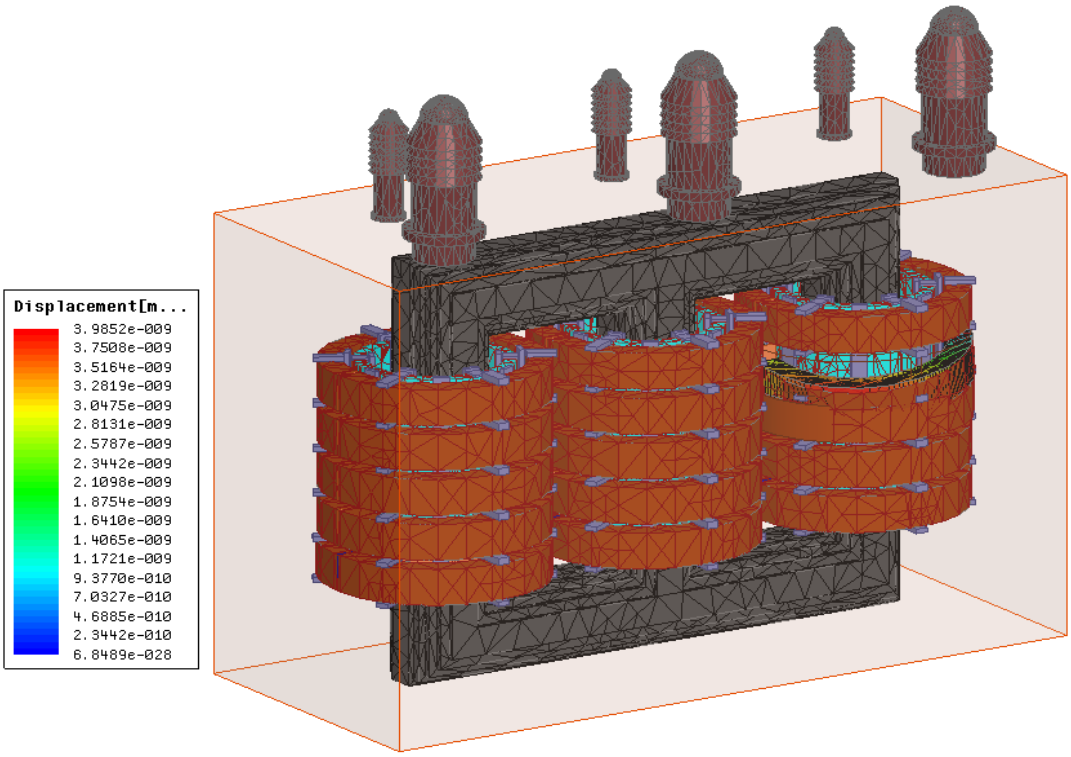

Figure 4-41. Disk space variation fault on Phase C

Table 4.7. Transformer FRA signature for disk space variation fault with and without a bushing model

Resonance Frequencies (Normal Condition; kHz)	***Δf FRA signature; kHz***	
	Without Bushing	With Bushing
330	+1.2	+ 1.6
380	+2.3	+ 2.8
752	-6.8	-7.6
986	-26.6	-31.6
1232	-32.5	-43.6
1745	-40.6	-56.2
2890	-69.3	- 78.3

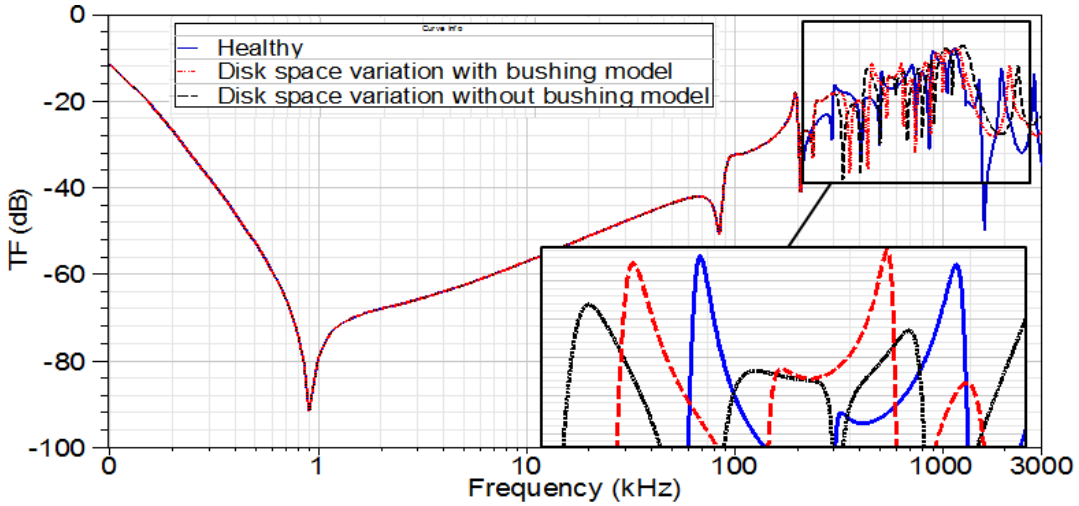

Figure 4-42 Impact of Disk space variations on the FRA signature with and without the bushing model (add square to zoned range)

4.8 EXPERIMENTAL RESULTS

To assess the accuracy of the proposed bushing model, the simulation results obtained as shown above are compared with a practical FRA signature. Measurements were conducted on three-phase 132kV, 35MVA power transformers at an ambient temperature of 25^{o} C. The FRA signature for phase A with and without the bushing is obtained using a frequency response analyser as shown in Figure 4-43 which reveals the impact of the bushing on the transformer FRA signature in the high-frequency range. This confirms the simulation results of Figure 4-37.

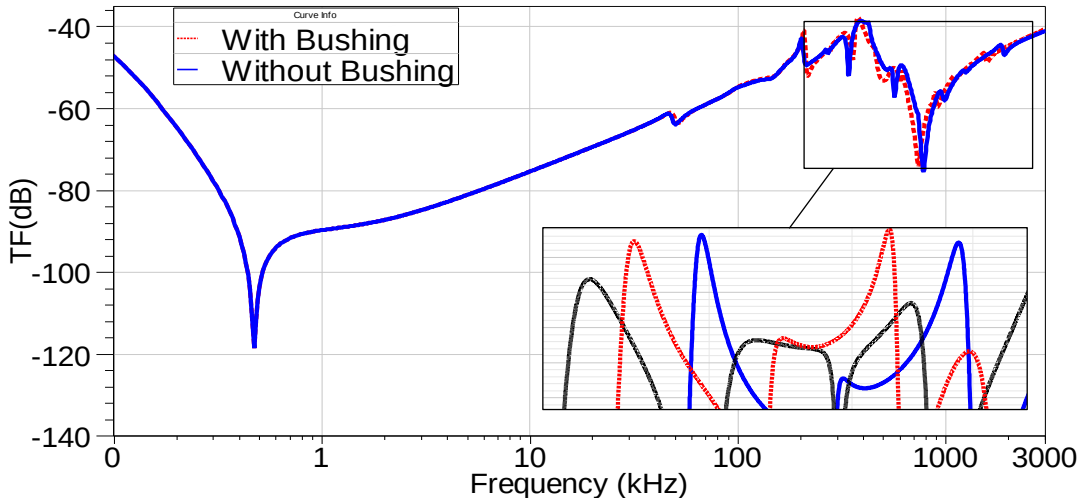

Figure 4-43. Practical FRA signatures with and without the bushing

The transformer bushing oil was tested and a moisture content of 3% was found in the Phase-A HV bushing. A FRA measurement was conducted on this phase and was compared with the same phase FRA signature with new oil to assess the impact of moisture content on the transformer's FRA signature. As shown in Figure 4-44, resonant peaks in the high-frequency range above 700 kHz shift to the left due to the existence of moisture in the bushing insulation oil. This aligns well with the FEM simulation shown in Figure 4-38.

To investigate the impact of insulating oil on the FRA signature, a FRA measurement is conducted on Phase A of the transformer with, and without, new insulation oil as shown in Figure 4-45. The FRA signature measured reveals that the whole frequency range varies due to the change in the total capacitance matrices as resonance peaks shift to the left. This is similar to the simulation results obtained in Figure 4-39 and the practical test presented in [1].

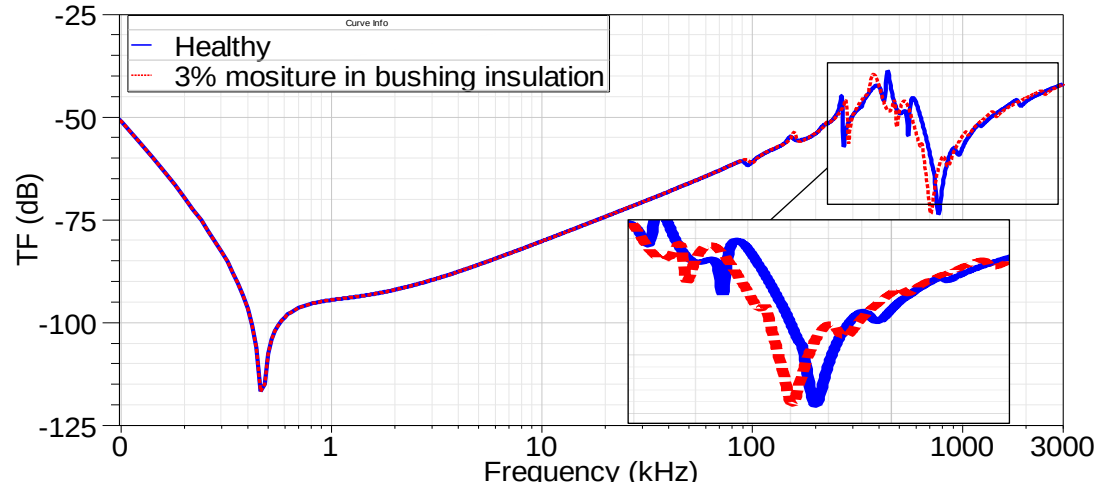

Figure 4-44. Practical FRA signature with 2 healthy conditions of insulating oil

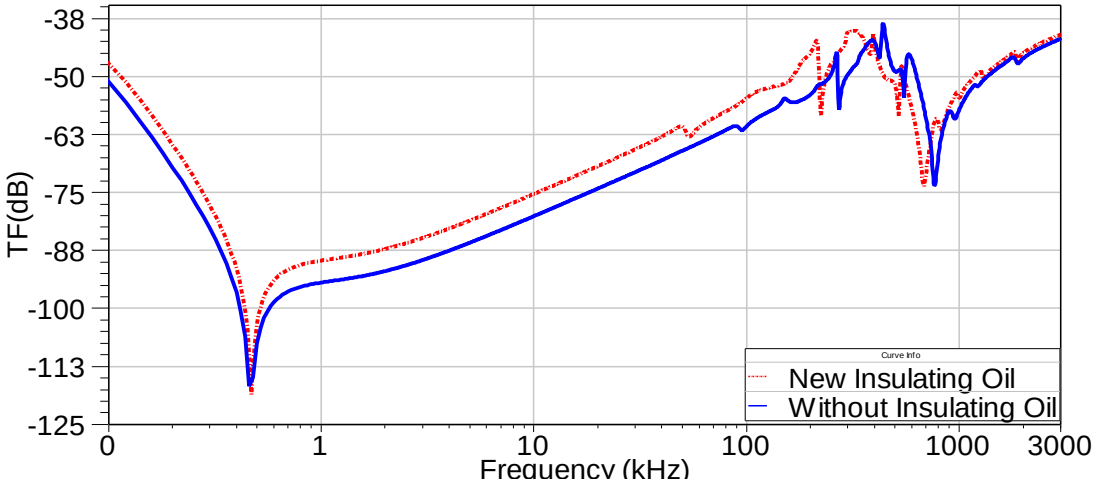

Figure 4-45. Practical FRA signature with and without insulating oil

5. CONCLUSION

The main aim of this thesis is to find the most appropriate technique to model high frequency power transformers in order to calculate internal stresses and effect of winding deformations using frequency response analysis (FRA) technique. FRA is a quite new diagnostic technique to detect the mechanical damages to transformer windings. This technique can be performed without opening the transformer tank which prevents the further damage to the insulation and windings. FRA is an offline test and is used to measure the input/output relationship as a function of frequency. This provides a fingerprint of a transformer which can be compared with a transformer future signature for fault diagnosis. The FRA technique calls for trained personnel to conduct the test and interpret its results for fault identification and quantification. Another drawback of the FRA test is that the transformer has to be de-energized and switched out of service causing severe interruption to the electricity grid.

Transformer modelling should support the real transformer geometry based on construction information from the manufacturer. In addition, the model should have the capability to compute the internal and external resonances due to bushing and leads.

In terms of computing the magnetic parameters accurately, a suitable and accurate representation of the iron-core is very vital. The computation of self- and mutual inductances depends on a precise description of the frequency-dependent behaviour of the core.

Based on the simulation results presented in this work, the following conclusions can be drawn:

1. Simple, analytical approaches based on transformer construction cannot be applied to establish a comprehensive high-frequency power transformer model .Since applying physical faults on the real transformer windings is very difficult and not applicable everywhere, the FEM can be used as an accurate and sophisticated method in its place. In comparison with a simple numerical method, the FEM increases the coherence of measurement results since a more accurate implementation of design details can be included, such

as properties of the materials for the windings and core as well as temperature.

2. This study introduces effective charts that correlate the percentage changes in each electrical parameter with various mechanical fault levels. This facilitates a precise simulation of mechanical failures using transformer equivalent circuits and the quantification analysis of the FRA signature.

3. FRA sensitivities are established for buckling deformations (free and forced) and axial displacements. Buckling deformations are heavily dependent on the shape of capacitance and inductance elements variations and accurate buckling deformations can be emulated by using the transformer equivalent circuit model. In addition, other previous studies [2, 85, 149] neglected the variations in capacitance elements in simulating transformer winding axial displacements. However, the FEM results showed that by considering capacitance and inductance element variations, accurate axial displacements can be emulated on the transformer lumped parameters model of deformation. In contrast to other previous studies that neglected the variations in inductance elements in simulating transformer winding radial deformations, the results of finite element analysis show them clearly.

4. This study shows that the percentage changes in the electrical parameters due to radial deformations are almost independent on the fault location. The shift in the entire frequency range of the FRA signature can be used as an index for the detection of the radial deformation and the amount of change is correlated to the severity of the fault level. Axial displacement causes the shift in resonance frequencies over 100 kHz to the high-frequency range. The FRA signature obtained from simulation coincides with the FRA signature obtained from practical measurements [10, 57].

5. Transformer sizing has a slight impact on the change in the electrical parameters due to different axial fault levels and can be overlooked.

6. Disk space variations significantly affect the series capacitance of the transformer equivalent electrical model and hence their impact on the FRA signature is seen in the high-frequency range. Disk space fault locations have

different impact on the FRA signature. Disk space variations are obviously detectable independently of their position within the winding because the magnetic behaviour is altered.

7. Core deformation changing winding inductance and its impact are shown in the low-frequency range of the FRA signature.

8. This study discussed the detection mechanism of the FRA method on bushing insulation through simulation and experiments. In contrast with other studies, where the bushing model is not considered for the FRA test, this study showed that the bushing model should be added to the transformer linear model for the purposes of the FRA test. It showed that the bushing model has an effect on the FRA signature and causes the variations in peak resonances from the medium- to high-frequency ranges and found that the frequency response is a capacitive characteristic curve.

9. In addition, the permittivity of dielectric materials and transformer oil is intensely affected by frequency, moisture, and temperature. Aging affects the high-frequency characteristics of transformer oil strongly. The impact of moisture content on the frequency response analysis of the transformer winding was investigated in detail. This study showed that transformer moisture deviation can affect the FRA trace variation significantly. It is clear that the moisture content in the oil insulation would result in the local resonances of the FRA signature moving horizontally from high-frequency range towards the low-frequency range. The finite element analysis showed that changes of moisture in the oil insulation significantly affect the transformer winding shunt and series capacitances. The result obtained by the simulation is confirmed by the practical test. It can be concluded that the FRA test can provide very significant information on moisture variations in the oil insulation and the bushing insulation.

5.1 FURTHER WORK

The following research avenues are suggested for future study in continuation of this work.

1. As the FRA test is an offline test and it has some disadvantages such as shutting down the transformer from the network which is very costly, the further research can be performed on On-line FRA test while the transformer is energized. FRA is an offline test based on the measurement of the impedance, admittance or transfer function of a particular phase as a function of a wide frequency range which is used as a transformer fingerprint that can be compared with its previous signatures to detect any winding displacements [8]. Although FRA is a powerful diagnostic tool for detecting winding deformation, its offline nature and reliance on graphical analysis are considered as the main drawbacks;
2. Several of the studied electromagnetic disturbances that impact transformers such as inrush, harmonic distortion and unbalanced operation are also known to affect transformer performance adversely. This should be further investigated through online condition monitoring. This can be done by investigating on online transformer internal fault detection technique and examining impact of harmonics through detailed nonlinear simulation of a transformer using three-dimensional finite element modelling.
3. Although FRA is a powerful method to detect mechanical faults within the windings, it cannot show the location of fault within the windings. This can be further investigation for using FRA test to show the location of fault within the windings. There is possibility to indicate the location of fault by using the information from the different resonance-frequencies in a voltage-ratio measurement or an admittance measurement. Since some of the resonances change less than others at certain types of faults, it gives an indication of the influence of each resonance.

REFERENCES

[1] M. Bagheri, B. T. Phung, and T. Blackburn, "Influence of temperature and moisture content on frequency response analysis of transformer winding," *Dielectrics and Electrical Insulation, IEEE Transactions on*, vol. 21, pp. 1393-1404, 2014.

[2] E. Rahimpour, J. Christian, K. Feser, and H. Mohseni, "Transfer function method to diagnose axial displacement and radial deformation of transformer windings," *Power Delivery, IEEE Transactions on*, vol. 18, pp. 493-505, 2003.

[3] V. Behjat and M. Mahvi, "Statistical approach for interpretation of power transformers frequency response analysis results," *Science, Measurement & Technology, IET*, vol. 9, pp. 367-375, 2015.

[4] J. C. Gonzales Arispe and E. E. Mombello, "Detection of Failures Within Transformers by FRA Using Multiresolution Decomposition," *Power Delivery, IEEE Transactions on*, vol. 29, pp. 1127-1137, 2014.

[5] W. Herrera Portilla, G. Aponte Mayor, J. Pleite Guerra, and C. Gonzalez-Garcia, "Detection of Transformer Faults Using Frequency-Response Traces in the Low-Frequency Bandwidth," *Industrial Electronics, IEEE Transactions on*, vol. 61, pp. 4971-4978, 2014.

[6] C. A2.26, "Mechanical Condition Assessment of Transformer Windings Using Frequency Response Analysis (FRA)," CIGRE Brochure 3422008.

[7] R. P. Jackson, "Recent Investigation of Lightning Protective Apparatus," *American Institute of Electrical Engineers, Transactions of the*, vol. XXV, pp. 881-900, 1906.

[8] D. A. K. Pham, T. M. T. Pham, H. Borsi, and E. Gockenbach, "A new diagnostic method to support standard frequency response analysis assessments for diagnostics of transformer winding mechanical failures," *Electrical Insulation Magazine, IEEE*, vol. 30, pp. 34-41, 2014.

[9] Z. W. Zhang, W. H. Tang, T. Y. Ji, and Q. H. Wu, "Finite-Element Modeling for Analysis of Radial Deformations Within Transformer Windings," *Power Delivery, IEEE Transactions on*, vol. 29, pp. 2297-2305, 2014.

[10] E. Rahimpour, M. Jabbari, and S. Tenbohlen, "Mathematical Comparison Methods to Assess Transfer Functions of Transformers to Detect Different Types of Mechanical Faults," *Power Delivery, IEEE Transactions on*, vol. 25, pp. 2544-2555, 2010.

[11] A. Abu-Siada and S. Islam, "A Novel Online Technique to Detect Power Transformer Winding Faults," *Power Delivery, IEEE Transactions on*, vol. 27, pp. 849-857, 2012.

[12] B. K. Gupta, J. Densley, and A. Narang, "Diagnostic Practices Used For Instrument Transformers," in *Electrical Insulation, 2008. ISEI 2008. Conference Record of the 2008 IEEE International Symposium on*, 2008, pp. 239-242.

[13] B. K. Gupta, J. Densley, and A. Narang, "Review of diagnostic techniques for oil-paper insulated instrument transformers," in *Electrical Insulation (ISEI), Conference Record of the 2010 IEEE International Symposium on*, 2010, pp. 1-5.

[14] B. H. Ward and S. Lindgren, "A survey of developments in insulation monitoring of power transformers," in *Electrical Insulation, 2000. Conference Record of the 2000 IEEE International Symposium on*, 2000, pp. 141-147.

[15] W. Zhongdong, W. Xin, Y. Xiao, L. Sitao, and J. V. Hinshaw, "Gas generation in natural ester and mineral oil under partial discharge and sparking faults," *Electrical Insulation Magazine, IEEE*, vol. 29, pp. 62-70, 2013.

[16] A. Santosh Kumar, R. P. Gupta, K. Udayakumar, and A. Venkatasami, "Online partial discharge detection and location techniques for condition monitoring of power transformers: A review," in *Condition Monitoring and Diagnosis, 2008. CMD 2008. International Conference on*, 2008, pp. 927-931.

[17] M. Stace and S. M. Islam, "Condition monitoring of power transformers in the Australian State of New South Wales using transfer function measurements," in *Properties and Applications of Dielectric Materials, 1997., Proceedings of the 5th International Conference on*, 1997, pp. 248-251 vol.1.

[18] N. Tapsi and S. Yaduvir, "Condition Monitoring and Diagnostics of Power Transformers Using WSNs," in *Computational Intelligence and Communication Networks (CICN), 2011 International Conference on*, 2011, pp. 274-278.

[19] H. Yann-Chang and H. Chao-Ming, "Evolving wavelet networks for power transformer condition monitoring," *Power Delivery, IEEE Transactions on*, vol. 17, pp. 412-416, 2002.

[20] Go, x, N. A. mez, H. M. Wilhelm, C. C. Santos, and G. B. Stocco, "Dissolved gas analysis (DGA) of natural ester insulating fluids with different chemical compositions," *Dielectrics and Electrical Insulation, IEEE Transactions on*, vol. 21, pp. 1071-1078, 2014.

[21] M. A. Elborki, P. A. Crossley, Z. D. Wang, A. Darwin, and G. Edwards, "Detection and characterisation of partial discharges in transformer defect models," in *Power Engineering Society Summer Meeting, 2002 IEEE*, 2002, pp. 405-410 vol.1.

[22] M. D. Judd, S. D. J. McArthur, J. R. McDonald, and O. Farish, "Intelligent condition monitoring and asset management. Partial discharge monitoring for power transformers," *Power Engineering Journal*, vol. 16, pp. 297-304, 2002.

[23] A. Akbari, P. Werle, H. Borsi, and E. Gockenbach, "Transfer function-based partial discharge localization in power transformers: a feasibility study," *Electrical Insulation Magazine, IEEE*, vol. 18, pp. 22-32, 2002.

[24] M. D. Judd, Y. Li, and I. B. B. Hunter, "Partial discharge monitoring for power transformer using UHF sensors. Part 2: field experience," *Electrical Insulation Magazine, IEEE*, vol. 21, pp. 5-13, 2005.

[25] M. S. Naderi, M. Vakilian, T. R. Blackburn, B. T. Phung, M. S. Naderi, and A. Nasiri, "A hybrid transformer model for determination of partial discharge location in transformer winding," *Dielectrics and Electrical Insulation, IEEE Transactions on*, vol. 14, pp. 436-443, 2007.

[26] T. V. Oommen and S. R. Lindgren, "Streaming electrification study of transformer insulation system using a paper tube model," *Power Delivery, IEEE Transactions on*, vol. 5, pp. 972-983, 1990.

[27] R. Sarathi and G. Koperundevi, "Investigation of partial discharge activity of single conducting particle in transformer oil under DC voltages using UHF technique," *Science, Measurement & Technology, IET*, vol. 3, pp. 325-333, 2009.

[28] K. Spurgeon, W. H. Tang, Q. H. Wu, Z. J. Richardson, and G. Moss, "Dissolved gas analysis using evidential reasoning," *Science, Measurement and Technology, IEE Proceedings*, vol. 152, pp. 110-117, 2005.

[29] H. Yann-Chang and S. Huo-Ching, "Dissolved gas analysis of mineral oil for power transformer fault diagnosis using fuzzy logic," *Dielectrics and Electrical Insulation, IEEE Transactions on*, vol. 20, pp. 974-981, 2013.

[30] W. G. Ariastina, I. A. D. Giriantari, I. K. Solin, and O. Yolanda, "Condition monitoring of power transformer: A field experience," in *Properties and Applications of Dielectric Materials, 2009. ICPADM 2009. IEEE 9th International Conference on the*, 2009, pp. 1051-1054.

[31] S. Ji, Y. Luo, and Y. Li, "Research on extraction technique of transformer core fundamental frequency vibration based on OLCM," *Power Delivery, IEEE Transactions on*, vol. 21, pp. 1981-1988, 2006.

[32] S. Ji, P. Shan, Y. Li, D. Xu, and J. Cao, "The vibration measuring system for monitoring core and winding condition of power transformer," in *Electrical Insulating Materials, 2001. (ISEIM 2001). Proceedings of 2001 International Symposium on*, 2001, pp. 849-852.

[33] K. Hiraishi, Y. Hori, and S. Shida, "Mechanical Strength of Transformer Windings Under Short-Circuit Conditions," *Power Apparatus and Systems, IEEE Transactions on*, vol. PAS-90, pp. 2381-2390, 1971.

[34] K. Hong, H. Huang, J. Zheng, J. Zhou, Y. Zhou, and J. Liu, "Time-frequency analysis for power transformer fault detection using vibration method," in *Industrial Electronics and Applications (ICIEA), 2014 IEEE 9th Conference on*, 2014, pp. 2110-2114.

[35] K. Hong and Z. Pan, "Vibration model of power transformer under short-circuit condition," in *Electrical Machines and Systems, 2009. ICEMS 2009. International Conference on*, 2009, pp. 1-5.

[36] E. Rivas, J. C. Burgos, Garci, x, and J. C. a-Prada, "Vibration Analysis Using Envelope Wavelet for Detecting Faults in the OLTC Tap Selector," *Power Delivery, IEEE Transactions on*, vol. 25, pp. 1629-1636, 2010.

[37] F. H. Wang and Z. J. Jin, "Using the vibration frequency response analysis method to detect the winding deformation of power transformer," in *Power and Energy Society General Meeting, 2011 IEEE*, 2011, pp. 1-6.

[38] F. H. Wang, J. Xu, Z. J. Jin, and S. S. Gui, "Experimental research of vibration sweep frequency response analysis to detect the winding deformation of power transformer," in *Transmission and Distribution Conference and Exposition, 2010 IEEE PES*, 2010, pp. 1-6.

[39] T.-T. He, J.-D. Wang, J. Guo, H. Huang, X.-x. Chen, and J. Pan, "A Vibration Based

Condition Monitoring System for Power Transformers," in *Power and Energy Engineering Conference, 2009. APPEEC 2009. Asia-Pacific*, 2009, pp. 1-4.

[40] B. S. Munir, J. J. Smit, and I. G. M. R. Rinaldi, "Diagnosing winding and core condition of power transformer by vibration signal analysis," in *Condition Monitoring and Diagnosis (CMD), 2012 International Conference on*, 2012, pp. 429-432.

[41] S. Borucki, T. Boczar, P. Fracz, and D. Zmarzly, "Diagnostics of power transformers cores using a modified vibroacoustic method," in *Electrical Insulation (ISEI), Conference Record of the 2012 IEEE International Symposium on*, 2012, pp. 179-183.

[42] A. Abu-Siada, S. Hmood, and S. Islam, "A new fuzzy logic approach for consistent interpretation of dissolved gas-in-oil analysis," *Dielectrics and Electrical Insulation, IEEE Transactions on*, vol. 20, pp. 2343-2349, 2013.

[43] A. Abu-Siada and S. Islam, "A new approach to identify power transformer criticality and asset management decision based on dissolved gas-in-oil analysis," *Dielectrics and Electrical Insulation, IEEE Transactions on*, vol. 19, pp. 1007-1012, 2012.

[44] S. Mofizul Islam, T. Wu, and G. Ledwich, "A novel fuzzy logic approach to transformer fault diagnosis," *Dielectrics and Electrical Insulation, IEEE Transactions on*, vol. 7, pp. 177-186, 2000.

[45] N. A. Muhamad, B. T. Phung, and T. R. Blackburn, "Dissolved gas analysis for common transformer faults in soy seed-based oil," *Electric Power Applications, IET*, vol. 5, pp. 133-142, 2011.

[46] A. Shintemirov, W. Tang, and Q. H. Wu, "Power Transformer Fault Classification Based on Dissolved Gas Analysis by Implementing Bootstrap and Genetic Programming," *Systems, Man, and Cybernetics, Part C: Applications and Reviews, IEEE Transactions on*, vol. 39, pp. 69-79, 2009.

[47] A. K. Mehta, R. N. Sharma, S. Chauhan, and S. Saho, "Transformer diagnostics under dissolved gas analysis using Support Vector Machine," in *Power, Energy and Control (ICPEC), 2013 International Conference on*, 2013, pp. 181-186.

[48] S. Singh and M. N. Bandyopadhyay, "Dissolved gas analysis technique for incipient fault diagnosis in power transformers: A bibliographic survey," *Electrical Insulation Magazine, IEEE*, vol. 26, pp. 41-46, 2010.

[49] Y. Wang, F. Lu, and H. Li, "The fault diagnosis method for electrical equipment based on Bayesian network," in *Electrical Machines and Systems, 2005. ICEMS 2005. Proceedings of the Eighth International Conference on*, 2005, pp. 2259-2261 Vol. 3.

[50] L. Ming-Jong and Y. Chao-Tang, "A Pragmatic Approach to Diagnose on Transformer's Insulating Oil with Gas Pattern," in *Computer, Consumer and Control (IS3C), 2014 International Symposium on*, 2014, pp. 1002-1005.

[51] S. S. Patil and S. E. Chaudhari, "An Attempt to Investigate the Transformer Failure by using DGA and SFRA Analysis," in *Properties and Applications of Dielectric Materials (ICPADM), 2012 IEEE 10th International Conference on the*, 2012, pp. 1-4.

[52] A. A. Suleiman, N. A. Mohamad, N. Bashir, A. S. AlGhamdi, and M. Aizam, "Improving accuracy of DGA interpreation of oil-filled power transformers needed for effective condition monitoring," in *Condition Monitoring and Diagnosis (CMD), 2012 International Conference on*, 2012, pp. 374-378.

[53] M. A. B. Amora, O. M. Almeida, A. P. S. Braga, F. R. Barbosa, L. A. C. Lisboa, and R. S. T. Pontes, "Improved DGA method based on rules extracted from high-dimension input space," *Electronics Letters*, vol. 48, pp. 1048-1049, 2012.

[54] ABB, *ABB Transformer hand book*. switzerland, 2009.

[55] F. L. Dixon, D. Steward, and J. Hoffmeister, "When to replace aging transformers," in *Petroleum and Chemical Industry Conference (PCIC), 2010 Record of Conference Papers Industry Applications Society 57th Annual*, 2010, pp. 1-14.

[56] E. T. Norris, "Mechanical strength of power transformers in service," *Proceedings of the IEE - Part A: Power Engineering*, vol. 104, pp. 289-300, 1957.

[57] K. Pourhossein, G. B. Gharehpetian, and E. Rahimpour, "Buckling severity diagnosis in power transformer windings using Euclidean Distance classifier," in *Electrical Engineering (ICEE), 2011 19th Iranian Conference on*, 2011, pp. 1-1.

[58] A. Bakshi and S. V. Kulkarni, "Analysis of Buckling Strength of Inner Windings in Transformers Under Radial Short-Circuit Forces," *Power Delivery, IEEE Transactions on*, vol. 29, pp. 241-245, 2014.

[59] L. Qingmin, Z. Tong, Z. Li, and J. Lou, "Mechanical Fault Diagnostics of Onload Tap Changer Within Power Transformers Based on Hidden Markov Model," *Power Delivery,*

IEEE Transactions on, vol. 27, pp. 596-601, 2012.
[60] E. Bjerkan, "High frequency modeling of power transformers stresses and diagnostics," Doctoral Thesis for the degree of Doctor Ingeniør, Trondheim, 2005.
[61] A. Hyun-Mo, L. Ji-Yeon, K. Joong-Kyoung, O. Yeon-Ho, J. Sang-Yong, and H. Sung-Chin, "Finite-Element Analysis of Short-Circuit Electromagnetic Force in Power Transformer," *Industry Applications, IEEE Transactions on*, vol. 47, pp. 1267-1272, 2011.
[62] P. S. Moses, M. A. S. Masoum, and H. A. Toliyat, "Dynamic Modeling of Three-Phase Asymmetric Power Transformers With Magnetic Hysteresis: No-Load and Inrush Conditions," *Energy Conversion, IEEE Transactions on*, vol. 25, pp. 1040-1047, 2010.
[63] P. S. Moses and M. A. S. Masoum, "Three-Phase Asymmetric Transformer Aging Considering Voltage-Current Harmonic Interactions, Unbalanced Nonlinear Loading, Magnetic Couplings, and Hysteresis," *Energy Conversion, IEEE Transactions on*, vol. 27, pp. 318-327, 2012.
[64] M. Arshad, S. M. Islam, and A. Khaliq, "Power transformer aging and life extension," in *Probabilistic Methods Applied to Power Systems, 2004 International Conference on*, 2004, pp. 498-501.
[65] P. Li, B.-h. Zhang, Z.-g. Hao, X.-j. Hu, and Y.-l. Chu, "Research on Monitoring of Winding Deformation of Power Transformer by On-line Parameter Estimation about Leakage Inductance," in *Power System Technology, 2006. PowerCon 2006. International Conference on*, 2006, pp. 1-6.
[66] S. Santhi, S. Jayalalitha, V. J. Kumar, and V. Jayashankar, "Detection of Winding Deformations During Short Time Current Tests," in *Instrumentation and Measurement Technology Conference, 2005. IMTC 2005. Proceedings of the IEEE*, 2005, pp. 203-208.
[67] L. Xiaodong, A. El-Kadri, J. Stevens, and R. Adedun, "Frequency Response Analysis for Phase-Shifting Transformers in Oil Field Facilities," *Industry Applications, IEEE Transactions on*, vol. 50, pp. 2861-2870, 2014.
[68] N. Abeywickrama, Y. V. Serdyuk, and S. M. Gubanski, "High-Frequency Modeling of Power Transformers for Use in Frequency Response Analysis (FRA)," *Power Delivery, IEEE Transactions on*, vol. 23, pp. 2042-2049, 2008.
[69] E. P. Dick, C. C. Erven, and S. M. Harvey, "Grounding System Tests for Analysis of Fault-Induced Voltages on Communication Cables," *Power Apparatus and Systems, IEEE Transactions on*, vol. PAS-98, pp. 2115-2125, 1979.
[70] R. Malewski and B. Poulin, "Impulse testing of power transformers using the transfer function method," *Power Delivery, IEEE Transactions on*, vol. 3, pp. 476-489, 1988.
[71] C. A2.26, "Mechanical Condition Assessment of Transformer Windings Using Frequency Response Analysis (FRA)," CIGRE Brochure 342April 2008.
[72] K. Kre , König, D., "Comparison of measured resonance frequencies of coilsat sinusoidal and impulse voltage excitation," *Proc. of the 7th Int. Symp. on High Voltage Engineering (ISH 1991), Technische universität Dresden*, August 26-30,1991.
[73] S. Tenbohlen, Ryder, S.A.,, "Making Frequency Response Analysis Measurements: A Comparison of the Swept Frequency and Low Voltage Impulse Methods," *Proc. of the 13th Int. Symp. on High-Voltage Engineering(ISH2003)*, Netherlands 2003.
[74] K. G. N. B. Abeywickrama, Y. V. Serdyuk, and S. M. Gubanski, "Exploring possibilities for characterization of power transformer insulation by frequency response analysis (FRA)," *Power Delivery, IEEE Transactions on*, vol. 21, pp. 1375-1382, 2006.
[75] A. Abu-Siada, N. Hashemnia, S. Islam, and M. A. S. Masoum, "Understanding power transformer frequency response analysis signatures," *Electrical Insulation Magazine, IEEE*, vol. 29, pp. 48-56, 2013.
[76] H. Firoozi, M. Kharezi, H. Rahimpour, and M. Shams, "Transformer Fault Diagnosis Using Frequency Response Analysis - Practical Studies," in *Power and Energy Engineering Conference (APPEEC), 2011 Asia-Pacific*, 2011, pp. 1-4.
[77] S. D. Mitchell, J. S. Welsh, and B. T. Phung, "Relating a distribution transformer's connection topology and the influence of inductive disparity to the observed frequency response," in *Power Engineering Conference, 2008. AUPEC '08. Australasian Universities*, 2008, pp. 1-6.
[78] S. D. Mitchell and J. S. Welsh, "Modeling Power Transformers to Support the Interpretation of Frequency-Response Analysis," *Power Delivery, IEEE Transactions on*, vol. 26, pp. 2705-2717, 2011.
[79] S. D. Mitchell and J. S. Welsh, "The Influence of Complex Permeability on the Broadband Frequency Response of a Power Transformer," *Power Delivery, IEEE Transactions on*, vol.

25, pp. 803-813, 2010.
[80] S. A. Ryder, "Diagnosing transformer faults using frequency response analysis," *Electrical Insulation Magazine, IEEE*, vol. 19, pp. 16-22, 2003.
[81] E. Bjerkan and H. K. Høidalen, "High frequency FEM-based power transformer modeling: Investigation of internal stresses due to network-initiated overvoltages," *Electric Power Systems Research*, vol. 77, pp. 1483-1489, 2007.
[82] T. Leibfried and K. Feser, "Off-line- and on-line-monitoring of power transformers using the transfer function method," in *Electrical Insulation, 1996., Conference Record of the 1996 IEEE International Symposium on*, 1996, pp. 34-37 vol.1.
[83] T. Leibfried and K. Feser, "Monitoring of power transformers using the transfer function method," *Power Delivery, IEEE Transactions on*, vol. 14, pp. 1333-1341, 1999.
[84] J. Christian, " Erkennung mechanischer Wicklungsschäden inTransformatoren mit der Übertragungsfunktion " Dissertation, ISBN 3-8322-0480-6 ,University of Stuttgart, 2001.
[85] J. Christian and K. Feser, "Procedures for detecting winding displacements in power transformers by the transfer function method," *Power Delivery, IEEE Transactions on*, vol. 19, pp. 214-220, 2004.
[86] E. Rahimpour, "Hochfrequente Modellierung von Transformatoren zur Berechnung der Übertragungsfunktion, ," Dissertation, ISBN 3-8265-9227-1, University of Stuttgart, 2001.
[87] M. Bigdeli, M. Vakilian, and E. Rahimpour, "Transformer winding faults classification based on transfer function analysis by support vector machine," *Electric Power Applications, IET*, vol. 6, pp. 268-276, 2012.
[88] M. J. Pykälä, "Transfer Function as a Diagnostic Tool in Testing of Power and Distribution Transformers, Report TKK-SJT-68, ISBN 951-22-6905-8, Helsinki University of Technology, High Voltage Institute,," Espoo, Finland,December 2003.
[89] A. J. Vandermaar, Wang, M.,, "Transformer Condition Monitoring by Frequency Response Analysis ., August 25-29, 1997, Montreal, ," *Proc. of the 10th Int. Symp. on High Voltage Eng(ISH1997)*, August 25-29, 1997Canada, pp. 119-122.
[90] M. Wang, A. J. Vandermaar, and K. D. Srivastava, "Transformer winding movement monitoring in service - key factors affecting FRA measurements," *Electrical Insulation Magazine, IEEE*, vol. 20, pp. 5-12, 2004.
[91] M. Wang, A. J. Vandermaar, and K. D. Srivastava, "Condition monitoring of transformers in service by the low voltage impulse test method," in *High Voltage Engineering, 1999. Eleventh International Symposium on (Conf. Publ. No. 467)*, 1999, pp. 45-48 vol.1.
[92] G. McDowell, "Condition Monitoring of Power Transformers to Assess Residual Life and Fault Damage " *ERA Report 88-0566R, 44 p.*, June 1989.
[93] W. Doble Engineering Company, Massachusetts. M5100 SFRA Instrument User's Guide [Online].
[94] H. K. Høidalen, Brede, A.P., Lundgaard, L.,, " "Transformer winding diagnosis using the transfer function approach," 2001 Nordic Symposium on Electrical Insulation, Stockholm, Sweden.
[95] L. Bolduc, Picher ,P., Pare, G., Demers, R.J., Belanger, J., ", "Detection of Transformer Winding Displacement by the Frequency Response of Stray Losses (FRSL)"," Cigre 12/33-02, 2000.
[96] C. Bartoletti, M. Desiderio, D. Di Carlo, G. Fazio, F. Muzi, G. Sacerdoti, and F. Salvatori, "Vibro-acoustic techniques to diagnose power transformers," *Power Delivery, IEEE Transactions on*, vol. 19, pp. 221-229, 2004.
[97] B. Weiser, H. Pfutzner, and J. Anger, "Relevance of magnetostriction and forces for the generation of audible noise of transformer cores," *Magnetics, IEEE Transactions on*, vol. 36, pp. 3759-3777, 2000.
[98] P. I. Fergestad and T. Henriksen, "Inductances for the Calculation of Transient Oscillations in Transformers," *Power Apparatus and Systems, IEEE Transactions on*, vol. PAS-93, pp. 510-517, 1974.
[99] D. J. Wilcox, M. Conlon, and W. G. Hurley, "Calculation of self and mutual impedances for coils on ferromagnetic cores," *Physical Science, Measurement and Instrumentation, Management and Education - Reviews, IEE Proceedings A*, vol. 135, pp. 470-476, 1988.
[100] L. F. Blume and A. Boyajian, "Abnormal Voltages within Transformers," *American Institute of Electrical Engineers, Transactions of the*, vol. XXXVIII, pp. 577-620, 1919.
[101] J. H. McWhirter, C. D. Fahrnkopf, and J. H. Steele, "Determination of Impulse Stresses within Transformer Windings by Computers [includes discussion]," *Power Apparatus and Systems, Part III. Transactions of the American Institute of Electrical Engineers*, vol. 75,

1956.
[102] R. B. Shipley, D. Coleman, and C. F. Watts, "Transformer Circuits for Digital Studies," *Power Apparatus and Systems, Part III. Transactions of the American Institute of Electrical Engineers,* vol. 81, pp. 1028-1030, 1962.
[103] C. M. Arturi, "Transient simulation and analysis of a three-phase five-limb step-up transformer following an out-of-phase synchronization," *Power Delivery, IEEE Transactions on,* vol. 6, pp. 196-207, 1991.
[104] K. W. Wagner, "The Progress of an Electromagnetic Wave in a Coil with Capacity between Turns," Elektrotechnik und Maschinenbau, Vol.33, 1915, pp. 89-92 & pp.105-108.
[105] B. Gustavsen and A. Semlyen, "Application of vector fitting to state equation representation of transformers for simulation of electromagnetic transients," *Power Delivery, IEEE Transactions on,* vol. 13, pp. 834-842, 1998.
[106] M. V. K. Chari, J. D'Angelo, M. Palmo, and D. K. Sharma, "Application of Three-Dimensional Electromagnetic Analysis Methods to Electrical Machinery and Devices," *Energy Conversion, IEEE Transactions on,* vol. EC-1, pp. 145-150, 1986.
[107] G. Lian, Y. Ruoping, and C. Pizhang, "An Equivalent Magnetization Surface Current Approach of Calculation 3-Dimensional Leakage Fields of a Transformer," *Power Delivery, IEEE Transactions on,* vol. 2, pp. 817-822, 1987.
[108] U. Gafvërt, Frimpong, G., Fuhr, J., "Modeling of Dielectric Measurements on Power Transformers," CIGRE, 15-103, 1998.
[109] T. Orosz, Z. A. Tamus, and I. Vajda, "Modeling the high frequency behavior of the Rogowski-coil passive L/r integrator current transducer with analytical and finite element method," in *Power Engineering Conference (UPEC), 2014 49th International Universities*, 2014, pp. 1-4.
[110] F. de León, "Transformer Model for the Study of Electromagnetic Transients," Dissertation, University of Toronto, 1992.
[111] S. Chimklay, "High-Frequency Transformer Model for Switching Transient Studies Doctoral Dissertation," University of British Columbia, 1995.
[112] W. L. A. Neves, "Transformer Modeling for Transient Studies", Doctoral Dissertation," University of British Columbia, 1994.
[113] P. I. Fergestad, " Transient oscillations in transformer windings", dissertation," NTH, Norway, 1971.
[114] D. J. Wilcox, W. G. Hurley, and M. Conlon, "Calculation of self and mutual impedances between sections of transformer windings," *Generation, Transmission and Distribution, IEE Proceedings C,* vol. 136, pp. 308-314, 1989.
[115] E. E. Mombello, " Modeling of a coil system considering frequency-dependent inductances and losses; I. Analysis of the impedance matrix characteristics", El. Eng. Springer Verlag, Vol. 84,, pp. 3-10," 2002.
[116] S. D. a. S. I. A. Abu-Siada, "Frequency Response Analysis using High Frequency Transformer Model " presented at the middle East Power Engineering conference MEPCON, Egypt, 2009. .
[117] S. V. Kulkarni and G. B. Kumbhar, "Analysis of Short Circuit Performance of Split-Winding Transformer Using Coupled Field-Circuit Approach," in *Power Engineering Society General Meeting, 2007. IEEE*, 2007, pp. 1-1.
[118] G. B. Kumbhar and S. V. Kulkarni, "Analysis of Short-Circuit Performance of Split-Winding Transformer Using Coupled Field-Circuit Approach," *Power Delivery, IEEE Transactions on,* vol. 22, pp. 936-943, 2007.
[119] A. D. Podoltsev, K. G. N. B. Abeywickrama, Y. V. Serdyuk, and S. M. Gubanski, "Multiscale Computations of Parameters of Power Transformer Windings at High Frequencies. Part II: Large-Scale Level," *Magnetics, IEEE Transactions on,* vol. 43, pp. 4076-4082, 2007.
[120] A. Group, "Ansoft Maxwell," 16.0.0 ed. Australia Leading Engineering Application Providers Australia, 2013.
[121] (2009). *ABB TRANSFORMER HANDBOOK*.
[122] M. Crow, *ELECTRIC POWER TRANSFORMER ENGINEERING*. The USA: Library of Congress Cataloging-, 2010.
[123] R. H. Larry Lawhead, John Horak Basler Electric Company, *Three Phase Transformer Winding Configurations and Differential Relay Compensation*, 2006.
[124] A. Mikulecky and Z. Stih, "Influence of temperature, moisture content and ageing on oil impregnated paper bushings insulation," *Dielectrics and Electrical Insulation, IEEE*

Transactions on, vol. 20, pp. 1421-1427, 2013.
[125] D. M. Sofian, W. Zhongdong, and L. Jie, "Interpretation of Transformer FRA Responses— Part II: Influence of Transformer Structure," *Power Delivery, IEEE Transactions on*, vol. 25, pp. 2582-2589, 2010.
[126] W. Zhongdong, L. Jie, and D. M. Sofian, "Interpretation of Transformer FRA Responses— Part I: Influence of Winding Structure," *Power Delivery, IEEE Transactions on*, vol. 24, pp. 703-710, 2009.
[127] O. A. Mohammed, Z. Liu, S. Liu, and N. Y. Abed, "Finite-element-based nonlinear physical model of iron-core transformers for dynamic simulations," *Magnetics, IEEE Transactions on*, vol. 42, pp. 1027-1030, 2006.
[128] E. Billig, "Mechanical stresses in transformer windings," *Electrical Engineers - Part II: Power Engineering, Journal of the Institution of*, vol. 93, pp. 227-243, 1946.
[129] M. Arshad and S. M. Islam, "Power transformer critical diagnostics for reliability and life extension," in *Electrical and Computer Engineering, 2004. Canadian Conference on*, 2004, pp. 625-628 Vol.2.
[130] A. G. Kladas, M. P. Papadopoulos, and J. A. Tegopoulos, "Leakage flux and force calculation on power transformer windings under short-circuit: 2D and 3D models based on the theory of images and the finite element method compared to measurements," *Magnetics, IEEE Transactions on*, vol. 30, pp. 3487-3490, 1994.
[131] R. Tang, S. Wang, Y. Li, X. Wang, and X. Cui, "Transient simulation of power transformers using 3D finite element model coupled to electric circuit equations," *Magnetics, IEEE Transactions on*, vol. 36, pp. 1417-1420, 2000.
[132] M. Bagheri, B. T. Phung, and T. Blackburn, "Transformer frequency response analysis: mathematical and practical approach to interpret mid-frequency oscillations," *Dielectrics and Electrical Insulation, IEEE Transactions on*, vol. 20, pp. 1962-1970, 2013.
[133] M. F. Beavers and C. M. Adams, "The Calculation and Measurement of Axial Electromagnetic Forces on Concentric Coils in Transformers," *Power Apparatus and Systems, Part III. Transactions of the American Institute of Electrical Engineers*, vol. 78, pp. 467-477, 1959.
[134] A. Hyun-Mo, O. Yeon-Ho, K. Joong-Kyoung, S. Jae-Sung, and H. Sung-Chin, "Experimental Verification and Finite Element Analysis of Short-Circuit Electromagnetic Force for Dry-Type Transformer," *Magnetics, IEEE Transactions on*, vol. 48, pp. 819-822, 2012.
[135] S. Liu, Z. Liu, and O. A. Mohammed, "FE-Based Modeling of Single-Phase Distribution Transformers With Winding Short Circuit Faults," *Magnetics, IEEE Transactions on*, vol. 43, pp. 1841-1844, 2007.
[136] R. Tang, Y. Li, D. Li, and L. Tian, "Numerical calculation of 3D eddy current field and short circuit electromagnetic force in large transformers," *Magnetics, IEEE Transactions on*, vol. 28, pp. 1418-1421, 1992.
[137] J. A. S. B. Jayasinghe, Z. D. Wang, P. N. Jarman, and A. W. Darwin, "Winding movement in power transformers: a comparison of FRA measurement connection methods," *Dielectrics and Electrical Insulation, IEEE Transactions on*, vol. 13, pp. 1342-1349, 2006.
[138] A. A. Reykherdt and V. Davydov, "Case studies of factors influencing frequency response analysis measurements and power transformer diagnostics," *Electrical Insulation Magazine, IEEE*, vol. 27, pp. 22-30, 2011.
[139] M. Wang, A. J. Vandermaar, and K. D. Srivastava, "Improved detection of power transformer winding movement by extending the FRA high frequency range," *Power Delivery, IEEE Transactions on*, vol. 20, pp. 1930-1938, 2005.
[140] C. Yao, Z. Zhao, Y. Chen, X. Zhao, Z. Li, Y. Wang, Z. Zhou, and G. Wei, "Transformer winding deformation diagnostic system using online high frequency signal injection by capacitive coupling," *Dielectrics and Electrical Insulation, IEEE Transactions on*, vol. 21, pp. 1486-1492, 2014.
[141] P. M. Nirgude, D. Ashokraju, A. D. Rajkumar, and B. Singh, "Application of numerical evaluation techniques for interpreting frequency response measurements in power transformers," *Science, Measurement & Technology, IET*, vol. 2, pp. 275-285, 2008.
[142] M. R. Patel, "Dynamic Response of Power Transformers Under Axial Short Circuit Forces Part I - Winding and Clamp as Individual Components," *Power Apparatus and Systems, IEEE Transactions on*, vol. PAS-92, pp. 1558-1566, 1973.
[143] M. R. Patel, "Dynamic Response of Power Transformers Under Axial Short Circuit Forces Part II - Windings and Clamps as a Combined System," *Power Apparatus and Systems, IEEE*

Transactions on, vol. PAS-92, pp. 1567-1576, 1973.
[144] M. Arshad, S. M. Islam, and A. Khaliq, "Power transformer asset management," in *Power System Technology, 2004. PowerCon 2004. 2004 International Conference on*, 2004, pp. 1395-1398 Vol.2.
[145] H. A. Thompson, F. Tillery, and D. U. Von Rosenberg, "The Dynamic Response of Low Voltage, High Current, Disk type Transformer Windings to through Fault Loads," *Power Apparatus and Systems, IEEE Transactions on*, vol. PAS-98, pp. 1091-1098, 1979.
[146] "The short-circuit strength of the inner windings of transformers against radial forces," CIGRE, Paris, France,1962.
[147] W. M. J. R. B. Steel, J. J.Narbus, M. R. Patel, R.A.Nelson, "Dynamic measurements in power transformers under short-circuit conditions," ed: CIGRE, 1972.
[148] K. Ludwikowski, K. Siodla, and W. Ziomek, "Investigation of transformer model winding deformation using sweep frequency response analysis," *Dielectrics and Electrical Insulation, IEEE Transactions on*, vol. 19, pp. 1957-1961, 2012.
[149] J. Christian, K. Feser, U. Sundermann, and T. Leibfried, "Diagnostics of power transformers by using the transfer function method," in *High Voltage Engineering, 1999. Eleventh International Symposium on (Conf. Publ. No. 467)*, 1999, pp. 37-40 vol.1.
[150] A. Shintemirov, W. H. Tang, and Q. H. Wu, "Transformer winding condition assessment using frequency response analysis and evidential reasoning," *Electric Power Applications, IET*, vol. 4, pp. 198-212, 2010.
[151] A. Shintemirov, W. H. Tang, and Q. H. Wu, "Construction of transformer core model for frequency response analysis with genetic Algorithm," in *Power & Energy Society General Meeting, 2009. PES '09. IEEE*, 2009, pp. 1-5.
[152] A. Shintemirov, W. H. Tang, and Q. H. Wu, "Transformer Core Parameter Identification Using Frequency Response Analysis," *Magnetics, IEEE Transactions on*, vol. 46, pp. 141-149, 2010.
[153] D. L. Alvarez, J. A. Rosero, and E. E. Mombello, "Circuit model of transformers windings using vector fitting, for frequency response analysis (FRA) PART II: Core influence," in *Power Electronics and Power Quality Applications (PEPQA), 2013 Workshop on*, 2013, pp. 1-5.
[154] E. Gomez-Luna, G. Aponte Mayor, J. Pleite Guerra, D. F. Silva Salcedo, and D. Hinestroza Gutierrez, "Application of Wavelet Transform to Obtain the Frequency Response of a Transformer From Transient Signals—Part 1: Theoretical Analysis," *Power Delivery, IEEE Transactions on*, vol. 28, pp. 1709-1714, 2013.
[155] M. B. Goff and A. H. Eltom, "Oil filled bushing secrets revealed," in *Industry Applications Society Annual Meeting, 2013 IEEE*, 2013, pp. 1-9.
[156] F. Meghnefi, I. Fofana, H. Hemmatjou, and M. Farzaneh, "Deriving an equivalent circuit of composite oil paper insulation for understanding the Frequency Domain Spectroscopic measurements," in *Electrical Insulation and Dielectric Phenomena, 2009. CEIDP '09. IEEE Conference on*, 2009, pp. 478-481.
[157] M. Melo, M. E. G. Alves, and G. A. Moura, "Experience with on-line monitoring of capacitance and tangent delta of condensive bushings," in *Transmission and Distribution Conference and Exposition: Latin America, 2008 IEEE/PES*, 2008, pp. 1-6.
[158] R. Nikjoo and H. Edin, "Effect of transformer winding on the transient response of power transformer bushings," in *Lightning Protection (ICLP), 2012 International Conference on*, 2012, pp. 1-5.
[159] Z. Daxiong, "An improved method of measuring C₁ power factor of resistance-graded bushings," *Power Delivery, IEEE Transactions on*, vol. 14, pp. 437-442, 1999.
[160] Y. Du, M. Zahn, B. C. Lesieutre, A. V. Mamishev, and S. R. Lindgren, "Moisture equilibrium in transformer paper-oil systems," *Electrical Insulation Magazine, IEEE*, vol. 15, pp. 11-20, 1999.
[161] J. A. Lapworth, "Detection of winding movement in power transformers by frequency response analysis (FRA)," presented at the Transformer Int'l. Conf. Power Transformers, Kolobrzeg, Poland, 1999.
[162] Z. Haijun, Y. Bin, X. Weijie, W. Shuhong, W. Guolin, H. Youpeng, and Z. Jingyin, "Dynamic Deformation Analysis of Power Transformer Windings in Short-Circuit Fault by FEM," *Applied Superconductivity, IEEE Transactions on*, vol. 24, pp. 1-4, 2014.
[163] M. Bagheri, M. S. Naderi, and T. Blackburn, "Advanced transformer winding deformation diagnosis: moving from off-line to on-line," *Dielectrics and Electrical Insulation, IEEE Transactions on*, vol. 19, pp. 1860-1870, 2012.

[164] M. Bagheri, M. S. Naderi, T. Blackburn, and T. Phung, "Practical challenges in online transformer winding deformation diagnostics," in *Electric Power and Energy Conversion Systems (EPECS), 2011 2nd International Conference on*, 2011, pp. 1-6.

[165] M. Bagheri, M. S. Naderi, T. Blackburn, and T. Phung, "FRA vs. short circuit impedance measurement in detection of mechanical defects within large power transformer," in *Electrical Insulation (ISEI), Conference Record of the 2012 IEEE International Symposium on*, 2012, pp. 301-305.

[166] A. Setayeshmehr, I. Fofana, C. Eichler, A. Akbari, H. Borsi, and E. Gockenbach, "Dielectric spectroscopic measurements on transformer oil-paper insulation under controlled laboratory conditions," *Dielectrics and Electrical Insulation, IEEE Transactions on*, vol. 15, pp. 1100-1111, 2008.

[167] J. A. Almendros-Ibaez, J. C. Burgos, and B. Garcia, "Transformer Field Drying Procedures: A Theoretical Analysis," *Power Delivery, IEEE Transactions on*, vol. 24, pp. 1978-1986, 2009.

[168] P. Hua-Dong, D. Ming, R. Ming, M. Jin, and Z. Zhi, "Insulation diagnosis for 220kV oil-immersed current transformer by frequency dielectric spectroscopy," in *Electrical Insulation Conference (EIC), 2011*, 2011, pp. 69-73.

Every reasonable effort has been made to acknowledge the owners of copyright material. I would be pleased to hear from any copyright owner who has been omitted or incorrectly acknowledged.

APPENDIX

Table A.1. Extracted parameters of the healthy transformer model by using FEA

	L_S	C_S	C_{H-L}	C_g	1/G	R_S
HV	180µH	2.20nF	3.5nF	37pF	7 MΩ	1.2Ω
LV	60µH	1.11nF	6nF	65pF	7 MΩ	0.8Ω

Table A.2. Transformer design data

Transformer Power	*1MVA*	*5 MVA*
Transformer ratio	22.9kV/3.3kV	66kV/6600 V
Outer radius HV	560 mm	747 mm
Outer radius LV	480 mm	576 mm
HV winding height	670 mm	1576 mm
LV winding height	670 mm	1576 mm

Table A.3. Dielectric properties of different oils

Dielectric properties	*Vegetable Oil*	*Mineral Oil*
ε_r	3.4	2.4
ϱ	$3*10^{-11}$	$9*10^{-12}$

Table A.4. Dielectric properties of bushing

Dielectric properties	*Oil*	*Paper layer*	*porcelain*
ε_r	2.4	2.5-16	6.5

Table A.5. Transformer Parameters (3 phase)

Description	*Value*
HV/LV Rating	11kV / 433V
Z%	9.49
HV Terminal Resistance	0.915Ω
HV Inductance	101mH
LV Inductance	20µH
HV-LV Cap	75 pF
LV-Core Cap	63pF
HV-Tank Cap	11pF

Table A.6. Extracted parameters of the healthy transformer model by using FEA

Electrical parameters	*C1*	*C2*	L_S	R_S
Value	2000pF	450pF	2.5µH	0.2Ω